THE EFFECT OF LYSOBISPHOSPHATIDIC ACID (LBPA) ON α-TOCOPHEROL TRANSFER PROTEIN (α-TTP) BINDING TO LIPID MEMBRANES

Matilda Baptist, BSc

Biotechnology

Submitted in partial fulfilment of the requirements
for the degree of Masters of Science

Faculty of Mathematics and Sciences
Brock University, St Catharines, Ontario

ABSTRACT

The α-tocopherol transfer protein (α-TTP) is responsible for the retention of the α-tocopherol form of vitamin E in living organisms. The detailed ligand transfer mechanism by α-TTP is still yet to be fully elucidated. To date, studies show that α-TTP transfers α-tocopherol from late endosomes in liver cells to the plasma membrane where it is repackaged into very low density lipoprotein (VLDL) and released into the circulation.

Late endosomes have been shown to contain a lipid known as lysobisphosphatidic acid (LBPA) that is unique to this cellular compartment. LBPA plays a role in intracellular trafficking and controlling membrane curvature. Taking these observations into account plus the fact that certain proteins are recruited to membranes based on membrane curvature, the specific aim of this project was to examine the effect of LBPA on α-TTP binding to lipid membranes. To achieve this objective, dual polarization interferometry (DPI) and a vesicle binding assay were employed. Whilst DPI allows protein binding affinity to be measured on a flat lipid surface, the vesicle binding assay determines protein binding affinity to lipid vesicles mimicking curved membranes.

DPI analysis revealed that the amount of α-TTP bound to lipid membranes is higher when LBPA is present. Using the vesicle binding assay, a similar result was seen where a greater amount of protein is bound to large unilamellar vesicles (LUVs) containing LBPA. However, the effect of LBPA was attenuated when small unilamellar vesicles (SUVs) were replaced with LUVs. The outcome of this project suggests that α-TTP binding to membranes is influenced by membrane curvature, which in turn is induced by the presence of LBPA.

ACKNOWLEDGEMENTS

First and foremost I wish to express my heartfelt gratitude to my supervisor, Dr Jeffrey Atkinson, for providing me the opportunity to pursue my graduate studies in his laboratory. I am also grateful for his patience, support and guidance throughout my studies and for fostering my development as a scientist. Dr Atkinson is truly a sincere man with lots of wisdom and knowledge and a great sense of humour – making my working experience with him a good and memorable one.

A note of thanks goes out also to Dr Heather Gordon and Dr Adonis Skandalis for being on my supervisory committee and for their invaluable input.

In addition, I wish to thank all the members of the Atkinson and Inglis research group during my time at Brock. Especially to Wendy Zhang who has shared her knowledge and skills and helped me a great deal; Ai Lin Beh for scientific discussions and helping in troubleshooting; Alessandro Virgulti for initial training on the DPI; Michael Flewelling for proofreading my introduction section and Kaleigh Giles for aiding in protein purification.

I am also grateful to Samantha Morley, from our collaborating group at Case Western Reserve University, who very patiently answered all my questions regarding the vesicle binding assay.

Last but not least I wish to thank my friends and family who have supported me throughout my time of study in every possible way.

TABLE OF CONTENTS

LIST OF TABLES

LIST OF FIGURES

LIST OF ABBREVIATIONS

PUFAs	Polyunsaturated fatty acids
LPL	Lipoprotein lipase
VLDLs	Very low density lipoproteins
HDLs	High density lipoproteins
LDLs	Low density lipoproteins
α-TTP	α-Tocopherol transfer protein
AVED	Ataxia with vitamin E deficiency
FRET	Fluorescence resonance energy transfer
GA	Golgi apparatus
RER	Rough endoplasmic reticulum
LAMP-1	Lysosome-associated membrane protein-1
C9-NBD-α-tocopherol	7-nitrobenz-2-oxa-1,-3-diazol-4-yl substituted tocopherol
LBPA	Lysobisphosphatidic acid
BMP	Bis(monoacylglycero)phosphate
PG	Phosphatidylglycerol
LPG	Lysophosphatidylglycerol
CL	Cardiolipin
EM	Electron microscopy
HPTS	8-hydroxypyrene-1, 3, 6–trisulfonic acid
ILVs	Intraluminal vesicles
MVBs	Multivesicular bodies
ECVs	Endosomal carrier vesicles
VSV	Vesicular stomatitis virus
MHC	Major histocompatibility complex
PI(3)P	Phosphatidylinositol-3-phosphate
EGFR	Epidermal growth factor receptor
MPR	Mannose-6-phosphate receptor
TGN	Trans-Golgi network
PC	Phosphatidylcholine

PE	Phosphatidylethanolamine
LPA	Lysophosphatidic acid
ArfGAP1	ADP-ribosylation factor GTPase activating protein 1
COP1	Coat protein complex 1
PI 3-kinase	Phosphoinositide 3-kinase
PI	Phosphatidylinositol
SPR	Surface plasmon resonance
DPI	Dual polarization interferometry
TE	Transverse electric
TM	Transverse magnetic
SDS-PAGE	Sodium dodecyl sulphate polyacrylamide gel electrophoresis
SUVs	Small unilamellar vesicles
LUVs	Large unilamellar vesicles
NaCl	Sodium chloride
IPTG	Isopropyl-D-thiogalactoside
Tris	Tris(hydroxymethyl)aminomethane
EDTA	Ethylenediaminetetraacetic acid
DTT	Dithiothreitol
PMSF	Phenylmethanesulphonylfluoride
$MgCl_2$	Magnesium chloride
IPA	Isopropanol
KCl	Potassium chloride
MES	2-(N-Morpholino)ethanesulphonic acid
DOPC	1, 2-dioleoyl-sn-glycero-3-phosphocholine
DOPS	1, 2-dioleoyl-sn-glycero-3-phospho-L-serine
DOPE	1, 2-dioleoyl-sn-glycero-3-phosphoethanolamine
SM	Sphingomyelin
PI	Phosphatidylinositol
LB	Luria Bertani
BSA	Bovine serum albumin
PBS	Phosphate buffered saline

TIFF	Tagged Image File Format
GST	Glutathione
SLBs	Supported Lipid Bilayers
CT	CTP (cytidine triphosphate):phosphocholine cytidyltransferase
pI	Isoelectric point
OD	Optical density
GUVs	Giant unilamellar vesicles

1. INTRODUCTION

1.1 Vitamin E: Structure and Function

Vitamin E refers to eight lipid-soluble molecules which can be grouped into two classes, tocopherols and tocotrienols. The general structure of vitamin E consists of a chromanol head group and an isoprenoid derived side chain [1]. Tocopherols and tocotrienols differ in the degree of saturation of the side chain. The tocopherols have a saturated chain giving rise to three chiral centres at C2, C4′ and C8′ [1]. As a result, eight stereoisomers are present in synthetic racemic vitamin E known as *all rac*-α-tocopherol. Only the *RRR*-α-tocopherol corresponds to the naturally occurring form [1-2]. The tocotrienols, on the other hand, have double bonds at C3′, C7′ and C11′ and a chiral centre at C2. The nomenclature of vitamin E is based on the methylation pattern of the chromanol head group which gives rise to α-, β-, γ- and δ-tocopherol and tocotrienol as shown in **Figure 1** [3]. Amongst the eight naturally occurring forms of vitamin E, α-tocopherol has the highest biological activity [3, 4].

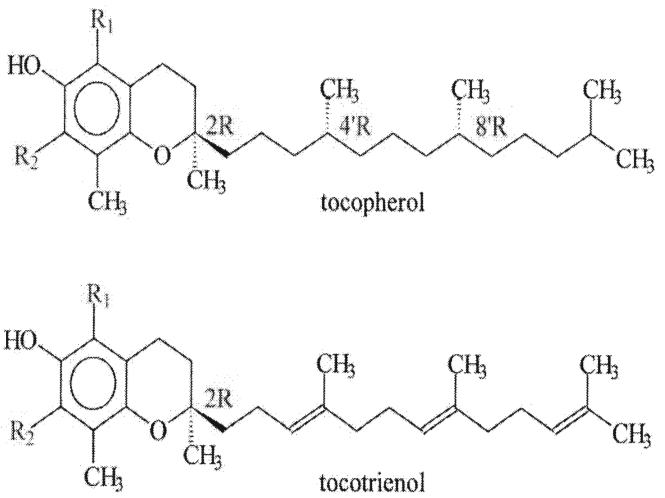

R_1	R_2	
CH_3	CH_3	α
CH_3	H	β
H	CH_3	γ
H	H	δ

***Figure 1**: Structure of tocopherols and tocotrienols. Taken from Azzi and Stocker [3].*

Since its discovery in 1922 by Evans and Bishop as a factor required for normal reproduction [5], vitamin E's most established role to date is its function as an antioxidant, protecting polyunsaturated fatty acids (PUFAs) in cell membranes against free radical damage [6-7]. A free radical is any species existing independently with one or more unpaired electrons making it highly reactive and causing it to attack biological molecules such as DNA, proteins and lipids [8].

Free radical attack on unsaturated lipids initiates lipid peroxidation; the process of oxidative degeneration of lipids which occurs as a chain reaction in three stages [9]. The first stage, which is known as the initiation phase, involves the generation of a carbon-centred radical (R•). This is usually the result of other free radicals such as hydroxyl (OH•) radicals attacking PUFAs via the abstraction of a hydrogen atom from the bis-allylic methylene between two double bonds [10]. Next is the propagation phase, which involves the production of the peroxyl radical (ROO•) when the carbon-centred radical reacts with molecular oxygen. The peroxyl radical formed is then capable of further propagating the chain reaction by abstracting another H-atom from a neighbouring PUFA, forming a hydroperoxide (ROOH) and a new carbon-centred radical [10]. A single initiation event is capable, in theory, of destroying hundreds of lipid molecules. Consequently the PUFAs that are consumed disrupt membrane structure and function, eventually affecting cell integrity [11].

Vitamin E, specifically α-tocopherol (α-TO-H), acts as a chain-breaking antioxidant by inhibiting the propagation phase of lipid peroxidation [10]. The hydrogen atom of the phenol on the chromanol ring is donated to the peroxyl radical resulting in the formation of a less reactive tocopheroxyl radical (α-TO•) [12]. The tocopheroxyl radical can then be reduced by glutathione, ascorbate or ubiquinol to

regenerate tocopherol [4, 13]. **Figure 2** illustrates the role of vitamin E in lipid peroxidation.

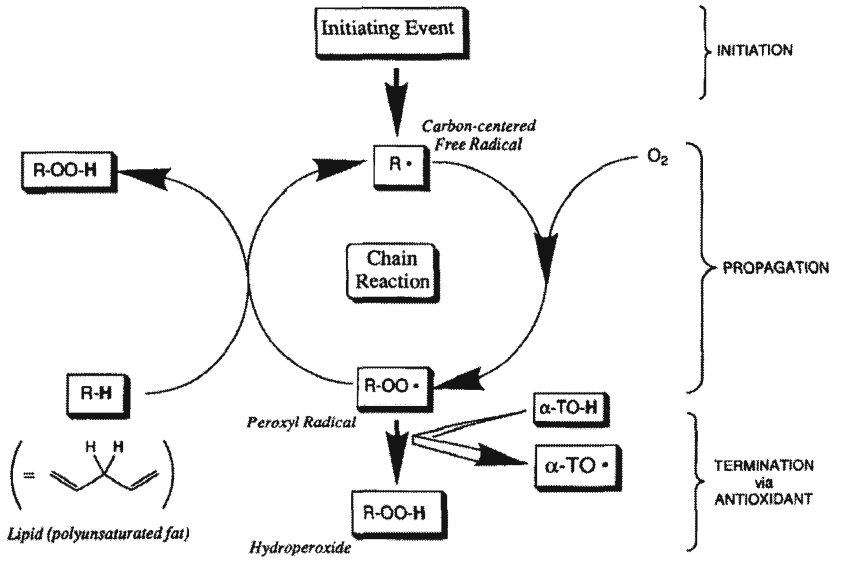

***Figure 2**: The role of α-tocopherol as a chain-breaking antioxidant in lipid peroxidation. A carbon-centred free radical from the hydrogen abstraction of PUFAs reacts with molecular oxygen to form a peroxyl radical. Donation of the phenolic hydrogen from α-tocopherol leads to the formation of hydroperoxide and a tocopheroxyl radical. The tocopheroxyl radical is regenerated to α-tocopherol through reduction by ascorbate and glutathione. Taken from Burton and Traber [10].*

Taking into account the significant role of vitamin E in maintaining cell membrane integrity and its occurrence in hydrophobic domains such as lipoproteins and cell membranes, many studies have been performed to determine its exact localization [14]. While the precise location of the chromanol ring within cell membranes has not been fully determined, the general position of vitamin E within membranes can be described as follows [15]. The side chain of vitamin E is oriented towards the hydrophobic core of membranes, facilitating its incorporation and retention in membranes, while the chromanol ring, primarily responsible for its

antioxidant activity, is located among the polar head groups [4, 14-15]. This is brought about by the amphiphilic nature of vitamin E due to its polar hydroxyl substituent on the chromanol ring and the greasy hydrophobic tail [14].

1.2 Vitamin E: Absorption and Delivery

One of the requirements for a compound to be classified as a vitamin is that it must be essential for human health [16]. Vitamin E is obtained from the diet. Vegetable oils, such as sunflower oil are the main sources of vitamin E in the human diet [6]. Since vitamin E is hydrophobic in nature, lipoproteins are its main transport system to tissues in the body [17]. Upon ingestion, vitamin E is absorbed in the small intestine with other lipid compounds and packaged into chylomicrons. It then enters the systemic circulation via the lymphatic system [18]. Following that, chylomicrons undergo transformation to chylomicron remnants by the action of lipoprotein lipase (LPL). As a result, a portion of the vitamin E is absorbed by surrounding tissues [17], while the rest is retained in chylomicron remnants and delivered to the liver. The chylomicron remnants are absorbed into liver cells via receptor-mediated endocytosis [17]. Vitamin E is then repackaged in liver cells, and secreted into the plasma in very low density lipoproteins (VLDLs). The vitamin E in VLDLs can either then be transferred to high density lipoproteins (HDLs) via lipolysis or to low density lipoproteins (LDLs) through the conversion of VLDLs [17].

However, it was discovered that only the *RRR*-α-tocopherol form of vitamin E is present in nascent VLDLs [19], while the remaining forms of vitamin E were found to be excreted in the bile [20]. Nearly two decades of investigation showed that a protein, known as α-tocopherol transfer protein (α-TTP) is responsible for this selective retention [21-25]. This is supported by its high binding affinity with α-

tocopherol in comparison with the other forms of vitamin E [26, 27] and also α-TTP's capability to transport α-tocopherol between liposomes [22, 23].

1.3 α-Tocopherol Transfer Protein (α-TTP)

α-TTP is a cytosolic protein, first isolated from rat liver [28]. Later, it was isolated from human liver [29] and found to have 94 % homology to rat α-TTP [30]. Though α-TTP is mainly expressed in the liver, it is also expressed in the brain, lung and kidney, but at much lower levels [20]. α-TTP has a molecular weight of about 32 kDa and is comprised of 278 amino acids [30]. It belongs to the CRAL-TRIO protein family, whose members contain the CRAL-TRIO domain, a lipid binding domain composed of an amino-terminal three-helix coil, and a larger C-terminal domain [31]. The CRAL-TRIO domain obtained its name from the cellular retinaldehyde-binding protein (CRALBP) and the Trio protein, a guanine exchange factor [27].

The significance of α-TTP in the regulation of vitamin E plasma levels was made clear when it was discovered that mutations in the *ttpA* gene resulted in very low plasma α-tocopherol levels and a neurological disorder termed ataxia with vitamin E deficiency (AVED) [32]. Similar symptoms were also observed in α-TTP knock-out mice [33]. In addition, α-TTP has also shown the ability to transfer α-tocopherol between liposomes and microsomes [22] and facilitate the secretion of α-tocopherol in cultured liver cells [34]. These observations further provide evidence supporting the role of α-TTP in α-tocopherol retention in the body.

The underlying mechanism of intermembrane tocopherol transfer by α-TTP is still not fully understood, however, its three-dimensional structure has given further insight into how α-TTP may possibly function. The structure of α-TTP has been solved by means of X-ray diffraction and the protein has been shown to exist in two conformations: open and closed (**Figure 3**) [35]. The closed form (**Figure 3A**) was

determined with the ligand (α-tocopherol) in the hydrophobic binding site, whereas the open form (**Figure 3B**), the detergent Triton X-100 replaced the ligand [35]. Comparison between both conformations revealed changes in residues 202 – 212, that reside within an α-helix (α-10) [36], which forms the 'lid' to the hydrophobic binding site. The closed conformation, which is thought to be the "carrier protein state", shows that the ligand is buried deeply in the hydrophobic pocket covered by the lid. In the open state, or the "membrane docking form", the lid changes its position exposing the hydrophobic binding pocket [35]. Hence it is proposed that α-TTP in the open state attaches to a lipid bilayer, where it picks up an α-tocopherol substrate and transports it in the closed conformation [35].

The notion that α-tocopherol transfer by α-TTP involves direct protein-membrane interaction is further supported by two recent studies using fluorescence resonance energy transfer (FRET) assays [37-38]. While the first study revealed an increase in the α-tocopherol transfer rate as α-TTP concentration increases [37], the second study also showed an increase in the transfer rate when the concentration of acceptor phospholipid vesicles was increased [38]. If α-TTP adopted a diffusional mechanism, as opposed to a collisional mechanism, then increasing either the protein or acceptor vesicle concentration as mentioned in the above studies would not enhance the transfer rate of α-tocopherol [37-38]. Therefore, the results from these two studies further support the proposed mechanism of α-TTP, that it first binds to lipid membranes and picks up its ligand in the open conformation, followed by ligand transfer in the closed conformation.

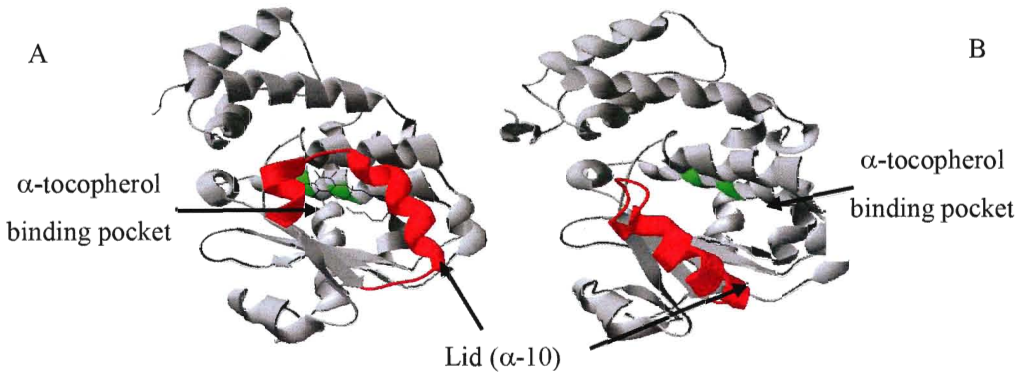

***Figure 3**: α-TTP structure. Shown here are the closed conformation with a-tocopherol in the binding site (A) and the open conformation (B). Taken from Meier et al. [35].*

1.4 α-TTP-Mediated Transfer of α-Tocopherol

To further understand the mechanism of α-TTP-mediated ligand transfer, where and how α-tocopherol is incorporated into VLDLs was investigated. Arita *et al.* demonstrated that the secretion of α-tocopherol is independent of the Golgi pathway where VLDL assembly occurs [34]. This was proven by over-expressing TTP in McARH7777 rat liver tumour cells in the presence of Brefeldin A, an inhibitor of VLDL secretion which disrupts the Golgi apparatus (GA) [34]. The secretion of triglyceride, a major lipid component of VLDL, was significantly inhibited, whereas α-tocopherol secretion was not affected [34]. This non-Golgi pathway of α-tocopherol secretion was further illustrated by Traber *et al.* through the isolation of nascent VLDLs from the rough endoplasmic reticulum (RER) and GA membrane fractions from the livers of rats fed with equimolar ratios of deuterated *RRR*- and *SRR*-α-tocopherol [39]. The membrane fractions of the RER and GA were selected, as it is believed that VLDL assembly occurs through this route, such that the core lipids are assembled at the RER and then transported to the GA for further modification [39]. It was observed that the deuterated *RRR*:*SRR* ratio was

approximately 1 in both the RER and Golgi fractions as opposed to the serum which had a ratio greater than 3 [39]. If α-tocopherol enrichment of VLDLs occurs in the RER or GA, then the ratios of the deuterated *RRR*:*SRR*-α-tocopherol should be approximately the same as in serum [39].

The localization of α-TTP at late endosomes has been recently determined by means of fluorescence microscopy techniques [40-41]. α-TTP was seen in a punctate pattern resembling vesicular structures surrounding the nucleus in both cultured and fresh hepatocytes. To identify the intracellular organelle that α-TTP associates with, several antibody markers were used [40]. The results showed that α-TTP colocalized significantly with the lysosome-associated membrane protein-1 (LAMP-1) marker, which is a resident protein of the late endosomes/lysosomes (**Figure 4)** [40]. This evidence supports the work of Horiguchi *et al.,* which demonstrated that chloroquine inhibits α-tocopherol secretion in cultured hepatocytes [41]. Chloroquine is known to accumulate within acidic compartments of late endosomes and lysosomes, neutralizing their luminal pH [41]. If the α-TTP-mediated-α-tocopherol secretion is affected when late endosomes and lysosomes are compromised, then an important role of TTP within these organelles is implied.

The colocalization of α-TTP with α-tocopherol was also investigated. Here, C9-NBD-α-tocopherol (7-nitrobenz-2-oxa-1,-3-diazol-4-yl substituted tocopherol), a fluorescent analog of vitamin E was used [40]. NBD-tocopherol emits green fluorescence aiding in visualization and it mimics natural vitamin E due to its high affinity to α-TTP and reversible binding capability [40]. α-TTP was found to colocalize with NBD-tocopherol – **Figure 5** [40]. These experiments demonstrated that α-tocopherol enters liver cells and follows the endocytic pathway where it eventually ends up in late endosomes/lysosomes. This is in line with a previous study

by Rupar *et al.* that revealed lysosomes from rat livers were enriched with α-tocopherol [42].

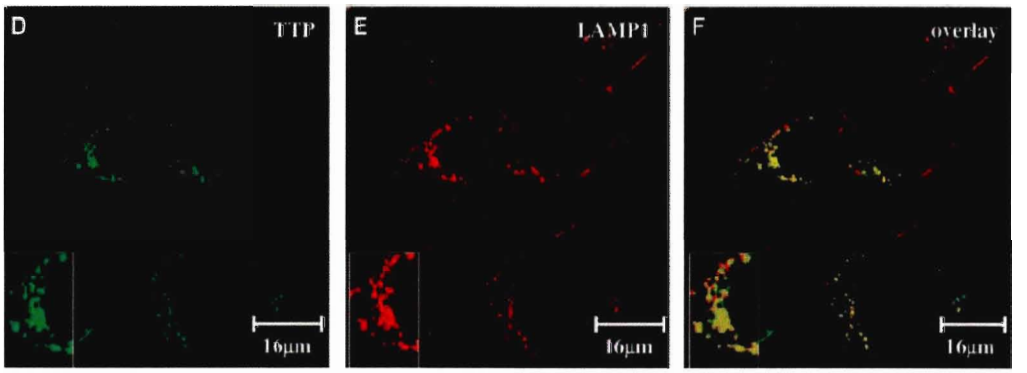

***Figure 4**: Colocalization of α-TTP with LAMP1 marker. When anti-α-TTP (green) (D) was overlaid with LAMP1 marker (red) (E) both anti-α-TTP and LAMP1 marker showed colocalization (F). Taken from Qian et al. [40].*

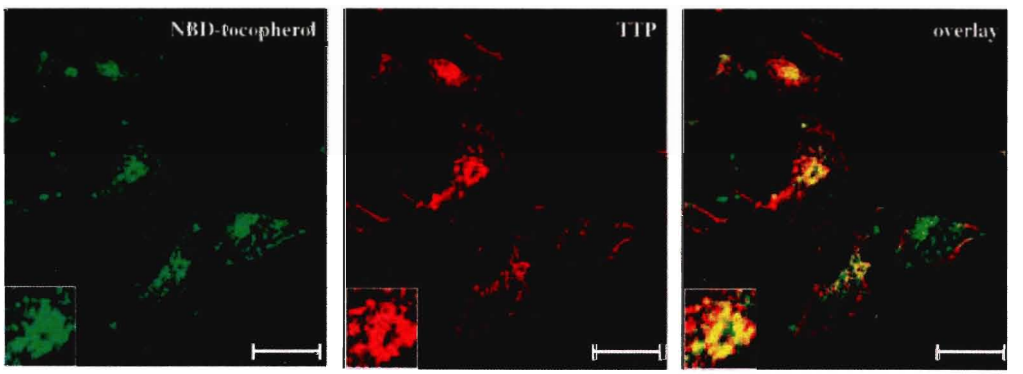

***Figure 5**: Colocalization of α-TTP with NBD-tocopherol. NBD-tocopherol (green) colocalizes with anti-α-TTP (red) in the overlay window. Bar = 16 μM. Taken from Qian et al. [40].*

A comparison between cells that express α-TTP and those that do not, showed that in α-TTP-expressing cells the NBD-tocopherol was found to be redistributed particularly around the cell periphery after 3 hours [40]. In cells that do not express α-TTP NBD-tocopherol remained in the perinuclear region, and only a small fraction was seen in the plasma membrane region [40].

Another important piece of evidence provided by Horiguchi *et al.* using a dual-label fluorescence technique showed that α-TTP colocalized with lysobisphosphatidic acid (LBPA) [41]. LBPA is found in late endosomes, where it makes up about 15 % of late endosomal total phospholipids [43]. All these studies suggest that α-tocopherol delivered to liver cells eventually ends up in the late endosome via endocytosis [40]. α-TTP, which is found in the cytosol around this compartment, then picks up α-tocopherol and transfers it to the plasma membrane region to be packaged into nascent VLDLs [40].

1.5 The Unique Properties of Lysobisphosphatidic acid (LBPA)

LBPA, also known as bis(monoacylglycero)phosphate (BMP) was first isolated from the lungs of rabbits and makes up less than 1 % of the total phospholipids of animal tissues [44]. LBPA is now known as a unique lipid that constitutes about 15 % of the total phospholipid content in late endosomes as mentioned above [43]. It possesses a distinct structure in that the phosphodiester moiety is attached to the *sn*-1 and *sn*-1′ positions of glycerol as opposed to the *sn*-3 position seen in most glycerol-phospholipids [45]. In addition, LBPA was thought to be esterified at the *sn*-3 and *sn*-3′ position but a recent study indicates that the 2, 2′-LBPA (**Figure 6**) is the major isoform in vivo [45]. Since LBPA is found predominantly in endosomal and lysosomal membranes, it is believed that its biosynthesis takes place here. Earlier investigation reveals that phosphatidylglycerol (PG) or lysophosphatidylglycerol (LPG) and cardiolipin (CL) are the main precursors of LBPA [46]. A recent study showed that PG was most likely the precursor of LBPA in mammalian cells; however the biosynthesis pathway of LBPA still remains to be elucidated [47].

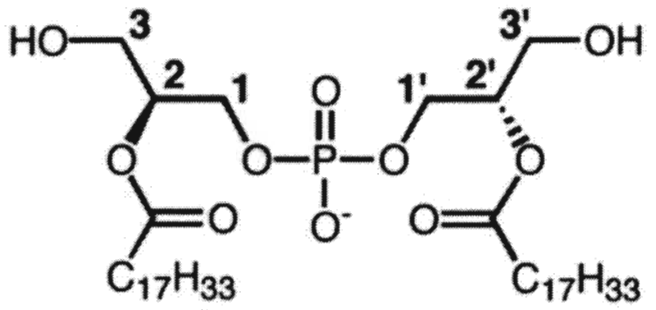

***Figure 6**: Structure of 2, 2'- dioleoyl-LBPA. Taken from Matsuo et al. [45].*

The unique characteristic of LBPA stems from its pH-dependent fusogenic property. At a low pH of about 5.6, LBPA-containing liposomes are highly fusogenic, with this characteristic diminishing at higher pH values [44]. In a recent study, LBPA was found to promote multivesicular formation in liposomes at acidic pH as observed by fluorescence and cryo-electron microscopy (EM) – **Figure 7** [45]. Liposomes with similar composition to late endosomes were prepared and were seen as unilamellar vesicles at neutral pH when LBPA was present (**Figure 7C**) [45]. When the luminal pH was dropped to about 5.5, multivesicular liposomes were seen only when LBPA was present (**Figure 7D & 7E**). Similar results were observed when the liposomes were observed by cryo-EM (**Figure 7F & 7G**). In addition, the invagination process of these liposomes was followed by the incorporation of the water-soluble dye 8-hydroxypyrene-1, 3, 6–trisulfonic acid (HPTS) at pH 5.5 [45]. Only in the presence of LBPA, the liposomes were capable of incorporating HPTS. Furthermore, when an antibody against LBPA was used, the invagination process was inhibited. This was not observed when an isotypic control antibody was used instead [45].

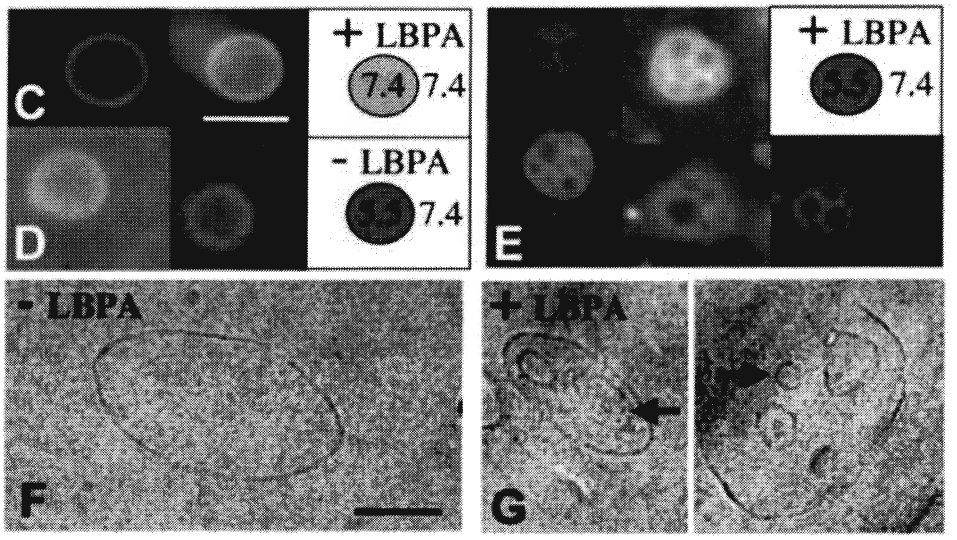

***Figure** 7: Formation of multivesicular liposomes. Liposomes observed with a neutral luminal pH with LBPA present (C). Liposomes observed with an acidic luminal pH in the absence (D) and presence of LBPA (E). C-E was obtained by fluorescence microscopy. Liposomes observed by cryo-EM in the absence (F) and presence (G) of LBPA at acidic pH. Taken from Matsuo et al. [45].*

The multivesicular structures formed in the presence of LBPA at low pH in liposomes resemble those seen in late endosomes via electron microscopy [45]. Since the pH conditions of late endosomes are also around 5.5, the results from the aforementioned study supports the idea that LBPA may play a role in this multivesicular formation [45]. Also, in this study, the investigators noted that mainly the 2, 2′-LBPA isoform rather than 3, 3′-LBPA was capable to stimulate internal vesicle formation, a 100 % activity compared to 19 % respectively [45].

1.6 The Endocytic Pathway

Endocytosis is the cellular uptake of substances from the extracellular environment via invagination and pinching-off of membrane-bound vesicles from the plasma membrane [48]. These vesicles, containing substances such as proteins and lipids, travel along a pathway that involves endosomes, eventually leading to the

lysosome for degradation [48]. Along the way, protein and lipid sorting takes place to ensure only those substances targeted for degradation arrive at the lysosome [48]. The process begins with the membrane-bound vesicles from the plasma membrane first fusing with early endosomes, the first sorting station [48]. Within the early endosomes, the pH is mildly acidic (6.2) and dissociation of some proteins and lipids from their receptors occurs [49]. The receptors are then recycled back to the plasma membrane via recycling endosomes [49]. The remaining substances targeted for the lysosome are packaged into intraluminal vesicles (ILVs). ILVs are small vesicles formed from the budding of the endosomal-limiting membrane into the endosomal lumen [48]. These early endosomes containing ILVs are believed to mature to form multivesicular bodies (MVBs) [50].

In recent literature, MVBs is used interchangeably with late endosomes [48, 50-51]. Three forms of late endosomes have been recognized in HeLa cells, namely dense tubular, multilamellar and multivesicular [52]. Hence, MVB specifically refers to the multivesicular late endosomes as opposed to the tubular and multilamellar forms. On the other hand, MVB has also been used interchangeably with endosomal carrier vesicles (ECVs) [49, 53]. These are recognized as intermediates between the early and late endosomes [49, 53]. In this thesis, the term MVB will be used for the late endosome.

The late endosome is characterized by a decrease in the luminal pH to about 5.5 [49] and an increase in the number of ILVs [54]. Fusion of MVBs to the lysosome results in the break-down of proteins and lipids that are no longer of functional value [55]. This was thought to be the only fate of MVBs [49]. However, current studies are showing that MVBs may possess other possible routes and therefore play a role in protein and lipid trafficking [55]. Hence, it appears that

MVBs act as the last sorting compartment before molecules are targeted for degradation in the lysosome [55]. An illustration of the endocytic pathway is seen in **Figure 8**.

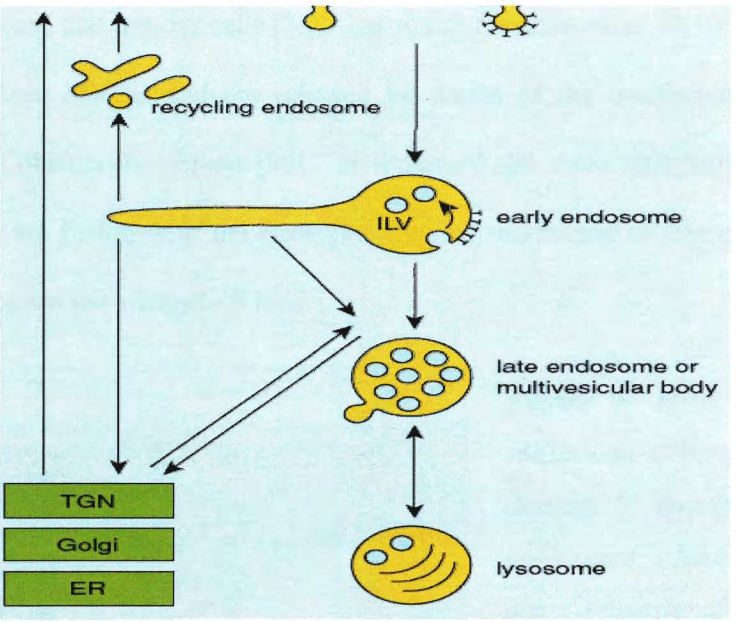

***Figure 8**: Key stages of the endocytic pathway. Endocytosed materials such as protein and lipids enter firstly into the early endosomes. Receptors are recycled back to the plasma membrane via recycling endosomes. The early endosome then matures into the late endosome and finally into the lysosome. Taken from Van Meel and Klumperman [48].*

In recent work with the vesicular stomatitis virus (VSV) and anthrax toxin, MVBs were shown to undergo back-fusion with the limiting membrane of endosomes [54]. This is required for the release of viral nucleocapsids and toxins respectively into the cytoplasm [54]. In addition, MVBs can also undergo fusion with the plasma membrane [54]. This was observed for the major histocompatibility complex (MHC) class II molecules which are stored in MVBs [54]. In dendritic cells, MVBs act as storage compartments for MHC class II molecules [55]. Antigens taken up by the dendritic cell bind to the MHC complex, and are presented on the cell surface via the

fusion of MVBs to the plasma membrane [55]. Similarly, MVBs can follow the same process releasing internal vesicles into the extracellular space [50]. These vesicles are known as exosomes and are observed in a variety of cells including dendritic cells, platelets, neurons and tumour cells [55]. Exosomes are defined as 30-100 nm vesicles originating from MVBs, and are released by fusion of the limiting membrane of MVBs to the plasma membrane [50]. In summary, the three recognized routes for MVBs so far are fusion with the lysosome, limiting membrane of late endosomes or the plasma membrane – **Figure 9** [56].

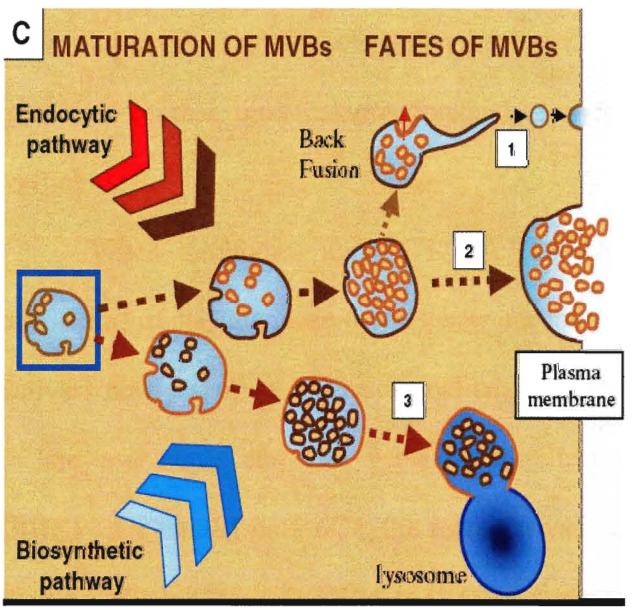

***Figure 9**: Fates of MVBs. MVBs can either fuse to the limiting membrane of endosomes where molecules are sequestered to the limiting membrane or cytosol (1). Fusion of MVBs to the plasma membrane results in the release of exosomes (2). Finally, fusion of MVBs to the lysosome results in degradation (3) Taken from Van Niel et al. [56].*

1.7 The Role of LBPA in the Endocytic Pathway

Lipid and protein composition, morphology, and function have been found to differ in endosomes along the endocytic pathway [57]. The early endosomes have a high amount of phosphatidylinositol-3-phosphate (PI(3)P), whereas the late endosomes have a significantly lower amount of this lipid. The reverse is true for LBPA, which is found predominantly in late but not early endosomes [58-59]. It has

been shown that MVBs targeted to different destinations have different lipid compositions in their membranes [59]. ILVs that develop into MVBs containing PI(3)P and ubiquitylated proteins are seen targeted to the lysosome as opposed to those enriched with LBPA [49]. White *et al.* demonstrated that MVBs containing the epidermal growth factor receptor (EGFR) are distinct from LBPA-enriched MVBs [60]. EGFR is known to associate with PI(3)P and both are required for MVB biogenesis. However, inhibition of PI-3-kinase activity did not prevent accumulation of LBPA-containing vesicles within the late endosome [60]. In addition, exosomes that are believed to be derived from MVBs show low LBPA content [61]. Instead, latest studies on exosomes reveal that these vesicles are rich in ceramides [62]. Hence it is evident that lipid composition and remodelling plays a role in intracellular trafficking.

When antibodies against LBPA (known as 6C4) were used, the proper trafficking of the mannose-6-phosphate receptor (MPR) was disrupted [63]. MPR delivers newly synthesized lysosomal enzymes from the trans-Golgi network (TGN) to late endosomes and vice versa for reutilization [63]. In baby hamster kidney (BHK) cells treated with 6C4, the receptor was found mainly in the late endosomes, where it colocalized with LBPA [63]. Under normal conditions, the receptor was seen primarily in the TGN and did not show any significant colocalization with LBPA [63]. In another investigation, accumulation of cholesterol in late endosomes was observed when anti-LBPA was present [64]. Furthermore, again using antibodies against LBPA, it was demonstrated that the release of nucleocapsids into the cytosol by VSV was inhibited [54]. A similar result was seen with studies involving the anthrax toxin [54]. VSV and anthrax are known to infect cells through the endocytic pathway [54]. Both models reveal that entry into the cytoplasm requires the fusion of

internal vesicles to the limiting membrane of late endosomes known as back-fusion [54]. The resistance of LBPA to lipase and phospholipase activity could possibly explain its resistance to degradation in lysosomes [53]. This may account for the lack of its presence in ILVs targeted to lysosomes [53]. Also, it may provide an explanation for the evolution of viruses to take advantage of these vesicles to avoid the lysosomal pathway allowing it to infect its host [54].

The evidence clearly implies that LBPA plays a role in intracellular trafficking. Although MVBs are responsible for targeting to different destinations, it is plausible that LBPA-containing vesicles may be mainly involved in trafficking molecules targeted to the cytoplasm via the back-fusion mechanism. Since LBPA is capable of generating the formation of multivesicular structures in liposomes without the presence of proteins, this suggests that cellular trafficking within late endosomes can also be lipid-driven [45].

1.8 LBPA and Membrane Curvature

The question on how LBPA is specifically involved in intracellular trafficking still remains to be answered. Biological membranes, which were once thought to mainly function as a barrier, are now proving to play more than one role. From the previous section, it is evident that membrane remodelling plays a role in intracellular trafficking. During membrane remodelling, budding and fusion of the membrane lipid bilayer are usually involved [65]. Budding and fusion of the membrane involves changes to the membrane curvature [65], hence there is interdependence between lipid domain formation and membrane curvature. This has been observed in both cell and model membranes [66]. So far five different mechanisms have been recognized that bring about membrane curvature: changes in lipid composition, influence of integral membrane proteins, cytoskeletal proteins and microtubule motor activity, scaffolding

by peripheral membrane proteins and active helix insertion into membranes [65]. Although specific proteins play an important role in the formation of membrane curvature, it is also highly dependent on the lipid composition [67]. Various parts of the bilayer structure and lipid physical properties are believed to contribute to the fusion/budding process [67]. These include imperfect lipid packing, and changes of elastic free energy and membrane fluidity [67]. The focus here will be on membrane curvature brought about by changes in lipid composition.

Membrane curvature can be positive, negative or zero. Positive curvature refers to the outer leaflet of a lipid bilayer that curves toward the aqueous phase due to the larger head-groups [65]. On the contrary negative curvature describes the outer leaflet curving away from the aqueous phase due to the smaller head-groups [65, 68-69]. Zero curvature is used to describe the lipid bilayer when it approximates a straight line i.e. lamellar shape [65]. Membrane curvature is largely determined by the packing characteristics of lipids present within the membrane [68]. For example, phosphatidylcholine (PC) is a cylindrical shaped lipid where the cross-sectional area of the head-groups is identical to that of the fatty acyl chains [68]. Therefore a bilayer consisting solely of PCs will produce a flat shape (zero curvature) – **Figure 10A** [68]. In contrast, phosphatidylethanolamine (PE) is a cone-shaped lipid [68]. As a result, this cone-shaped lipid exerts a negative curvature (**Figure 10B**) on the membrane due to the tighter packing of the smaller head-groups compared to the tail end [68]. On the contrary, an inverted cone-shaped lipid such as lysophosphatidic acid (LPA) will generate a positive curvature (**Figure 10C**) [68].

In support of the role of lipid composition in membrane fusion and fission, it has been observed that some lipids are required for certain fusion/fission reactions [70]. For example, PE appears to be required for the fusion of Golgi membranes,

while sphingolipid and cholesterol are necessary for the fusion mediated by Semliki Forest virus [70]. In the case of LBPA, we have seen from the work of Matsuo *et al.* that this lipid promotes multivesicular morphology [45]. In addition, the fusion of intraluminal vesicles to late endosomes to release viral nucleocapsids during VSV infection is also dependent on the presence of LBPA [71]. It is noteworthy to mention here that although recent literature suggests that LBPA is a cone-shaped lipid by citing remarks made by Matsuo *et al.*, there is no concrete evidence proving this. In fact, in Matsuo's 2004 paper, he only suggested that the 2, 2′-LBPA may be cone-shaped. Even though the effect of LBPA on phospholipid bilayer polymorphism has not been fully established, it is clear that this lipid is able to regulate membrane curvature in the above-mentioned fusion processes.

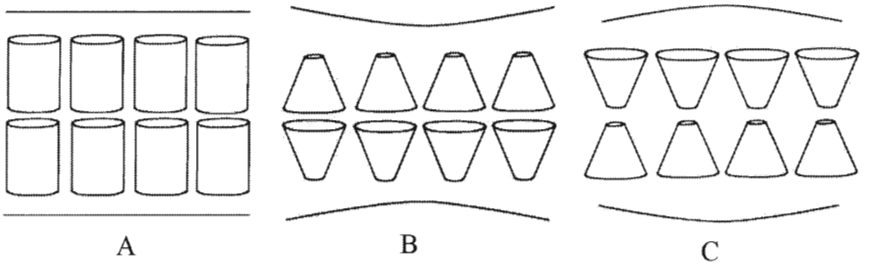

***Figure 10**: A schematic diagram describing membrane curvature. A flat bilayer produced by PC (A); negative curvature due to cone-shaped lipids such as PE (B); positive curvature due to inverted cone-shaped lipids such as LPA (C). Taken from Atkinson et al. [15].*

The idea of membrane curvature being used as a means of recruiting proteins to membranes is one that cannot be dismissed. One protein that has been identified as associating with membranes in a curvature-dependent manner at the Golgi complex is the ArfGAP1 protein (ADP-ribosylation factor GTPase activating protein 1) [69]. ArfGAP1 is responsible for the dynamics of the COP1 (coat protein complex 1) coat

at the Golgi complex [72]. Current investigations suggest that binding of Arf-GAP1 is based on the shape of the lipid molecule and membrane curvature [72]. ArfGAP1 activity showed an increase when conical shaped lipids was introduced at a constant liposome radius. On the other hand, when the lipid composition was kept constant, ArfGAP1 activity increased with membrane curvature [72]. Another example is the phosphoinositide 3-kinase (PI 3-kinase), which phosphorylates phosphatidylinositol (PI) [73]. When PI was presented in a convex (positive curvature) surface as opposed to a flat bilayer, the activity of PI-3 kinase showed an increase [73]. In addition, PI-3 kinase activity was also increased when vesicles with an average diameter of 50 nm were used as compared to vesicles with an average diameter greater than 300 nm [73].

1.9 Characterization of Protein-Lipid Interactions

Understanding macromolecular interactions is vital in elucidating many biological processes in living organisms. Here, the focus is to study protein-lipid or protein-membrane interactions. Surface plasmon resonance (SPR) is an established method for measuring such interactions [74]. It involves the immobilization of one reactant (the ligand) onto a biosensor chip surface and its interaction with a second component (the analyte) is monitored in solution [74]. The sensor chip in SPR is a glass slide coated with a thin layer of gold [75]. Polarized light is directed to the sensor chip and the change in refractive index caused by the binding of the analyte to the ligand is measured [74-75]. In protein-lipid interaction assays, the lipid is normally immobilized on the sensor chip followed by the injection of the protein across the chip [75]. The increase in protein mass due to lipid binding on the chip surface then causes an increase in the response [75]. SPR allows real time measurements without the need of protein and lipid labelling, requires small quantities

of samples (nearly nM concentrations of proteins) and also provides a rapid and direct mean of measuring the association and dissociation of binding processes [74-75].

Another technique that uses a similar approach is dual polarization interferometry (DPI). DPI is an optical sensing technique that involves two polarized light paths, hence the term 'dual polarization'. A sensor chip is also required, which consists of two optical waveguides stacked on top of each other, made of silicon dioxide doped with silicon nitride [76]. The top waveguide acts as a sensing waveguide, while the bottom is termed the reference waveguide. On the surface of the sensing waveguide are two etched sample wells, which allow the analyte to bind [77].

The theory behind DPI can be explained as follows. Polarized light is fed into the short end of the sensor chip [77]. When the polarized light enters the top and bottom waveguide, they are in phase. After passing through the sensor, the two beams from the two waveguides are allowed to diverge and form an interference pattern that is detected in the far-field [77]. The precise position of these bands is dependent upon the phase relationship of the light as it emerges from the two waveguides. **Figure 11** illustrates the physical setup of the sensor chips and light paths used in DPI.

Exposing the sensor chip to a sample changes the refractive index at the waveguide surface. This in turn alters the speed of light travelling through the sensing guide, whereas the speed of light passing through the reference guide remains the same since it has no contact with the analyte – **Figure 12** [77]. The light travelling at constant velocity acts as an optical reference. The light emitted from both waveguides is now no longer in phase. Hence this results in a change in the interference pattern. This change in phase can be converted to refractive index and

thickness values using Fourier transformation [77]. The use of two components of the polarized light – transverse electric (TE) and transverse magnetic (TM) – allows measurements to be taken at right angles of each other [78]. Both components will respond differently, providing independent measurements. Since the refractive index value obtained is proportional to density, the layer density and mass of layer can therefore be calculated [78].

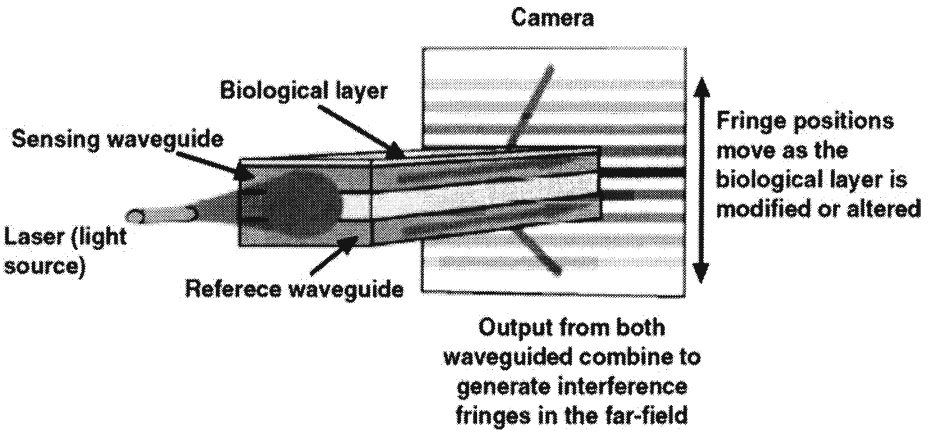

***Figure 11**: A schematic representation of the setup of DPI. Light waves from a laser source pass through the sensor chip and produce an interference pattern in the far-field. Taken from Terry et al. [79].*

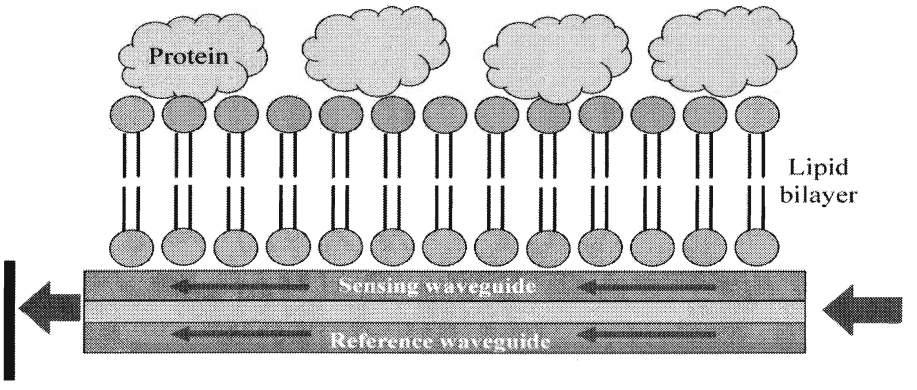

***Figure 12**: Illustration of the adsorbed analyte (lipid bilayer for example) on the chip surface. Upon binding of a second component (protein), the light path through the sensing waveguide is altered which results in a changed interference pattern.*

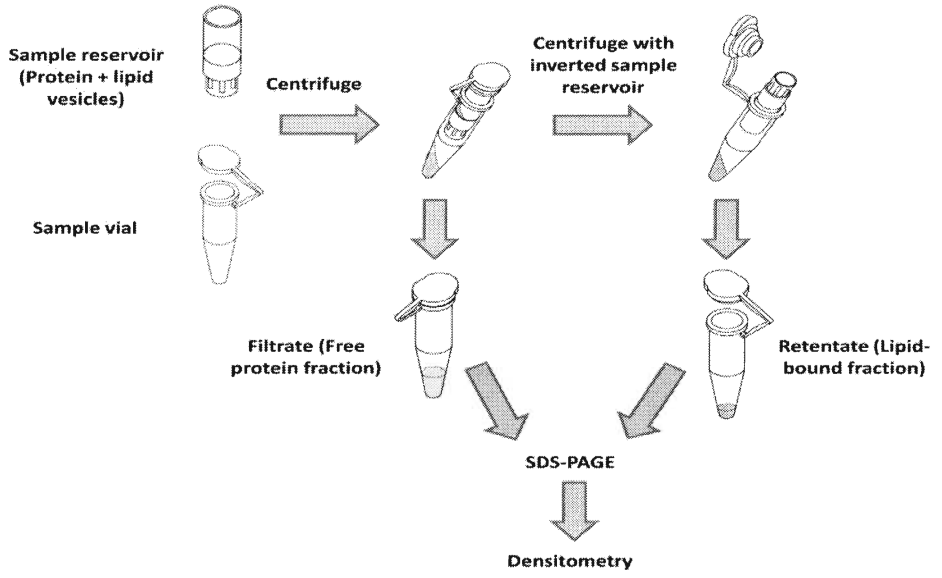

***Figure 13**: Summary of the vesicle binding assay. The protein and lipid vesicles held within the sample reservoir are centrifuged to first produce the free protein fraction (filtrate). A further centrifugation step with the sample reservoir inverted yields the lipid-bound fraction (retentate). The individual fractions are analysed by SDS-PAGE followed by densitometry.*

DPI only allows protein interactions with planar lipid bilayers to be determined; hence another method is required to study protein-lipid interactions that allow the comparison of lipid vesicles of different sizes. One such method is the vesicle binding assay (**Figure 13**). In addition to evaluating the role of lipid vesicle size, protein binding to the vesicles can also be assessed based on lipid composition, similarly to DPI. The vesicle binding assay involves the incubation of the protein of interest at a fixed concentration with varying amounts of the lipid. The sample mixture is then passed through a centrifugal filtration device with a molecular weight cut-off of 100 kDa to retain the lipid-bound proteins [37, 80]. This yields a filtrate containing the free protein fraction and a retentate holding the lipid-bound fraction. These fractions can then be further analysed with SDS-PAGE (Sodium Dodecyl

Sulphate Polyacrylamide Gel Electrophoresis) and densitometry to determine the protein binding affinity [79-80].

1.10 Project Outline

Current studies reveal that α-TTP associates with late endosomes and possibly transfers α-tocopherol from here to the plasma membrane to be packaged into VLDLs [40]. However the detailed mechanism is not fully established. The late endosomes have been shown to be enriched with the lipid LBPA [44]. Moreover, LBPA appears to promote multivesicular formation as seen in late endosomes [45]. An initial study employing DPI analysis has demonstrated that α-TTP binding to artificial endosomal membranes containing LBPA shows some differences when compared to endosomal membranes without LBPA [81]. Using fluorescence resonance energy transfer (FRET) to study the transfer rate of the α-tocopherol ligand by α-TTP, it has been shown that small unilamellar vesicles (SUVs) containing only PC have higher transfer rates than LUVs [38].

Taking all these observations into account, it is plausible that LBPA may play a crucial role in the binding of α-TTP to late endosomes. Therefore, the aim of this project is to investigate the effect of LBPA on α-TTP binding to membranes – specifically to determine whether α-TTP binds to membranes due to the presence of LBPA itself or due to the curvature effect generated by LBPA. To answer these questions, DPI will be used to determine the binding affinity of α-TTP to flat lipid bilayers in the presence and absence of LBPA. Since low pH (pH 5.5) is important for LBPA to generate multivesicular structures [44-45], the binding affinity of α-TTP to LBPA-containing membranes will also be explored with DPI at this pH range in addition to physiological pH.

Since DPI only allows flat lipid bilayers to be investigated, it does not provide a proper means to study the curvature effect. Although one should be aware that the presence of LBPA in a flat membrane may cause its shape to be irregular due to curvature stress if LBPA truly regulates membrane curvature. This is based on the following assumption. A membrane bilayer that is naturally flat in structure will undergo curvature stress when it is forced to adopt a positive or negative curvature [82]. Similarly, a positive or negative curvature membrane will be stressed when it is forced to adopt a flat structure [82]. If LBPA truly produces curvature in membranes, its presence will cause curvature stress in the flat bilayer on the sensor chip. However, the DPI method does not differentiate between the two effects that is the presence of LBPA itself and membrane curvature caused by LBPA.

To further investigate the curvature effect on α-TTP binding to LBPA-containing membranes, a vesicle binding assay will be employed. In the previous section, it is mentioned that the vesicle binding assay can be used to examine protein-lipid interactions based on lipid composition and vesicle size. Here, both SUVs and large unilamellar vesicles (LUVs) will be used with and without LBPA present. In addition, the vesicle binding assays will also be compared at both physiological and low pH ranges as for the DPI experiments. Therefore, this method will allow us to determine whether α-TTP binding to membranes is dependent solely on the presence of LBPA or due to the curvature effect generated by LBPA.

Finally, also using the vesicle binding assay, both forms of LBPA will be studied, that is the 3, 1′-LBPA and 2, 2′-LBPA form. The 3, 1′-LBPA is used instead of the 3, 3′-LBPA mainly because it is the only commercially available form of LBPA closest to the 3, 3′ form. All studies will be conducted with the 3, 1′-LBPA except where indicated since 2, 2′-LBPA is a costly lipid. The purpose of the final

investigation is to explore the effect of the two LBPA forms on α-TTP binding to LBPA-containing membranes. This is important since the 2, 2′-LBPA form has shown to possess a higher activity in multivesicular formation at pH 5.5 [45]. Therefore it is crucial to also investigate whether α-TTP binding changes when 2, 2′-LBPA is present in vesicles as opposed to the 3, 3 ′-LBPA form.

Examining the effects of LBPA on α-TTP binding to membranes will provide further insight into the mechanism of α-TTP- mediated transfer of α-tocopherol. This is important since α-TTP is responsible for the plasma levels of vitamin E in the body. Consequently this work will provide further understanding of vitamin E nutrition in health and disease.

2. MATERIALS AND METHODS

2.1 Chemicals and Stock Solutions

Sodium Chloride (NaCl) (Bioshop, Burlington, ON, Canada)

Yeast extract (Bioshop, Burlington, ON, Canada)

Tryptone (Bioshop, Burlington, ON, Canada)

Ampicillin (Bioshop, Burlington, ON, Canada): 100 mg/mL in milliQ water, stored at -20°C

Isopropyl-D-thiogalactoside (IPTG) (Bioshop, Burlington, ON, Canada): 1 M in milliQ water, stored at -20°C

Tris(hydroxymethyl)aminomethane (Tris) (Bioshop, Burlington, ON, Canada)

Ethylenediaminetetraacetic acid (EDTA) (Bioshop, Burlington, ON, Canada)

Dithiothreitol (DTT) (Sigma-Aldrich, St. Louis, MO, USA)

Phenylmethanesulphonylfluoride (PMSF) (Sigma-Aldrich, St. Louis, MO, USA)

Glycerol (Caledon Laboratory Chemicals, Georgetown, ON, Canada)

Triton X-100 (Sigma, St Louis, MO, USA)

Magnesium Chloride ($MgCl_2$) (Bioshop, Burlington, ON, Canada)

Lysozyme (Bioshop, Bioshop, Burlington, ON, Canada)

Deoxyribonuclease I (Invitrogen, Carlsbad, CA, USA)

RNase A, Pancreatic (Bioshop, Burlington, ON, Canada)

Glutathione-Sepharose Beads (Sigma, St Louis, MO, USA)

Thrombin protease (Amersham Biosciences now part of GE Healthcare, Piscataway, NJ, USA)

Glutathione (Bioshop, Burlington, ON, Canada)

Precision Plus Unstained Protein Marker (Biorad, Hercules, CA, USA)

Potassium Phosphate Dibasic (Bioshop, Burlington, ON, Canada)

Bradford Reagent (Sigma-Aldrich, St Louis, MO, USA)

Glycine (Sigma, St Louis, MO, USA)

Acetic Acid (Caledon Laboratory Chemicals, Georgetown, ON, Canada)

Sodium Dodecyl Sulfate (SDS) (Sigma, St Louis, MO, USA)

Anhydrous Ethyl Alcohol (Commercials Alcohols Inc., Brampton, ON, Canada)

Methanol (Fisher Scientific, Fair Lawn, NJ, USA)

Isopropanol (IPA) (Caledon Laboratory Chemicals, Georgetown, ON, Canada)

Sucrose (Bioshop, Burlington, ON, Canada)

Potassium Chloride (KCl) (Bioshop, Burlington, ON, Canada)

ProtoBlue Safe (Colloidal Coomasie Stain) (National Diagnostics, Atlanta, GA, USA)

2-(N-Morpholino)ethanesulphonic acid (MES) (Bioshop, Burlington, ON, Canada)

S, S Bisoleoyl-LBPA (Echelon Biosciences, Salt Lake City, UT, USA)

1, 2-dioleoyl-sn-glycero-3-phosphocholine (DOPC) (Avanti Polar Lipids Inc., Alabaster, AL, USA)

1, 2-dioleoyl-sn-glycero-3-phospho-L-serine (DOPS) (Avanti Polar Lipids Inc., Alabaster, AL, USA)

1, 2-dioleoyl-sn-glycero-3-phosphoethanolamine (DOPE) (Avanti Polar Lipids Inc., Alabaster, AL, USA)

Sphingomyelin (Brain, Porcine) (Avanti Polar Lipids Inc., Alabaster, AL, USA)

L-α-phosphatidylinositol (Liver, Bovine) (Avanti Polar Lipids Inc., Alabaster, AL, USA)

Bis(monooleoylglycero)phosphate (S, R) (Avanti Polar Lipids Inc., Alabaster, AL, USA)

2.2 Buffers and Solutions

2.2.1 Bacterial cell culture and protein expression

Luria Bertani (LB) Broth: 5 g/L NaCl, 5 g/L yeast extract, 10 g/L tryptone

LB-Amp medium: LB medium supplemented with 50 µg/mL ampicillin

2.2.2 Protein purification

Buffer A: 150 mM Tris pH 8, 150 mM NaCl, 1 mM EDTA pH 7.5, 10 % glycerol, 0.1 mM DTT, 0.1 mM PMSF

Buffer B: Buffer A supplemented with 0.5 % Triton X-100 & 10 mM $MgCl_2$

Buffer C: 50 mM Tris pH 8, 150 mM NaCl, 10 mM $MgCl_2$, 0.1 mM DTT

Phosphate Buffered Saline (PBS): 25 mM potassium phosphate dibasic, 137 mM NaCl pH 8

Glutathione Elution Buffer: 1X PBS supplemented with 4 mg/mL glutathione

Cleansing Buffer 1: 0.1 M borate buffer (boric acid), 0.5 M NaCl pH 8.5

Cleansing Buffer 2: 0.1 M acetate buffer (sodium acetate), 0.5 M NaCl pH 4.5

Storage Buffer: 2 M NaCl

2.2.3 SDS-PAGE electrophoresis

SDS-PAGE Stacking Buffer: 0.5 M Tris pH 6.8

SDS-PAGE Separating Buffer: 1.5 M Tris pH 8.8

SDS-PAGE Running Buffer: 125 mM Tris, 960 mM glycine, 0.5 % SDS pH 8.3

SDS-PAGE Loading Dye: 50 mM Tris, 16 % glycerol, 16 % SDS (10 %), 0.02 % DTT, 0.08 % bromophenol blue (1 %)

Fixing Solution: 50 % methanol, 10 % acetic acid

Gel Drying Solution 1: 40 % methanol, 10 % glycerol, 7.5 % acetic acid

2.2.4 Dual polarization interferometry

DPI Running Buffer: 10 mM potassium phosphate dibasic, 137 mM NaCl pH 7.4

Calibration Solutions: 80 % ethanol, milliQ water

Wash Solutions: 2 % SDS, 50 % isopropanol (IPA)

2.2.5 Vesicle binding assay

SET Buffer: 250 mM Sucrose, 1 mM EDTA, 50 mM Tris, 100 mM KCl pH 7.5

SET Buffer + Triton X-100: SET buffer supplemented with 100 μM TritonX-100

MES Buffer: 250 mM Sucrose, 1 mM EDTA, 50 mM MES, 100 mM KCl pH 5.5

MES Buffer + Triton X-100: MES buffer supplemented with 100 μM Triton X-100

2.3 Equipment

Spectronic® Genesys™ 2 spectrophotometer (Spectronic Instruments, Leeds, UK)

Sorvall® MC 12 microcentrifuge (Mandel Scientific Co. Ltd., Guelph, Ontario)

Sorvall® RC 5C Plus with SLA-3000 and SS-34 rotors (Mandel Scientific Co. Ltd., Guelph, Ontario)

Sorvall® RMC14 (Mandel Scientific Co. Ltd., Guelph, Ontario)

Corning pH meter 445 (Corning, Lowell, Massachusetts)

TC-7 test tube roller (New Brunswick Scientific Co. Inc., Edison, New Jersey)

Shaker Incubator (Gallenkamp, Loughborough, UK)

Mini-PROTEAN III Cell (Bio-Rad Laboratories, Mississauga, ON, Canada)

101U Peristaltic Pump (Watson Marlow, Concord, ON, Canada)

Farfield Analight® Bio200 (Farfield Scientific Ltd., Crewe, UK)

Microcon (Millipore Corporation, Bedford, MA, USA)

Mini-Extruder (Avanti Polar Lipids Inc., Alabaster, AL, USA)

Liposofast-Basic (Avestin, Ottawa, ON, Canada)

Polycarbonate filters – 100, 200 and 400 nm (Avestin, Ottawa, ON, Canada)

W-375 Sonicator cell disruptor (Misonix, Inc., Farmindale, NY, USA formerly known as Heat Systems-Ultrasonics, Inc.)

Cellulose Dialysis Tubing (Fisherbrand, Nepean, ON, Canada)

Unmodified sensor chip – FB85 (Farfield Scientific Ltd., Crewe, UK)

Ready gels – 15 % Tris-HCl (Biorad, Hercules, CA, USA)

Optima XL-100K Ultracentrifuge (Beckman Coulter, Missisauga, ON, Canada)

Gel Drying Film (Promega Corporation, Madison, WI, USA)

2.4 Software

Scion Image for Windows (Scion Corporation, Frederick, MD, USA)

GraphPad Prism for Windows, Version 5.0 (GraphPad Software Inc., La Jolla, CA, USA)

Farfield Analight® Bio200, Version 2.1.21 (Farfield Scientific Ltd., Crewe, UK)

2.5 Bacterial Strain

BL21(DE3) *Escherichia coli* (*E. coli*) was used for protein expression (Stratagene, La Jolla, CA, USA)

2.6 Plasmid

pGEX 4T-3 (GE Healthcare) was used for the expression of wild-type α-TTP. The α-TTP gene was previously cloned into the pGEX 4T-3 vector at the SalI and NotI sites [83].

2.7 Methods

2.7.1 Protein expression of wild-type α-TTP

Four test tubes containing 10 mL each of autoclaved LB Broth were supplemented with 100 μg/mL ampicillin. Each test tube was inoculated from a frozen culture of BL21(DE3) *E. coli* cells containing pGEX 4T-3/ α-TTP construct. The cultures were then grown overnight at 37°C in a test tube roller. On the next day, six 1 L baffled flasks containing 500 mL of autoclaved LB broth were inoculated with 5 mL of the overnight culture to produce a 1:100 dilution factor. The cultures were allowed to grow at 37°C on a shaker at 180 rpm until an OD_{600} of 0.4 – 0.6 was achieved. The flasks were then left to cool at room temperature. Following that, TTP expression was induced by the addition of 200 μL of 1 M IPTG (final concentration of 0.4 mM). The flasks were left overnight at room temperature on a shaker. The cells were harvested by centrifugation at 9000 rpm for 10 minutes. The supernatant were decanted and the remaining cell pellets were stored at -80°C.

2.7.2 Purification of GST-Fusion α-TTP

A frozen cell pellet was thawed and frozen at -80°C three times for cell lysis purposes. Then the cells were suspended in 10 mL of Buffer A with 400 μL of 100 mg/mL lysozyme to yield a final concentration of 4 mg/mL. The solution was left to incubate for 30 minutes on ice. Following that the solution was treated with the following: 20 μL of 5 M $MgCl_2$ (final concentration of 10 mM), 10 μL 100 % Triton X-100 (final concentration 0.1 %), 1000 units DNAse, 50 μL of 10 mg/mL RNAse (final concentration of 50 μg/mL) and left to incubate for a further 30 minutes on ice. Then, the lysate was passed through an 18G1 ½ needle attached to a 10 ml syringe for 5 to 6 times followed by sonication three times for 30 seconds at approximately 10 –

15 watts. The cell debris was removed by centrifugation at 17500 rpm for 25 minutes at 4°C.

A column containing 1 mL of glutathione-sepharose beads was prepared and washed with 10 mL of 1X PBS followed by 10 mL of Buffer B. All solutions were passed through the column by means of a peristaltic pump with a flow rate of 25 rpm. Then the supernatant was added to the pre-washed column. Subsequently the column was washed first with a 10 mL of Buffer B and secondly Buffer C. 50 µL (50 units) of thrombin were diluted in 950 µL of 1X PBS and added to the column and allowed to incubate for 2 hours at room temperature on a bench top roller. The protein was eluted from the column with 5 mL Buffer C giving a total of 5 1 mL fractions. Next, the column was washed with a further 10 mL of Buffer C. The GST tags were then eluted from the column with 4 mL of Glutathione Elution Buffer. The column was regenerated with Cleansing Buffer 1 and milliQ water followed by Cleansing Buffer 2 and milliQ water. Finally the column was stored in 2 mL of 2 M NaCl at 4°C.

2.7.3 Protein quantitation: Bradford assay

The protein concentration from a given purification was quantified using the Bradford assay. A standard curve of absorbance measured at 595 nm versus the concentration of bovine serum albumin (BSA) ranging between 0 – 1 mg/mL was prepared. Each standard was prepared by adding 50 µL of BSA solution to 1 mL of Bradford reagent. After incubation for 5 minutes at room temperature, the absorbance was measured. The concentration of unknown protein samples were then determined from the standard curve and the conditions used were similar to those applied to the BSA samples. Protein samples exceeding 1 mg/mL were diluted with PBS buffer and the final concentration was corrected for the dilution factor used.

2.7.4 Protein characterization: SDS-PAGE analysis

SDS-PAGE analysis was used to determine the purity of the purified protein. SDS-PAGE loading buffer was added to each sample to yield a final amount of 5 μg of protein. A 15 % acrylamide separating gel with a 5.5 % stacking gel was prepared in a Mini-Protean 3 casting system according to manual specifications. The protein samples were treated by heating at 95°C for 10 minutes to fully denature the proteins. Samples were then loaded onto the gel along with a protein molecular weight marker and ran for two hours at 100 – 110 V. After that the gel was soaked in fixing solution for an hour with gentle rocking. Then the gel was washed with distilled water followed by overnight staining in Coomasie Brilliant Blue staining solution again with gentle rocking. Next, the gel was soaked in destaining solution to remove background dye. Finally, the gel was soaked in gel preserving solution for 30 minutes and clamped between two acetate sheets and allowed to dry to create a permanent record.

2.7.5 Protein dialysis

All protein samples that were run on the Analight Bio200 were dialysed with DPI running buffer to avoid bulk phase changes. Approximately 1 mL of protein sample was loaded into a regenerated cellulose dialysis tube with a molecular weight cut-off of 3.5 kDa. The dialysis tubing was regenerated in milliQ water for 20 minutes followed by DPI running buffer for a further 20 minutes. Protein samples were dialyzed for approximately one hour in DPI running buffer at 4°C to minimize protein loss.

2.7.6 Large unilamellar vesicle (LUV) preparation for DPI

LUVs were prepared with a final concentration of 2.54 mM. When mixed lipid composition was used, the preparation was based on mole fractions of the final

concentration. **Table 1** summarizes the lipid composition and concentration of the three lipid membrane system investigated in this project.

Lipid stocks were purchased dissolved in chloroform. The desired volumes of lipids were transferred to an 8 mL glass vial and dried under nitrogen gas to remove the solvent. The glass vials were then transferred to a high vacuum apparatus for an hour to completely remove residual chloroform. The remaining lipid stocks were stored in 8 mL glass vials at -20°C flushed with nitrogen gas. The dried lipids were rehydrated with DPI running buffer for one hour at room temperature. After hydration, the lipids were extruded using the Mini-Extruder or Liposofast-Basic through a 100 nm polycarbonate filter for fifteen times to produce 100 nm LUVs. Rehydrated LUVs were stored at 4°C until further use. LUVs stored at 4°C were used for up to three to five days.

Membrane System	**Lipid**	**% Composition**	**Concentration (mM)**
90:10 DOPC:DOPS	DOPC	90	2.28
	DOPS	10	0.25
Endosomal lipids without LBPA	DOPC	65	1.65
	DOPS	5	0.13
	DOPE	20	0.51
	SM	5	0.13
	PI	5	0.13
Endosomal lipids with LBPA	DOPC	50	1.27
	DOPS	5	0.13
	DOPE	20	0.51
	SM	5	0.13
	PI	5	0.13
	LBPA	15	0.38

***Table 1**: Summary of lipid composition and concentration of 90:10 DOPC: DOPS, endosomal lipids with and without LBPA for DPI.*

2.7.7 LUV preparation for vesicle binding assay

For the vesicle binding assay, LUVs were prepared as in Section 2.7.6 with a final concentration of 2 mM. The lipid composition and concentration used here are shown in **Table 2**. In this case, the dried lipids were rehydrated with the buffers used in the vesicle binding assay – SET and MES buffer respectively. In addition, 200 nm and 400 nm polycarbonate filters were used to prepare 200 and 400 nm LUVs respectively.

Membrane System	Lipid	% Composition	Concentration (mM)
90:10 DOPC:DOPS	DOPC	90	1.80
	DOPS	10	0.20
Endosomal lipids without LBPA	DOPC	65	1.30
	DOPS	5	0.10
	DOPE	20	0.40
	SM	5	0.10
	PI	5	0.10
Endosomal lipids with LBPA	DOPC	50	1.00
	DOPS	5	0.10
	DOPE	20	0.40
	SM	5	0.10
	PI	5	0.10
	LBPA	15	0.30

***Table 2**: Summary of lipid composition and concentration of 90:10 DOPC: DOPS, endosomal lipids with and without LBPA for vesicle binding assay.*

2.7.8 Small unilamellar vesicle (SUV) preparation for vesicle binding assay

The initial steps in SUV preparation for vesicle binding assay purposes were similar to LUV preparation with a final concentration of 2 mM. The lipid composition and concentration used are similar to those in **Table 2**. SUVs were

prepared by rehydrating the dried lipids in SET or MES buffer for one hour at room temperature. The rehydrated lipids were then sonicated with a probe sonicator for 45 minutes. Titanium particles from the probe sonicator were removed by ultra-centrifugation at 30 000 rpm (100 000 g) for one hour and 30 minutes. The SUVs were similarly stored at 4°C until further use. The shelf-life for SUVs stored at 4°C was typically up to 3 – 4 days.

2.7.9 Dual polarization interferometry

The Analight Bio200 was set up by allowing DPI running buffer to pump through for an hour prior to running an experiment. Following that an unmodified sensor chip was cleaned with isopropanol and loaded into the machine according to the manufacturer's protocol. The sensor chip was then calibrated with 80 % ethanol and milliQ water. Once calibration was completed, a 400 µL sample containing the desired 100 nm LUVs was injected onto the sensor chip at a flow rate of 25 µl/min for 8 minutes. The phospholipid layer was allowed to adsorb unto the chip until a stable layer was formed. Then a 400 µL sample of α-TTP solution of the desired concentration was injected with similar conditions as the phospholipid layer. The volume for both protein and lipid samples are as recommended by the manufacturer and are sufficient to produce a signal at a flow rate of 25 µl/min. The protein layer was monitored for a further 10 minutes after the 8 minute injection to ensure sufficient data collection. The sensor chip was then regenerated with 2 % SDS solution followed by 50 % IPA solution. Upon regeneration, subsequent lipid and protein injections were performed. Generally, to determine the binding affinity of TTP to an adsorbed phospholipid layer, an increasing amount of α-TTP concentration was used, typically between 62.5 – 2000 nM. In the case of measuring the thickness

of a phospholipid layer, only the phospholipid solution was injected unto the chip. The lifetime of a single sensor chip is averagely between 50 – 70 sample injections.

2.7.10 DPI data analysis

The signal elicited by the association of α-TTP to lipid membranes on the Analight Bio200 is determined by the maximum mass of α-TTP deposited on to the lipid layer. To obtain a K_d value, data were collected for a series of injections at eight different concentration of protein. All protein and lipid samples are injected twice. However, due to the two-channel geometry of the sensor chip in the DPI instrument, two measurements are obtained for a single injection. Since two injections were performed for each protein concentration, the four resulting measurements were used for data analysis. All graphs were plotted using GraphPad Prism. The mass data over a 480 s time frame for each α-TTP concentration were fit to a one phase exponential association model. The equation is as follows:

$$Y = Y_{max} (1 - e^{-kt}) \qquad (1)$$

With reference to (1), Y = mass of α-TTP bound, Y_{max} = maximum mass of α-TTP bound, t = time, k = rate constant. The maximum mass of α-TTP bound to the lipid bilayer for each α-TTP concentration was then used to plot a saturation binding curve with the following equation to obtain the K_d value:

$$Y = B_{max} * X / (K_d + X) \qquad (2)$$

With reference to (2), Y = maximum mass of protein deposited at a given concentration, B_{max} = maximum number of binding sites, X = α-TTP concentration and K_d = dissociation constant. The binding curves were treated with relative weighting. According to Prism, relative weighting is used when the average distance of the data points from the curve increases as Y increases.

2.7.11 Vesicle binding assay

YM-100 microcons were pre-wet with 100 μL SET or MES buffer and spun at 7500 rpm for 30 minutes in a microcentrifuge. At the same time, 31.5 μg of TTP was incubated with 0 – 1.5 mM vesicles (SUVs or LUVs) in a total volume of 200 μL for 30 minutes at room temperature with constant and gentle mixing. The TTP-vesicle complex was then added to the hydrated microcons and spun for 20 minutes at 9500 rpm. After that, an additional 100 μL of SET or MES buffer was added unto the microcon and the centrifugation was repeated. The resultant flow-through from the two spins is known as the filtrate or free protein fraction. The microcon was then inverted and transferred to a new collection tube. 100 μL of SET or MES buffer supplemented with 150 μM Triton X-100 was added unto the microcon and spun at 3500 rpm for 3 minutes. This process was repeated an additional two times. The flow-through from the three spins represents the retentate or membrane-bound fraction. The fractions were then characterized by SDS-PAGE followed by densitometry.

2.7.11 SDS-PAGE analysis of vesicle binding assay fractions

The procedure used here are similar to those described in Section 2.7.4 but in this case commercial ready-made gels were used. Also, instead of staining the gels with Coomasie Brilliant Blue solution, Colloidal Coomassie stain was used. The gels were then destained with distilled water.

2.7.12 Densitometry analysis

The gels containing the vesicle binding assay fractions were scanned and saved as a TIFF (Tagged Image File Format) file. Using the software Scion Image for Windows, band intensities were obtained. The band intensities were then used to plot a binding affinity curve – see Results & Discussion for further details. All band intensities were treated by removal of the background gel intensity.

2.7.13 Investigation of α-TTP stability at low pH conditions

315 μg of α-TTP was mixed in 2 mL of MES buffer of pH values of 6.5, 6.0 and 5.5. The mixture was mixed thoroughly and centrifuged for 5 minutes at 12000 rpm. A 50 μL sample was removed to test for protein concentration using the Bradford assay. The original mixture was resuspended and left to stand at room temperature. Protein concentration measurements were taken at one hour intervals starting from time = 0 hour over a three hour period.

3. RESULTS AND DISCUSSION

3.1 Characterization of TTP by SDS-PAGE

The purification of α-TTP was carried out by means of affinity chromatography using agarose beads containing immobilized glutathione. The glutathione-agarose beads bind GST-TTP and the GST-tag is then removed by cleavage using thrombin, a serine protease. **Figure 14** shows a typical SDS-PAGE gel demonstrating the purification procedure.

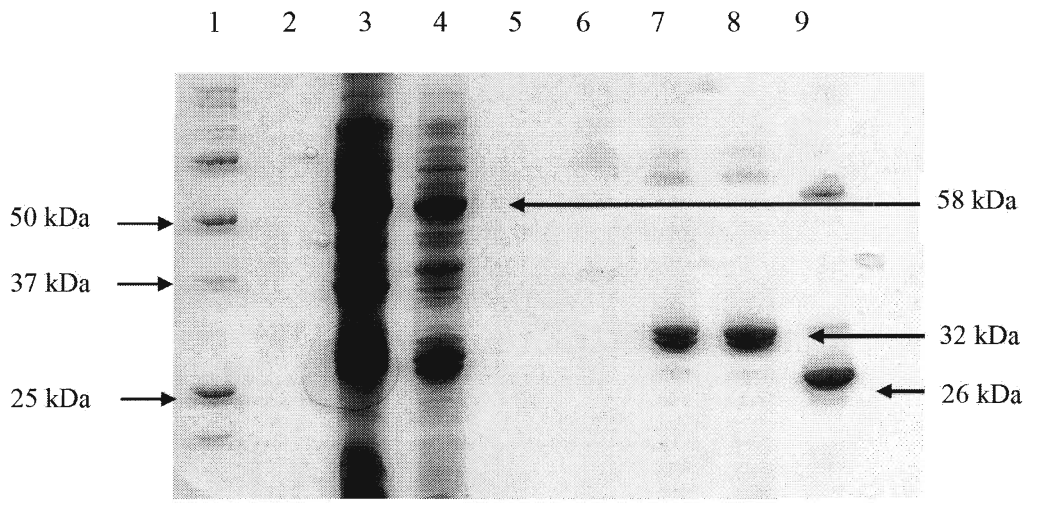

***Figure 14**: SDS-PAGE gel of α-TTP purification. Molecular weight marker (1), empty (2, 5 & 10), cell lysate (3), supernatant (4), flow through (6), pure α-TTP from fraction one (7), pure α-TTP from fraction two & GST tag (9).*

Lane one contains the molecular weight marker. Lanes three and four were loaded with bacterial cell lysate and supernatant respectively. The band at 58 kDa corresponds to GST-TTP while the band at 32 kDa represents α-TTP. Lane six holds the flow-through. No visible band observed here indicates the binding of GST-TTP to the agarose beads. The 32 kDa band in lanes seven and eight corresponds to pure α-TTP after treatment with thrombin. However, it should be noted that there are some traces of impurities in lanes seven and eight but they do not correspond to GST-TTP,

since these impurities are of higher molecular weight. Finally the band at 26 kDa in lane nine represents the GST-tag after elution with glutathione. A typical yield can vary between 3 to 5 mg/mL of pure α-TTP from 3 g of wet cell pellet.

3.2 Investigation of α-TTP-Lipid Membrane Interactions Using DPI at Physiological pH Conditions

3.2.1 Deposition of phospholipid vesicles on to silicon oxynitride sensor chips

In order to investigate the interactions of α-TTP with lipid membranes on the Analight Bio200, LUVs were first deposited on to the surface of unmodified silicon oxynitride sensor chips. A convenient method for creating supported lipid bilayers (SLBs) is through vesicle fusion, a method developed by McConnell and co-workers as cited by Schonherr *et al.* [84]. The solution containing the LUVs of interest is injected into the Analight Bio200 and when the vesicles come into contact with the silicon sensor chip, they undergo vesicle rupture and adsorption to the surface. Much investigation has been conducted to understand the detailed mechanism of vesicle adsorption on solid supports [84]. The current model for the formation of SLBs can be described as follows and will serve as a general model for the deposition of LUVs unto the sensor chip in the Analight Bio200. Firstly, the vesicle approaches and adsorbs unto the solid support – **Figure 15 (1)**. The adsorbed vesicle then deforms or flattens. Next, vesicle fusion may occur to form larger vesicles – **Figure 15 (2)** – followed by vesicle rupture to form SLBs – **Figure 15 (3).** Finally, merging occurs to form a continuous bilayer over the solid support – **Figure 15 (4)** [84].

An important prerequisite in examining protein-lipid interactions in the Analight Bio200 is the formation of a stable phospholipid bilayer. This stability is characterized by the thickness of the flat phospholipid layer formed and that it remains constant throughout the entire period of protein deposition. A stable bilayer

is considered to have been produced when a measurement of bilayer thickness has reached a constant value. Therefore, before the binding of α-TTP to lipid membranes was assessed, the deposition of phospholipid vesicles onto sensor chips was first examined by means of bilayer thickness measurements. In this project, three different lipid mixtures were used in the investigation of α-TTP binding to lipid membranes, including 90:10 DOPC:DOPS, endosomal lipids with and without LBPA. The bilayer thickness measurements obtained for these lipid systems are shown in **Table 3**. The measured thickness of a 90:10 DOPC:DOPS (which from here onwards will be referred to as just DOPC:DOPS) lipid bilayer ranged between 4 to 4.5 nm. These values are an indication that the DOPC:DOPS vesicles form a single planar bilayer, since the thickness of a single planar bilayer has been found to be approximately 5 nm [85].

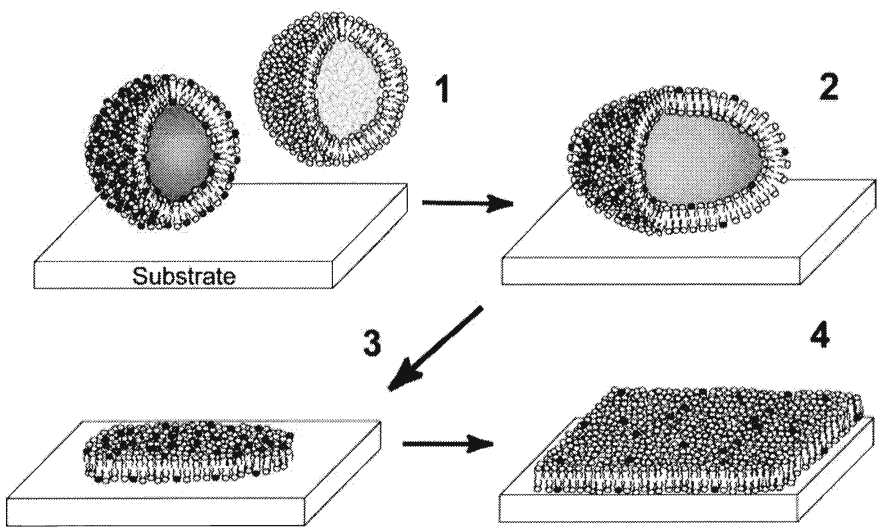

Figure 15: *Formation of supported lipid bilayers (SLBs). Lipid vesicle adsorbs and flattens on the solid support (1). Vesicle fusion may occur to form larger vesicles (2). Vesicle rupture then takes place to form the SLB (3) and finally a continuous bilayer is produced through merging (4). Taken from Schonherr et al. [84].*

LUV Composition	Bilayer Thickness Measurements (nm)
90 % DOPC:10 % DOPS	**4 – 4.5**
Endosomal lipids without LBPA	**≈ 5.5**
Endosomal lipids with LBPA	**≈ 6.5**

***Table 3**: Lipid bilayer thickness measurements from DPI analysis.*

The ability of a lipid vesicle to adsorb to a surface and transform into a planar bilayer can be influenced by many factors [84], including the presence of curvature-forming lipids or non-bilayer lipids [86]. Hamai and co-workers demonstrates this point clearly. Using fluorescence microscopy, the effect of average phospholipid curvature on SLB formation by vesicle fusion was investigated [86]. The investigation showed that the ability of vesicles to rupture and form SLBs is affected by the geometry of the lipids present within the vesicle. As the proportion of curvature-forming lipids such as PE increases within the vesicle, the ability to form planar bilayers diminishes [86]. When the proportion of non-bilayer lipids is sufficiently high, vesicles will rather remain intact than form a planar bilayer. On the other hand, when non-bilayer lipids are present at low quantities or not at all, the vesicles are more easily deformed and can rupture to form an adsorbed single bilayer.

The inclusion of non-bilayer lipids into a monolayer will result in the monolayer adopting a certain curvature. The consequence of forcing two monolayers of the same curvature into a flat bilayer leads to a build up of curvature stress (or elastic stress), since the monolayers' natural tendency is to curve rather than remain flat [87-88]. As a result of this curvature stress, the bilayer can undergo physical changes such as an increase in the overall bilayer thickness [88-89]. The

aforementioned description may then account for the increased lipid bilayer thickness observed for both the endosomal lipids with and without LBPA present when compared to DOPC:DOPS lipids. This is because endosomal lipids without LBPA contain DOPE which induces negative curvature. On the other hand, endosomal lipids with LBPA present contain PE and LBPA, which both are non-bilayer lipids. In addition, a recent study showed that LBPA-containing vesicles spontaneously form highly curved vesicles [90]. Therefore, the increase in the proportion of non-bilayer lipids within the LBPA-containing lipids can rationalize the further increase in thickness layer as seen in **Table 3**.

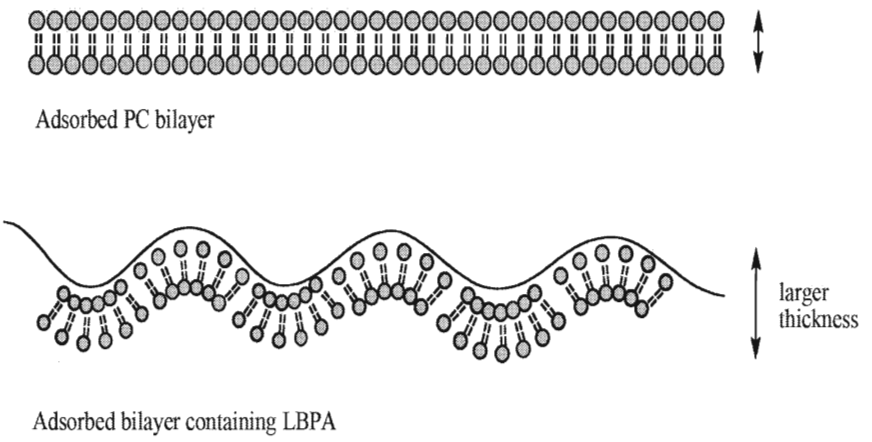

***Figure 16**: An illustration of how non-bilayer lipids may affect the SLB thickness. The presence of curvature-inducing lipids such as LBPA causes the planar lipid bilayer to be stressed. The stressed bilayer is represented as an irregular surface (but may not necessarily depict the true condition) which results in an increased bilayer thickness on average. Partially uncollapsed vesicles on the sensor chip surface may also contribute to an increased bilayer thickness.*

Also, partially uncollapsed vesicles on the sensor chip surface may explain the increased bilayer thickness. These partially uncollapsed vesicles possess a greater layer thickness and therefore contribute to the overall increased bilayer thickness,

since DPI measures the average thickness of the bilayer on the sensor chip. An illustration of this rationalization is provided in **Figure 16.**

3.2.2 Interaction of α-TTP with 90:10 DOPC:DOPS lipid layer

In order to show that α-TTP binds to lipid membranes, it was first necessary to investigate α-TTP's interaction with a simple lipid system. The DOPC:DOPS lipid system was chosen due to its ability to form a stable bilayer on the DPI rapidly and reproducibly. **Figure 17** shows the saturation binding curve of α-TTP with DOPC:DOPS with a K_d value of 877 ± 102 nm (B_{max} = 1.98 ± 0.134 ng/mm^2). This result indicates that α-TTP possesses the ability to bind to lipid membranes.

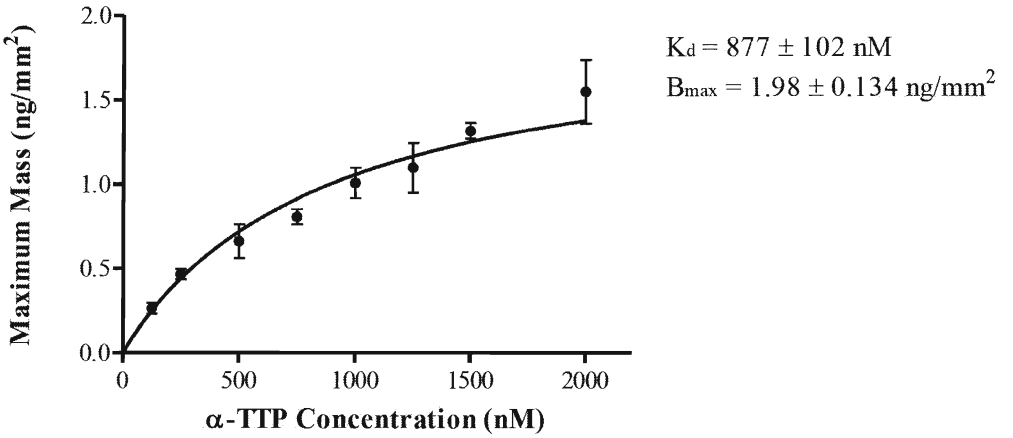

***Figure 17**: Plot of maximum specific mass of α-TTP bound to DOPC:DOPS lipid layer. DOPC:DOPS lipid is made up of 90 mol% DOPC and 10 mol% DOPS with a final lipid concentration of 2.54 mM. Data are representative of four measurements from two independent sample injections.*

3.2.3 Interaction of α-TTP with endosomal lipids with and without LBPA

Since the objective of this project is to investigate the effect of LBPA on α-TTP binding to lipid membranes, it was necessary to investigate α-TTP binding to lipid membranes without the presence of LBPA as a comparison. Here the lipid

membrane composition of interest is the endosomal lipid mixture as described by Kobayashi *et al.* [44]. The affinity of α-TTP for endosomal lipids without LBPA present were close to that of the DOPC:DOPS lipids with a K_d value of 902 ± 191 nM (B_{max} = 1.42 ± 0.176 ng/mm^2). **Figure 18** shows the binding affinity curve for α-TTP to endosomal lipids without LBPA.

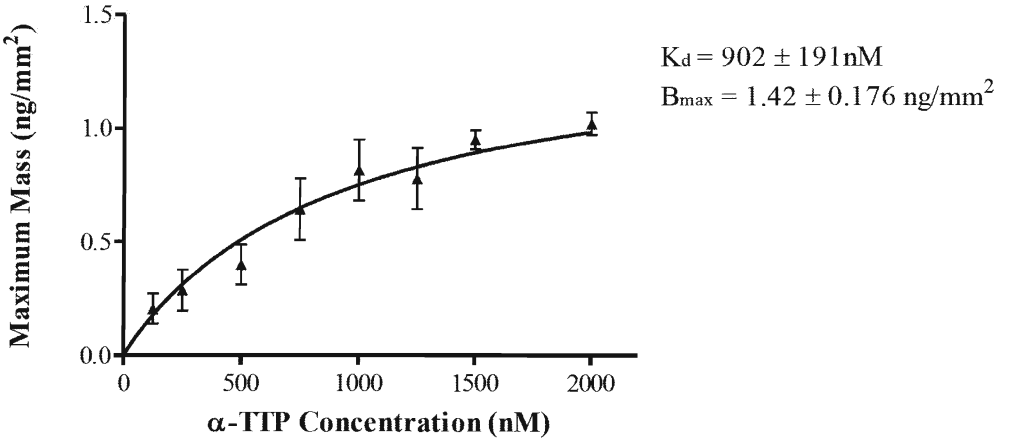

***Figure 18**: Plot of maximum specific mass of α-TTP bound to an artificial endosomal lipid mixture without LBPA. Endosomal lipids without LBPA are made up of 65 mol% DOPC, 20 mol% DOPE and 5 mol% DOPS, SM and PI with a final lipid concentration of 2.54 mM. Data are representative of four measurements from two independent sample injections.*

However, when LBPA was present, the affinity of α-TTP for lipid membranes increased by two-fold as reflected by the lower K_d value of 328 ± 64.6 nM (Bmax = 1.24 ± 0.096 ng/mm^2). **Figure 19** illustrates the binding affinity curve for α-TTP to endosomal lipids with LBPA.

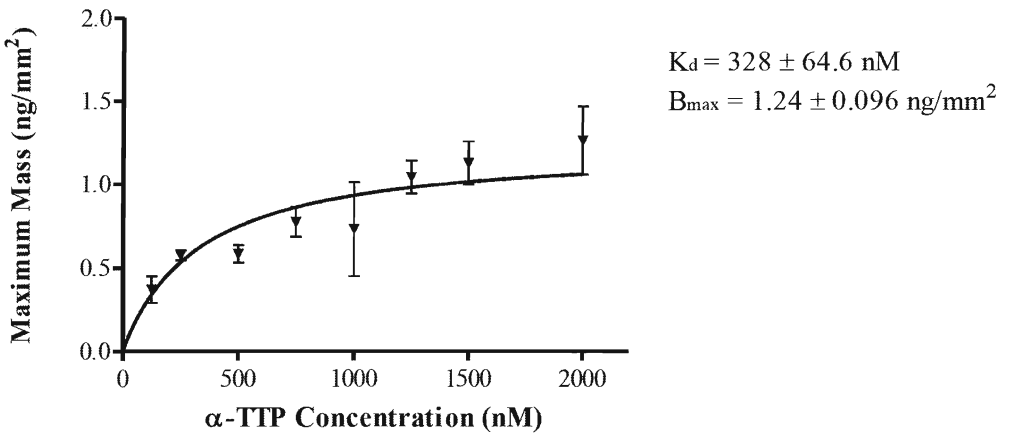

***Figure 19**: Plot of maximum specific mass of α-TTP bound to an artificial endosomal lipid mixture with LBPA. Endosomal lipids with LBPA is made up of 50 mol% DOPC, 20 mol% DOPE, 5 mol% DOPS, SM and PI and 15 mol% LBPA with a final lipid concentration of 2.54 mM. Data are representative of four measurements from two independent sample injections.*

In protein-ligand interactions, the K_d corresponds to the concentration when half of the protein concentration is ligand-bound. Therefore a lower K_d value signifies a stronger binding affinity between the protein and ligand. However, in this case, the lipid membrane is not the ligand for α-TTP rather it is the location for α-TTP to release or retrieve its ligand. Therefore the K_d does not signify half of the concentration of α-TTP being occupied, instead, the K_d represents the half the maximum possible association of α-TTP to the membrane. In DPI analysis, the amount of lipid present is fixed on the sensor chip. However, the amount of protein introduced on to the chip is varied. The general trend observed for α-TTP is that as protein concentration increases, more protein was bound regardless of lipid composition. In Section 1.3, earlier studies proposed that α-TTP associates to membranes via its lid helix (α-10) [35]. Since there are no specific sites on the membrane that favour α-TTP's binding to it, when α-TTP is introduced on to the

sensor chip, the way it recognizes and binds to the membrane surface is similar regardless of where it lands on a homogeneous sample of adsorbed vesicles. However, the lower K_d value seen with the LBPA-containing lipids is an indication of a stronger binding affinity between α-TTP and LBPA-containing lipids. This means that in comparison with the other lipid mixtures, a lesser amount of protein was required to saturate the lipid surface on the sensor chip, given that the lipid surface area available to the protein is limited on a sensor chip.

The B_{max} value represents the maximum specific mass of protein bound to the sensor chip. For the DOPC:DOPS lipid mixture, the B_{max} obtained from the DPI measurement was 1.98 ± 0.143 ng/mm^2. This means that approximately 1.98 ng of α-TTP are bound to one mm^2 area of the sensor chip. It appears that the B_{max} value decreases slightly with the endosomal lipids without LBPA and with LBPA, 1.42 ± 0.176 ng/mm^2 and 1.24 ± 0.096 ng/mm^2 respectively, when compared to the DOPC:DOPS lipid mixture. This means that the amount of bound protein decreased with the inclusion of endosomal lipids. The reduced amount of protein bound to the sensor chip might be explained with reference to the increased average thickness bilayer as seen in **Table 3**. It was described in Section 3.2.1 that the endosomal lipids seem to possess a thicker bilayer. This increased bilayer thickness was rationalize by the presence of non-bilayer lipids and the presence of partially uncollapsed vesicles. Consequently, this implies that the surface of the lipid bilayer is no longer homogenous. As a result, there are fewer binding sites available for α-TTP to bind to. The maximum specific mass of α-TTP did not vary significantly between endosomal lipids without LBPA (1.42 ± 0.176 ng/mm^2) and endosomal lipids with LBPA (1.24 ± 0.096 ng/mm^2). However the decrease in K_d for endosomal lipids with LBPA

indicates a stronger affinity of the protein to the lipid mixture, suggesting a possible role of LBPA in α-TTP binding to lipid membranes.

3.3 Investigation of α-TTP-Lipid Membrane Interactions Using Vesicle Binding Assay at Physiological pH Conditions

The examination of α-TTP interactions with lipid membranes using DPI suggests that LBPA increases the affinity of α-TTP binding to membranes. However, this does not discriminate whether α-TTP binding to membranes is based on its affinity for LBPA itself or the curvature effect generated by LBPA in membranes. Thus, the vesicle binding assay was employed to investigate the binding of α-TTP to lipid vesicles mimicking curved membranes. It is important to emphasize here that the vesicle binding assay utilized in this project is a semi-quantitative measure of binding affinity as compared to the DPI analysis. It is used mainly as a complementary technique to DPI to observe binding trends. This is due to the nature of the assay which caused large errors to occur especially when LUVs were employed, since the amount of protein bound to LUVs is less than to SUVs of the same lipid composition. As a result, the K_d and B_{max} values were not extracted from the binding curves except in a few instances where the errors are minimal. All binding curves were plotted using GraphPad Prism. The vesicle binding data could not be treated using data weighting methods, possibly suggesting that the assumption of 'one-site binding' is not accurate for this system.

In this assay, lipid-bound proteins were separated from free proteins using a centrifugal filter. Both lipid-bound and free protein fractions were then analyzed by SDS-PAGE. Band intensities were evaluated by densitometry and the values for lipid-bound fractions were fit to a binding saturation curve to show the binding trend. For each assay, lipid-bound fractions were normalized against the highest lipid

concentration fraction, which represents the maximum amount of bound protein in any particular instance. On the other hand, the free protein fractions can also be used to show binding trends (**Appendix I**). In this case, the curves are the mirror-images of the lipid-bound fractions and the results generally show similar binding trends. Here, the free protein fractions were normalized against the amount of protein recovered when no lipid was present, which is taken as the total amount of free protein and fitted to a one phase exponential decay curve.

It is also noteworthy that the densitometry values can be assessed by an alternative method. In this case, the lipid-bound fractions are calculated from the free protein fractions [91-92]. Based on Feng *et al.*'s work, lipid-bound fractions were determined by $(1 - P_f/P_t)$ [91]. P_f represents the free protein recovered when lipid was present, while P_t is the free protein recovered when no lipid was present. Therefore P_t represents the total amount of free protein. The lipid-bound fractions are represented as P_b/P_t where P_b is the amount of lipid-bound protein [91]. The data was fit to a one-site saturation binding curve. Again, the results obtained from this manner of data analysis are closely similar to those obtained from the previously mentioned analysis (**Appendix II**). The use of two different data analysis methods reveals that the results obtained from the vesicle binding assay are qualitatively reproducible. This means that either the free protein or the lipid-bound fractions can be used to show binding trends. However, it should be mentioned that a discrepancy was observed when low pH conditions were introduced into this assay that affected both the free and lipid-bound protein fractions. This discrepancy is due to the insolubility of the lipid and/or protein at low pH conditions rather than the assay itself and will be discussed further in Section 3.4.2. For clarification and consistency, the data analysis method that measures the lipid-bound fractions directly will be used in the following sections.

3.3.1 Effect of lipid composition on α-TTP's interaction with lipid vesicles

Prior to employing the vesicle binding assay to investigate α-TTP's binding to lipid membranes, the assay was first examined with DOPC:DOPS lipid vesicles. DOPC:DOPS vesicles (200 nm in diameter) of increasing concentration were incubated with α-TTP at a fixed concentration. The results obtained showed that α-TTP does bind to DOPC:DOPS vesicles. When DOPC:DOPS vesicles were replaced with vesicles containing endosomal lipids without LBPA, the amount of lipid-bound-α-TTP was comparable to that with DOPC:DOPS lipids. However, a further increase in the amount of lipid-bound protein was observed when LBPA was present (**Figure 20**).

The SDS-PAGE analysis of the free and bound protein fractions clearly demonstrates this distinction in the binding of α-TTP to lipid vesicles based on their composition (**Figure 20 A-C**). The trend observed here is that more protein is retained in the lipid-bound fractions as lipid concentration increases and more so when LBPA is present. When the densitometry values for lipid-bound fractions were plotted against LUV concentration, a similar trend was observed (**Figure 20 D**). Interestingly, these findings correspond to those observed in the DPI analysis, further supporting the fact that LBPA does have an effect on α-TTP's binding to membranes.

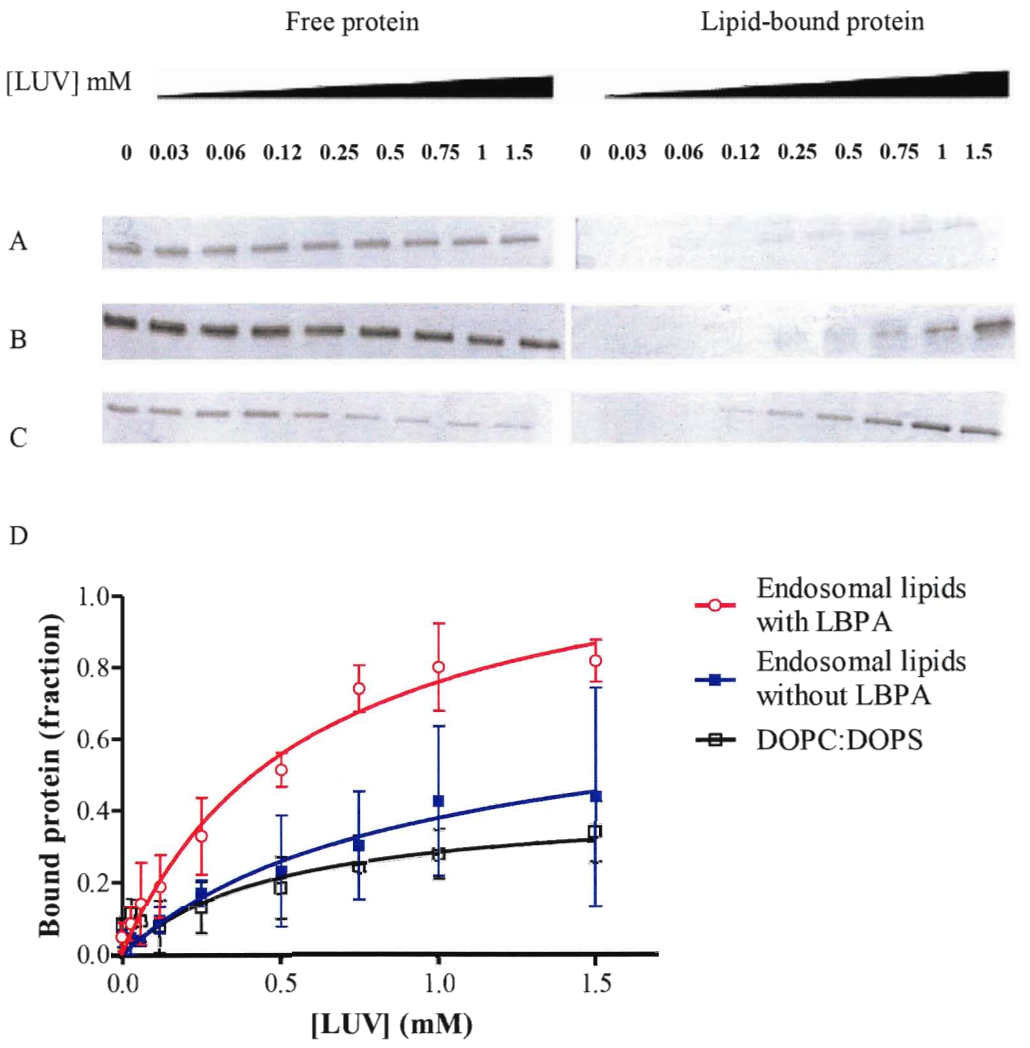

***Figure 20**: Effect of lipid composition on α-TTP binding to lipid vesicles at pH 7.5. SDS-PAGE analysis of free and bound α-TTP to 200 nm LUVs of (A) DOPC:DOPS, (B) endosomal lipids without LBPA and (C) endosomal lipids with LBPA present. Binding curves plotted from lipid-bound fractions (D). Data are taken from three separate measurements.*

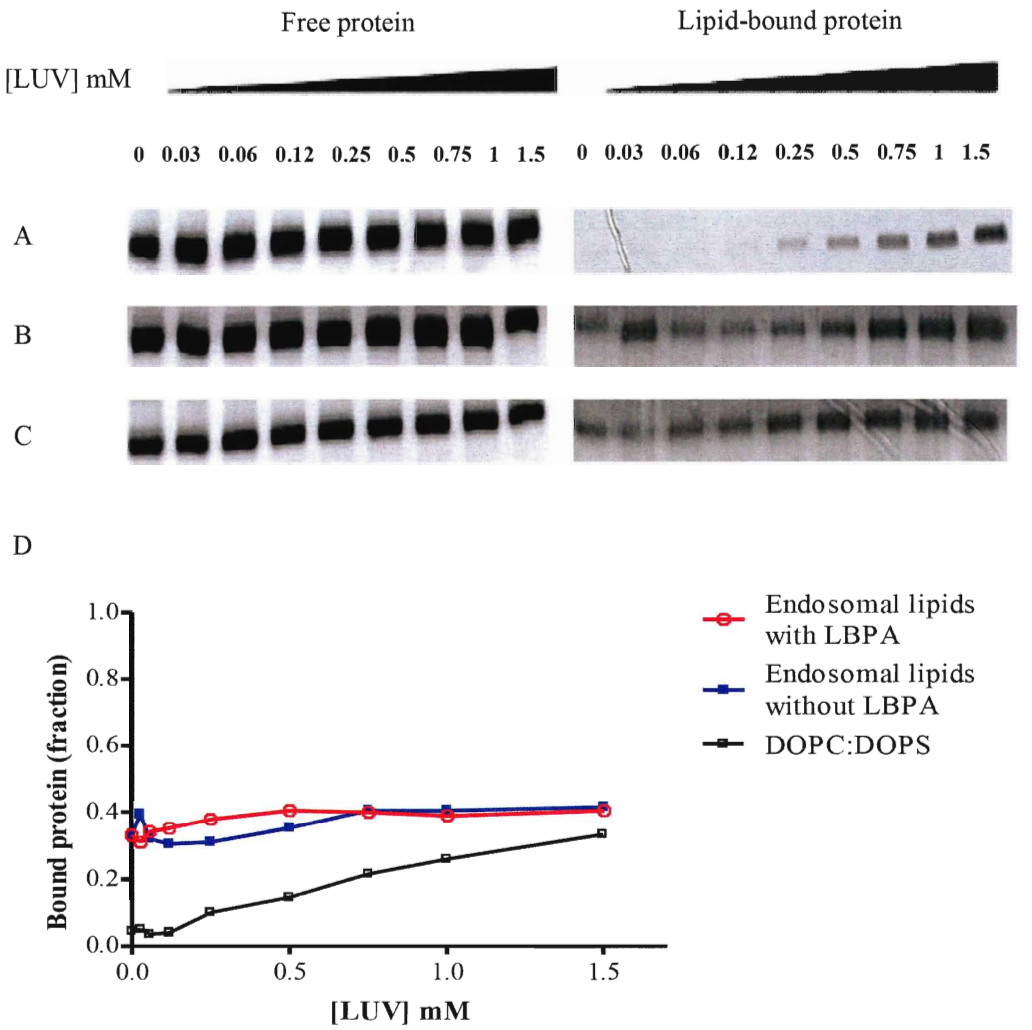

***Figure 21**: BSA binding to 200 nm LUVs at pH 7.5. SDS-PAGE analysis of free and bound BSA to 200 nm vesicles of (A) DOPC:DOPS, (B) endosomal lipids without LBPA and (C) endosomal lipids with LBPA present. Binding curves plotted from lipid-bound fractions (D). Data are from one measurement.*

As a control measure, another soluble protein, bovine serum albumin (BSA) was used in this assay under similar conditions. In general, BSA did not demonstrate any specific binding toward all three lipid systems used here (**Figure 21D**). However, it should be noted that some non-specific binding occurs between BSA and the lipid mixtures as observed in the weaker bands present in the lipid-bound fraction for all three lipid mixtures (**Figure 21 A-C**). It was also noticed that more BSA were

present in the lipid-bound fractions when endosomal lipids were used. Why this occurs remains unanswered. The main deduction from this study was to show that the association of α-TTP to membranes is not a result of non-specific binding of the protein to lipids or to the centrifugal filter. It also excludes the notion that α-TTP may be trapped by the lipid vesicles. Instead, this analysis reveals that α-TTP possesses the ability to bind to lipid membranes and this ability is specifically influenced by lipid composition.

3.3.2 Effect of membrane curvature on α-TTP binding to lipid vesicles

The next objective was to investigate the effect of bilayer curvature on α-TTP's binding to membranes. Under similar conditions, α-TTP was incubated with SUVs for all three lipid systems. SUVs produced by probe sonication generally yield vesicles about 25 – 30 nm in diameter [94].

From the results seen in **Figure 22**, it is evident that the amount of α-TTP bound to all three lipid systems is similar. This is further substantiated by the B_{max} values which represent the maximum amount of bound protein for each lipid system, as shown in **Table 4**. This implies that the amount of α-TTP bound to SUVs is the same regardless of the lipid composition of the vesicles. However the K_d values from these curves, as shown in **Table 5**, reveal that α-TTP has a higher binding affinity to endosomal lipids with LBPA. This suggests that LBPA plays a role in α-TTP binding to lipid membranes even in SUVs. However, comparing between the binding curves, the increased amount of α-TTP bound to SUVs compared to LUVs cannot be excluded here. This suggests that membrane curvature plays a significant role in α-TTP's binding to membranes. These observations are in line with recent findings that the ligand transfer rate by α-TTP is greater with SUVs containing only PC compared to LUVs [38]. Therefore, α-TTP's preference to bind to highly curved membrane

surfaces, regardless of lipid composition, as seen here is consistent with the higher ligand transfer rate seen with SUVs versus LUVs. However, it is still not possible to conclude at this point that no specific interaction exists between α-TTP and LBPA.

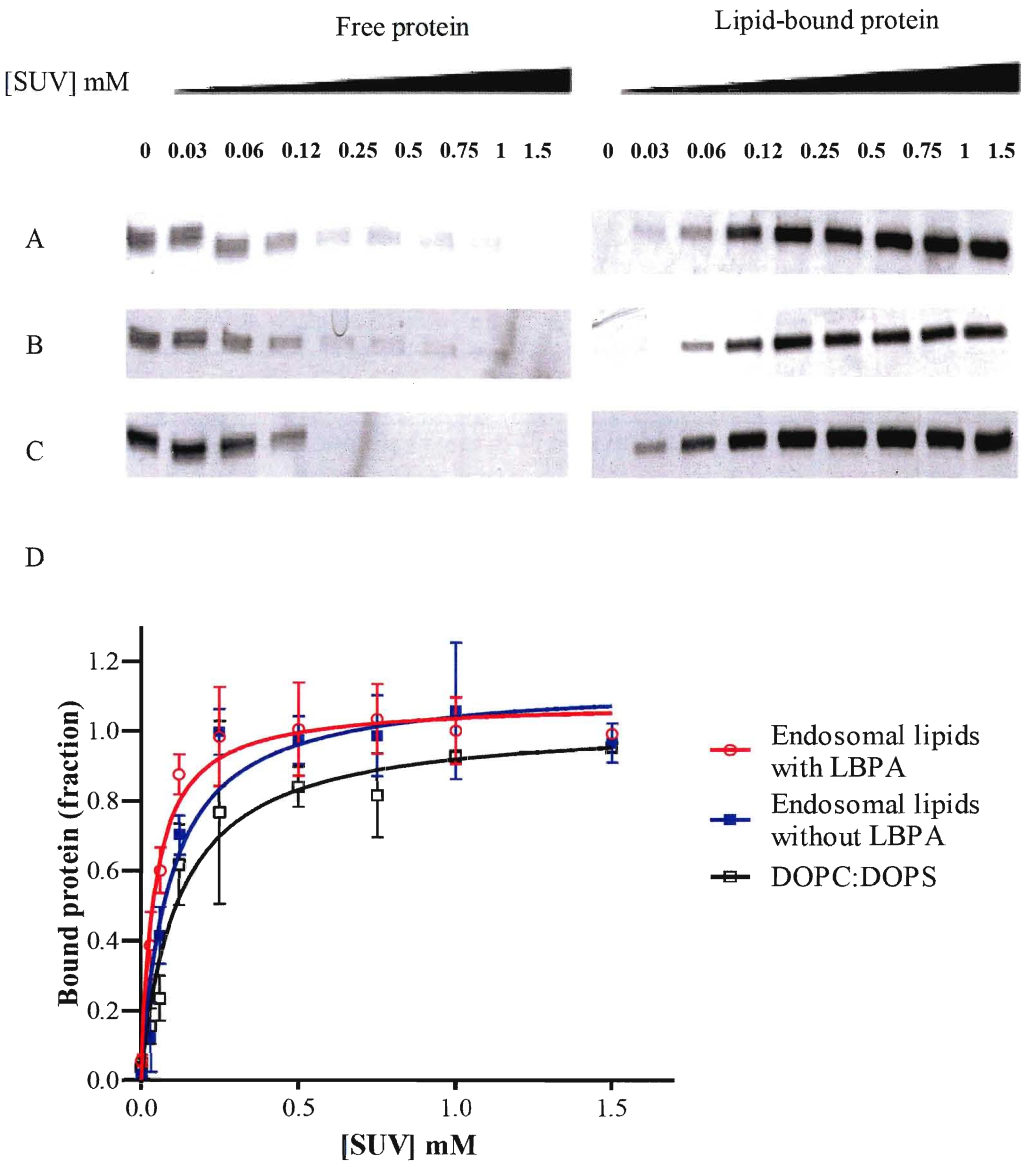

***Figure 22**: α-TTP binding to SUVs at pH 7.5. SDS-PAGE analysis of free and bound α-TTP to SUVs of (A) DOPC: DOPS, (B) endosomal lipids without LBPA and (C) endosomal lipids with LBPA. Binding curves plotted from lipid-bound fractions (D). Data are from three independent measurements.*

Lipid system	B_{max} (Bound protein fraction)
DOPC:DOPS	1.03 ± 0.053
Endosomal lipids without LBPA	1.13 ± 0.051
Endosomal lipids with LBPA	1.08 ± 0.031

***Table 4**: B_{max} values obtained from α-TTP-SUV binding curves at pH 7.5.*

Lipid system	K_d (mM)
DOPC:DOPS	0.118 ± 0.025
Endosomal lipids without LBPA	0.090 ± 0.018
Endosomal lipids with LBPA	0.043 ± 0.007

***Table 5**: K_d values obtained from α-TTP-SUV binding curves at pH 7.5.*

To show that α-TTP's binding to SUVs was not a result of non-specific binding, BSA was tested in the similar fashion. Results are shown in **Figure 23**. No specific binding was observed between BSA and the three lipid systems. However, the presence of the weaker bands in the lipid-bound fractions again indicates that non-specific binding exists to some degree to the lipids. On the whole, the use of BSA in this study further supports α-TTP's preference to bind to highly curved membrane surfaces.

The results so far reveal that more α-TTP is bound to larger vesicles when LBPA is present, but the LBPA effect is reduced or insignificant when small vesicles are used instead. The next aim was to investigate the binding of α-TTP to larger vesicles; in this case, LUVs of 400 nm in diameter were used, which are double the diameter of the 200 nm LUVs. Since DOPC:DOPS vesicles had already been used to show that α-TTP was able to bind to membranes in this assays, this lipid mixture was

not included in the following trial. Moreover, since a similar amount of α-TTP bound to endosomal lipids without LBPA compared to DOPC:DOPS vesicles, only the endosomal lipids with and without LBPA were examined for the 400 nm LUVs.

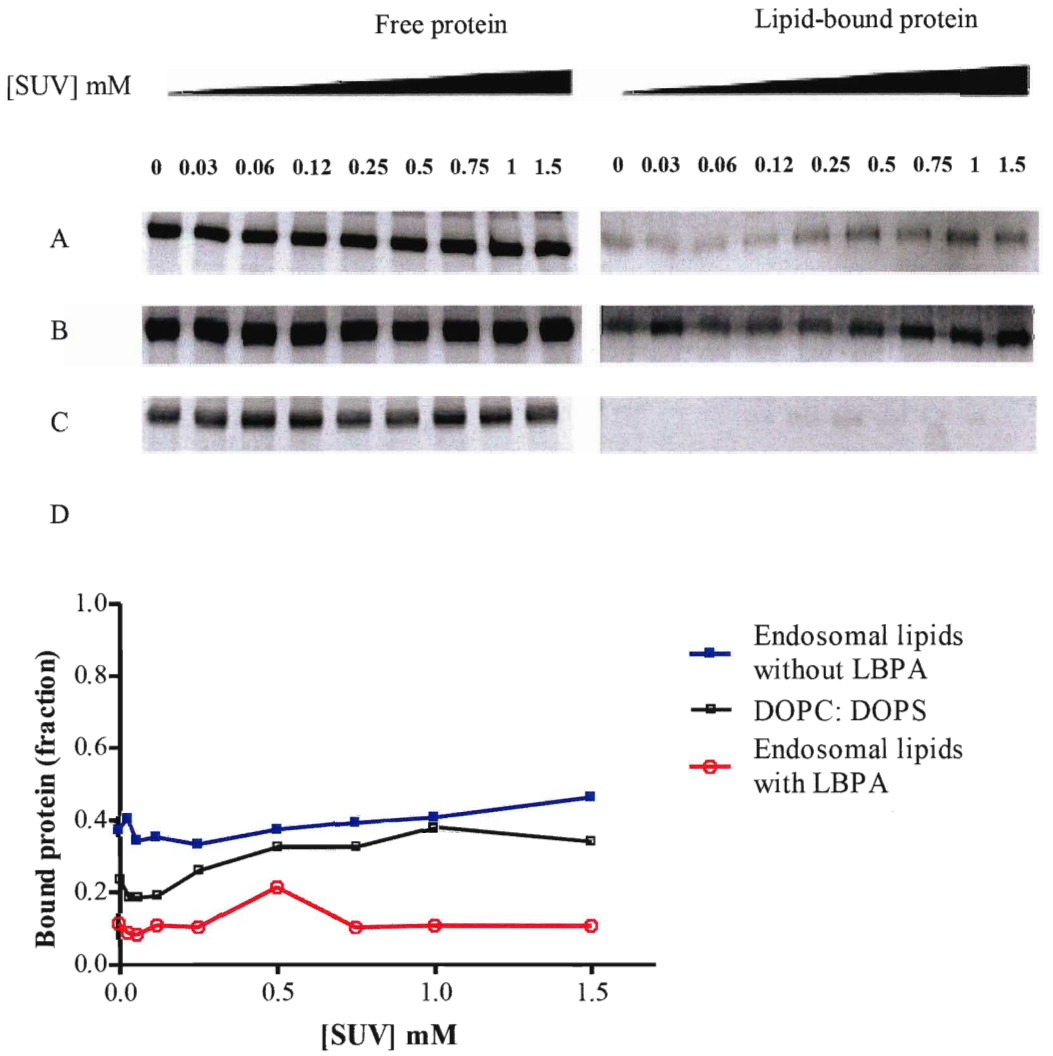

***Figure 23**: BSA binding to SUVs at pH 7.5. SDS-PAGE analysis of free and bound BSA to SUVs of (A) DOPC: DOPS, (B) endosomal lipids without LBPA and (C) endosomal lipids with LBPA present. Binding curves plotted from lipid-bound fractions (D). Data are from one measurement.*

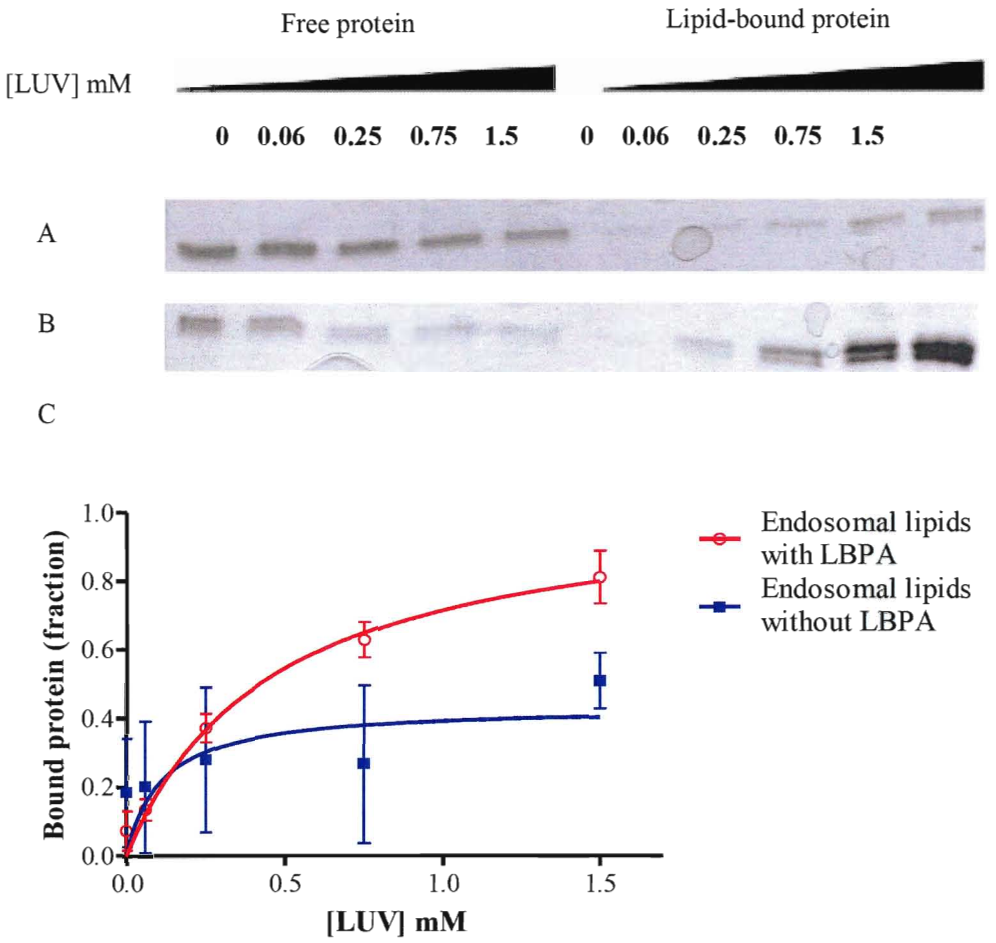

***Figure 24**: α-TTP binding to 400 nm LUVs at pH 7.5. SDS-PAGE analysis of free and bound α-TTP to LUVs of (A) endosomal lipids without LBPA and (B) endosomal lipids with LBPA. Binding curves plotted from lipid-bound fractions (C). Data are from three independent measurements.*

Results from the analysis showed a similar pattern as seen with the 200 nm LUVs – more α-TTP were bound to endosomal lipids when LBPA was present (**Figure 24**). Since the main focus is on the endosomal lipids with LBPA present, a comparison of α-TTP's binding trend to LBPA-containing vesicles based on vesicle size is shown in **Figure 25**.

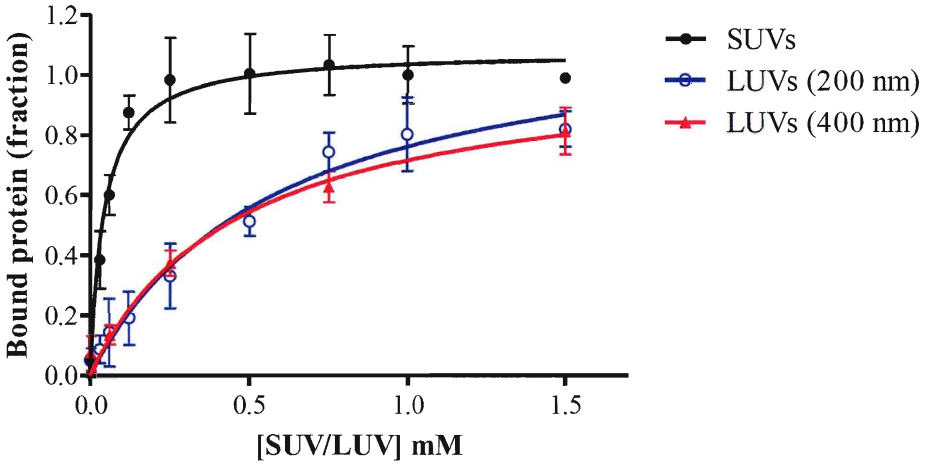

***Figure 25**: Curvature effect on α-TTP binding to membranes at pH 7.5. Shown here is a greater amount of α-TTP bound to SUVs containing endosomal lipids with LBPA compared to 200 and 400 nm LUVs of similar lipid composition. Data are from three independent measurements.*

Comparison between the K_d and B_{max} values obtained from **Figure 25** are shown in **Table 6**. The B_{max} values are similar between SUVs and LUVs implying that the maximum amount of bound protein is the same for all three types of vesicles. It should be noted that the B_{max} values are greater than one possibly due some data points that exceeds the fraction of the highest lipid concentration. The K_d values for both 200 and 400 nm LUVs are similar. However, the K_d value for SUVs is approximately ten times less than those of the LUVs, indicating a stronger affinity between α-TTP and SUVs. This evidently shows that α-TTP binding to membranes is influenced by the curvature of the membrane structure to which it binds.

Endosomal Lipids with LBPA	K_d (mM)	B_{max} (Bound protein fraction)
SUVs	0.043 ± 0.007	1.08 ± 0.031
LUVs (200 nm)	0.581 ± 0.134	1.21 ± 0.119
LUVs (400 nm)	0.463 ± 0.103	1.05 ± 0.103

***Table 6**: Comparison between K_d and B_{max} values for α-TTP bound to SUVs, LUVs of 200 nm and 400 nm diameters.*

The vesicle binding assay results obtained so far clearly shows that α-TTP prefers to bind to a highly curved membrane surface as opposed to a flatter one. The degree of curvature of a lipid vesicle is proportional to 1/R, where R is the diameter of the vesicle [95]. Therefore, the spontaneous curvature of a 25 nm SUV is greater than a 200 and 400 nm LUV by eight and sixteen times respectively. This means that when α-TTP approaches a LUV of a diameter ranging between 200 and 400 nm compared to a 25 nm SUV, the surface of the LUV would appear essentially flat rather than curved as with the SUV (**Figure 26**).

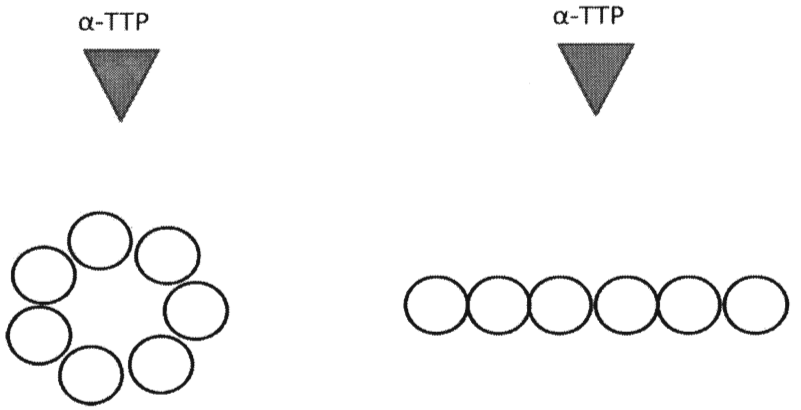

***Figure 26**: An illustration to show how α-TTP views a SUV versus a LUV or flat bilayer. α-TTP sees the SUV surface as highly curved with more free space within the lipid head-groups allowing easier access to bind. In contrast, α-TTP sees the LUV and flat bilayers as a flat surface. Shown here is just the representation of lipid head-groups of the outer monolayer to which α-TTP associates.*

In the introductory section, it was shown that LBPA plays a role in generating curvature in lipid membranes. Taking this into account and α-TTP's preference to bind to highly curved membrane surfaces indicates that α-TTP binding to LBPA-containing LUVs is a result of local curvature generated by LBPA. The ability of LBPA to form multivesicular structures, which also means generating local curvature within a liposome, is dependent upon a low pH environment [45]. However, in this case, an enhanced binding is observed despite the fact that the pH conditions were near neutral. A recent study investigating the morphology of LBPA vesicles showed that hydrated LBPA vesicles at neutral pH formed non-spherical vesicles with small budlike protrusions [90]. This may suggest that the presence of LBPA within the vesicle causes the lipid bilayer to want to bud and form multivesicular structures but is unable to do so due to the neutral pH. The uneven bilayer surface and budlike protrusions (both indicative of higher curvature membrane morphologies) of LBPA-containing LUVs at neutral pH may then explain the increased amount of α-TTP bound to these vesicles. It should be mentioned that in the same study, extruded LBPA vesicles formed well-rounded vesicles at neutral pH [90]. However it should also be noted that the methodology in LUV preparation and number of extrusion times used in this project differs from those used in Frederick *et al.*'s work. This may mean that even though extruded LBPA-containing vesicles produce well-rounded vesicles at neutral pH, the amount of time for them to remain stable in this spherical shape may vary with the previously mentioned factors. Another factor to be considered is that in Frederick *et al.*'s work, vesicles were made of 100 mol% LBPA as opposed to our vesicles which contain only 15 mol% LBPA; therefore any local curvature effect of LBPA will be reduced. In the situation where LBPA-containing lipids are forced into a flat bilayer such as during DPI analysis, it is uncertain whether

the membrane surface is irregular or whether any budlike protrusions exist. If truly budlike protrusions exist, such structures may be able to enhance the binding of α-TTP to the LBPA-containing bilayer.

An alternative rationalization to account for the increase in α-TTP binding to LBPA-containing LUVs and flat bilayers is based on curvature stress. The concept of peripheral proteins binding to lipid membranes dictated by curvature stress in the lipid bilayer is one that cannot be dismissed [88]. Two examples of proteins that are regulated this way are the CTP (cytidine triphosphate):phosphocholine cytidyltransferase (CT) and leader peptidase [96-98]. While CT catalyzes the key step in phosphatidylcholine synthesis, leader peptidase cleaves signal peptides from translocated precursor proteins. Both proteins have been shown to preferentially interact with membranes containing the non-bilayer lipid DOPE as opposed to just DOPC. In section 3.2.1 it was discussed that the presence of non-bilayer lipids such as DOPE increases curvature stress within the bilayer. In addition, the smaller head-group of DOPE results in exposed hydrophobic sites, also known as insertion sites [96-98]. It was then proposed that the presence of the insertion sites allows easier access of peripheral proteins to bind to the bilayer, especially those that bind via hydrophobic interactions. The binding of peripheral proteins to membranes aids in relieving curvature stress by allowing the lipids that are within close proximity of the protein to splay apart [96]. It should be mentioned that at present there are many terms used to describe the role of lipid regulation of protein function. The description used here is curvature stress, but a few other examples include lipid packing stress, lateral pressure profile and bilayer deformation energy [99]. At the moment, there is no agreement as to which is the correct phenomenon to be used in any description of peripheral protein binding to membranes.

Since LBPA does not normally form lamellar shaped lipid bilayers, it is not surprising that its presence will cause curvature stress within a lipid bilayer. Whether LBPA forms negative or positive curvature is yet to be determined. However there is evidence that shows LBPA is able to induce some kind of curvature as mentioned earlier, with the formation of budlike protrusions at neutral pH and the multivesicular liposomes at pH 5.5 [90, 45]. Due to the curvature forming properties by LBPA, its presence within a lipid bilayer – in this case the extruded vesicles that are well rounded without any protrusions and the flat bilayer on the sensor chip - will result in curvature stress. As there are no concrete measurements at present to state whether LBPA has a smaller or larger head-group, we cannot be certain that LBPA has the same effect as DOPE – the formation of insertion sites allowing easier access of proteins to the membrane. Whether LBPA induces positive or negative curvature, forcing it into a bilayer structure, will no doubt produce some form of curvature stress. One method for the membrane to relieve this stress is through the binding of proteins. Previously, it was mentioned that the insertion of a peripheral protein into the bilayer causes the surrounding lipids to splay apart. This slight change in orientation may aid in relieving the build-up of stress within the bilayer (**Figure 27**) [95]. This explanation may explain the results obtained from DPI analysis which showed a two-fold increase in binding affinity when LBPA was present, albeit in this case in a flat lipid surface. Also, if the extruded LBPA-LUVs remain in a well-rounded shape without any budding surfaces being formed [90], then the above description can be used here. It should be noted that even though DOPE is a non-bilayer lipid, yet its curvature effect does not appear to influence α-TTP binding to membranes. This could simply mean that the 20 mol% of DOPE present in

endosomal lipids is insufficient to have a large effect on α-TTP binding to membranes.

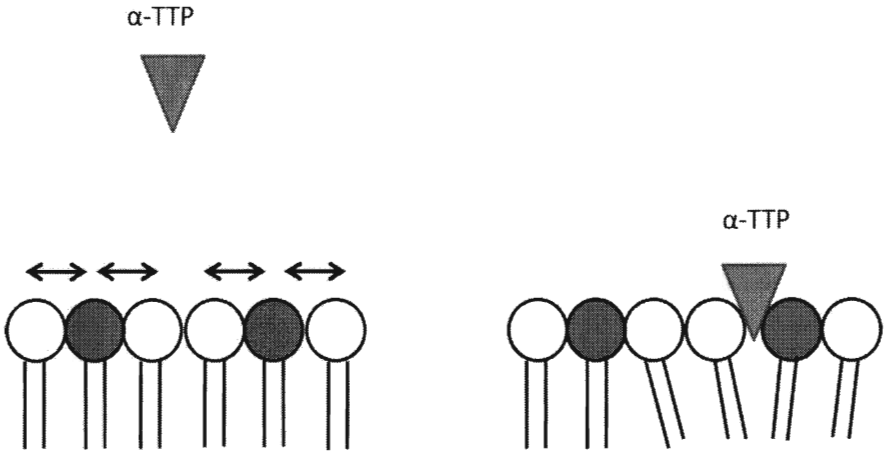

***Figure 27**: An illustration of the rationalization of how α-TTP binding to membranes may be influenced by LBPA. The presence of the non-bilayer LBPA (shaded lipids) within the bilayer results in increase curvature stress (shown as the black arrows). Binding of α-TTP to the stressed bilayer helps to relieve the curvature stress by splaying apart the neighbouring lipids.*

The increased binding affinity of α-TTP to SUVs can be explained as follows. SUVs are highly curved vesicles that have a higher curvature stress [100-101] which is reflected by their tendency to fuse over time. They also contain more free space between the lipid head-groups of the outer monolayer. This available free space is analogous to the insertion sites described previously. Both the available free space between the head-groups which allows easier access and the higher curvature stress may account for the increased affinity of α-TTP for SUVs.

3.4 pH Effect on α-TTP's Interactions to Lipid Membranes

Up to now, the discussion has concerned measurements that were conducted under physiological pH conditions. However, in both Matsuo and Kobayashi *et al.*'s work, it was apparent that low pH conditions (pH 5.5) were required for LBPA to form multivesicular liposomes and to manifest its fusogenic properties [44-45]. Therefore, it was important to investigate the effect of low pH conditions on the association of TTP with lipid membranes.

3.4.1 Investigation of α-TTP's solubility at low pH conditions

α-TTP possesses an isoelectric point (pI) of approximately 5.1 [30]. This value is close to the optimal pH value (pH 5.5) for LBPA to produce multivesicular morphology. Since pH 5.5 is close to α-TTP's pI, we were concerned that α-TTP may precipitate at this pH level. Therefore it was important to investigate the stability of α-TTP under this condition or at least determine the lowest pH that still allows us to perform the assay with a soluble protein. A simple test was done by incubating α-TTP in 2-(N-morpholino)ethanesulphonic acid (MES) buffer at different pH values of 6.5, 6.0 and 5.5. MES was chosen as it has a pKa value of 6.15, which is suitable to buffer the pH ranges being tested without the need of using different buffer systems. A small volume from each mixture was removed and tested for protein concentration using the Bradford assay. Prior to that, the mixture was centrifuged to remove any precipitates. Protein concentration was measured at intervals of one hour for up to three hours. A time span of three hours was chosen as it provides sufficient time to perform a vesicle binding assay. Generally, a vesicle binding assay for one replicate requires about 1.5 to 2 hours. The aim of this test was to observe any decline in protein concentration over the three hour period which would indicate that the protein is precipitating. This test was conducted at room temperature. Initially, the

experiment was done with 200 mM of potassium chloride (KCl) present. However, with the protein in the pH 6.0 and 5.5 buffers, a gradual decline in protein concentration was observed. Moreover, with pH 5.5, an approximately 50 % reduction was seen at the initial measurement (time = 0 hour), signifying that the protein was falling out of solution as soon as it came into contact with the buffer solution (**Figure 28 A**). Although the pH of the buffer had a value of 5.5, after the addition of the protein (in elution buffer at pH 7.5), the mixture had an overall pH of 5.7. Therefore, the final pH value will be reported as 5.7. Since α-TTP is purified in Tris(hydroxymethyl)aminomethane (Tris) buffer, as a control measure, the test was also conducted with α-TTP in Tris buffer at pH 7.5. α-TTP's solubility was plotted as optical density (O.D.) values at absorbance of 595 nm against time. The protein concentrations from the O.D. values were determined and it should be noted that the concentrations corresponding to the O.D. values ranging between 0.4 and 0.5 is comparable to the initial protein concentration added to the mixture.

Since salt plays a role in protein solubility, the next step was to conduct the same analysis with only the pH 6.0 and 5.7 conditions without the presence of salt. Interestingly, the protein concentration at both pH values was maintained over the three hour period (**Figure 28 B**). However to maintain consistency with the buffer system used in the vesicle binding assay at neutral pH, salt was added back to the buffer system at pH 5.7 but at a lower concentration of 100 mM. This time no reduction was observed in the protein concentration (**Figure 28 C**). Having established α-TTP's stability at pH 5.7 with this buffer condition, the investigation of the effect of pH on α-TTP binding to membranes was able to proceed.

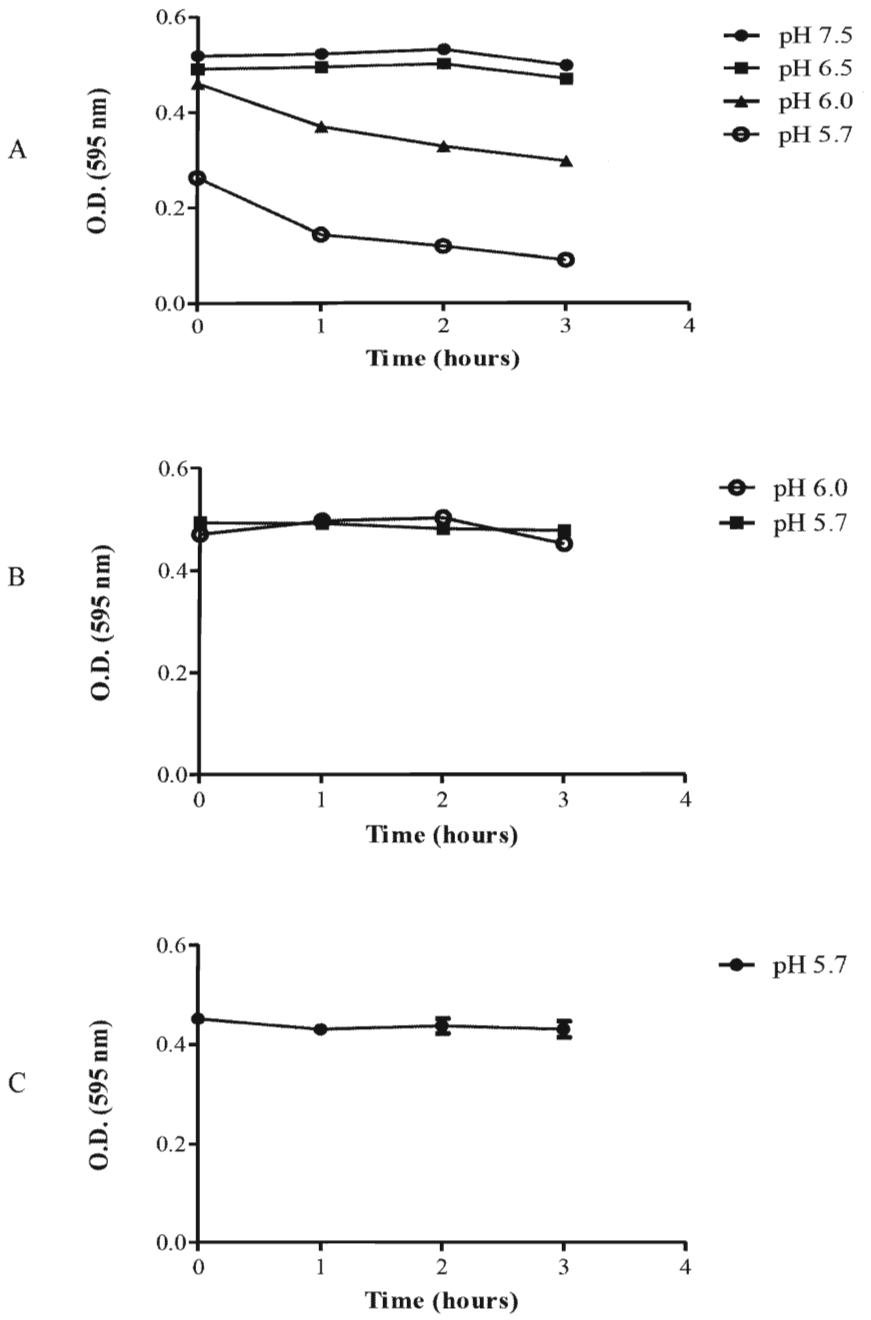

***Figure 28**: Effect of pH on α-TTP solubility. α-TTP in MES buffer with 200 mM KCl at different pH ranges except for pH 7.5 which uses Tris buffer (A). α-TTP in MES buffer without KCl at pH 6.0 and 5.5 (B). α-TTP in MES buffer at pH 5.5 with 100 mM KCl (C). All data shown are from single measurements except for (C) which are in duplicates.*

3.4.2 Effect of pH on α-TTP's association to lipid vesicles using the vesicle binding assay

It should be mentioned here that performing the vesicle binding assay at low pH conditions had one drawback. It was noted that a white precipitate was visible only in the lipid-bound fractions regardless of the type of lipid mixture used. However, no precipitate was observed in the fractions when the lipid concentration was zero. In addition, there seemed to be an increase in precipitation in the lipid-bound fractions as lipid concentration increased. An investigation was carried out to determine the cause of this precipitation. The assay was first done with just a single sample containing the buffer alone. No precipitation was visible, ruling out the idea that the buffer solution was the source of the precipitation. In an additional assay, a single sample containing lipid (1.5 mM DOPC:DOPS) was introduced into the buffer but no protein was added. In this case, the precipitate was visible. From this test, it appears that the lipids were precipitating. However, during the actual assay, we cannot rule out that the precipitates are protein-free. It is possible that as the lipid falls out of solution, any bound-protein may also precipitate along with it. An attempt was made to isolate the precipitate and test for proteins, however it was unsuccessful. It should be pointed out that during the preparation of the lipid vesicles at pH 5.7, no precipitates were observed. Another test was also conducted which involved setting aside two samples: one containing the lipid alone and the other containing both the lipid and protein in the buffer and leaving both samples out at room temperature for as long as three hours. The idea of this test was to see if any precipitation occurred over this time span. After the three hour period no solid deposits were observed in either sample, as seen in the lipid-bound fractions.

One difference observed in the vesicle binding assay at pH 5.7 compared to pH 7.5 was that the centrifugation time (during separation of free protein from bound) increased significantly, especially for the higher concentrations of lipids. An assay at neutral pH that on average took about 1.5 to 2 hours to complete was now taking about 4 hours to complete. This was true for all lipid systems. So far, all the assays were centrifuged at room temperature. This did not pose a problem with the neutral pH conditions. But with the acidic conditions, as spin time increased, one thing that was noticeable was the heat generated within the microfuge. To maintain a stable temperature environment, the assays were conducted in a refrigerated microfuge and the temperature was maintained at 25°C. When a trial run was conducted using the refrigerated microfuge with the endosomal lipids without LBPA (400 nm LUVs), interestingly, a significant reduction in the precipitation was observed. However, when the remaining lipid systems were used under this new condition, some discrepancies were observed – in that the precipitation was seen again but not in all trials. Unfortunately, there was no visible trend in the formation of these precipitates. One rationale for this precipitation can be explained as follows. As the protein-lipid mixture is being centrifuged to separate the free protein from the bound protein, the sample mixture is being concentrated, meaning less solvent is available causing the lipids and/or proteins to aggregate and fall out of solution. As the lipids and/or proteins fall out of solution, the remaining solution takes longer to pass through the filter unit, therefore increasing the spin times significantly. Since this occurred only at low pH, it is clear that the acidic conditions play a role in this problem.

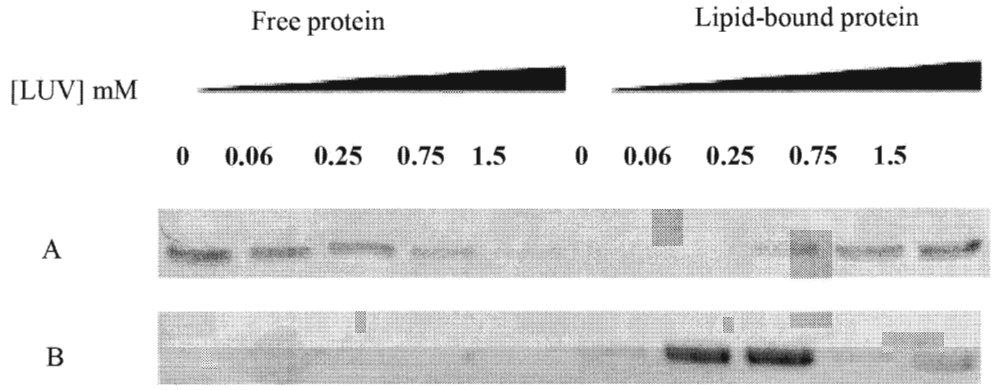

***Figure 29**: Comparison of vesicle binding assay at acidic conditions with the use of refrigerated microfuge (A) in contrast to without the use of it (B). Shown here are α-TTP bound to endosomal LUVs (400 nm) without LBPA.*

Two significant observations were also made in the SDS-PAGE analysis when the assay was conducted in a refrigerated microfuge as opposed to a non-refrigerated microfuge. Firstly, there was a significant reduction in the band intensities for the free protein fractions, especially when no lipid was present for the non-refrigerated microfuge samples. Secondly, the band intensities for the lipid-bound fractions were inconsistent with the lipid concentrations for the non-refrigerated microfuge samples. It seems that stronger band intensities were observed at lower lipid concentrations as opposed to higher ones (**Figure 29**).

What is believed to have taken place in both instances can be explained in two ways: 1) some protein is lost during the filtration step through non-specific binding to the filter unit; 2) protein precipitation is taking place. It is expected that although the results show α-TTP is soluble at pH 5.7 for at least three hours (Section 3.4.1), at this pH (close to its pI) it has near neutral charge and thus a tendency to become more hydrophobic. As a result of this, α-TTP may have a higher preference to stick to either lipids or the filter unit. As a consequence of a more hydrophobic protein at pH 5.7, it also likely that the amount of Triton X-100 used for the rinsing step may not be

sufficient to remove the non-specifically bound protein from the filter unit. On the other hand, protein precipitation may also account for the decreased band intensity for the free protein fraction. Based on the following – that the average time of the assay was increased to more than three hours and the solubility of α-TTP was not examined for more than three hours – the notion that over time α-TTP precipitates cannot be dismissed.

To rationalize the decreased intensity of protein bands at higher lipid concentrations, recall that lipid precipitation is more prominent at higher concentrations as well. The protein is again either non-specifically bound to the filter unit or precipitating out along with the lipids. Although the use of the refrigerated microfuge did not solve the precipitation problem entirely, it did improve the assay by increasing the band intensities for the free protein fraction and also enhanced the band intensity trends for the lipid-bound fractions for most of the trials (**Figure 29**).

Having discussed the issues faced whilst performing the vesicle binding assay at acidic conditions, the results obtained from the assay can now be reviewed. Since changing the pH of the buffer solution meant changing the conditions of the assay, DOPC:DOPS lipids were included in the SUV and 200 nm LUV measurements at pH 5.7 as a comparison. α-TTP binding to SUVs at pH 5.7 showed similar results as at neutral pH (**Figure 30**). Regardless of lipid mixtures, α-TTP bound with similar amounts to SUVs. Again, we see that there is no distinction between the association of α-TTP and the lipid vesicles based on lipid composition, similar to what was seen with the SUVs at neutral pH. For comparison purposes, the binding curves for the endosomal lipids with LBPA at both pH 7.5 and 5.7 are shown in **Figure 31**.

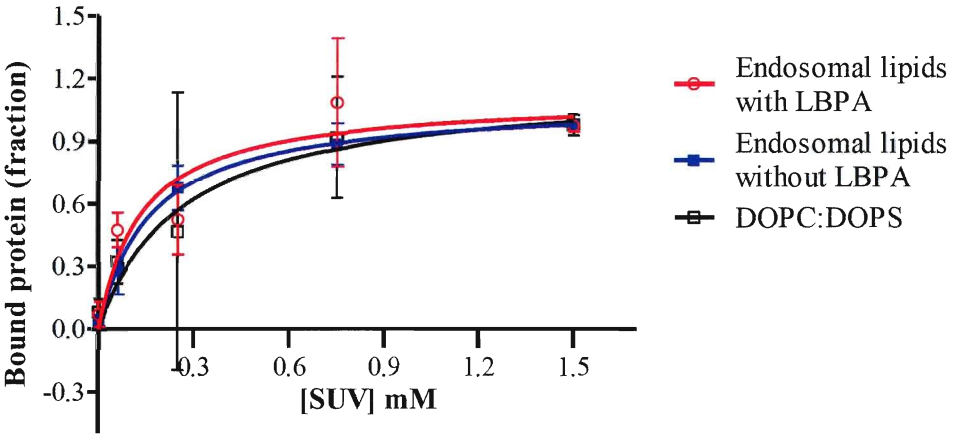

***Figure 30**: Binding curves for α-TTP to SUVs of DOPC: DOPS, endosomal lipids with and without LBPA at pH 5.7. Data are taken from three separate measurements.*

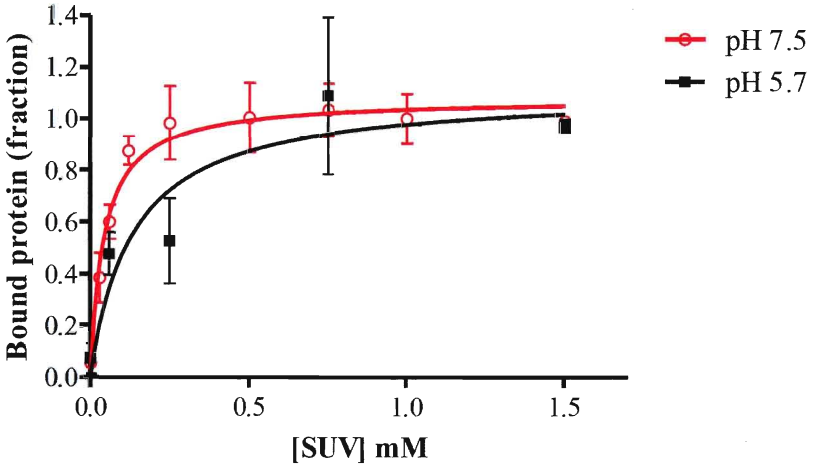

***Figure 31**: Comparison between the binding trends of α-TTP to SUVs containing 15 mol% LBPA at neutral and acidic pH conditions. Data are taken from three independent measurements.*

When SUVs were replaced with 200 nm LUVs, comparing all three lipid systems at pH 5.7, the binding trend was closely similar, although more protein was bound to the DOPC: DOPS lipids (**Figure 32**). The amount of α-TTP bound to DOPC:DOPS vesicles at pH 5.7, increased when compared to those at neutral pH (**Figure 33 A**), testifying to the increased hydrophobicity of α-TTP at this pH. This increase was also observed for the endosomal lipids without LBPA at pH 5.7 (**Figure 33 B**). But the amount of protein bound to the endosomal lipids with LBPA did not vary significantly compared to pH 7.5 (**Figure 33 C**). It seems that at pH 5.7 the enhancement of α-TTP-vesicle binding by LBPA is diminished in the 200 nm LUVs.

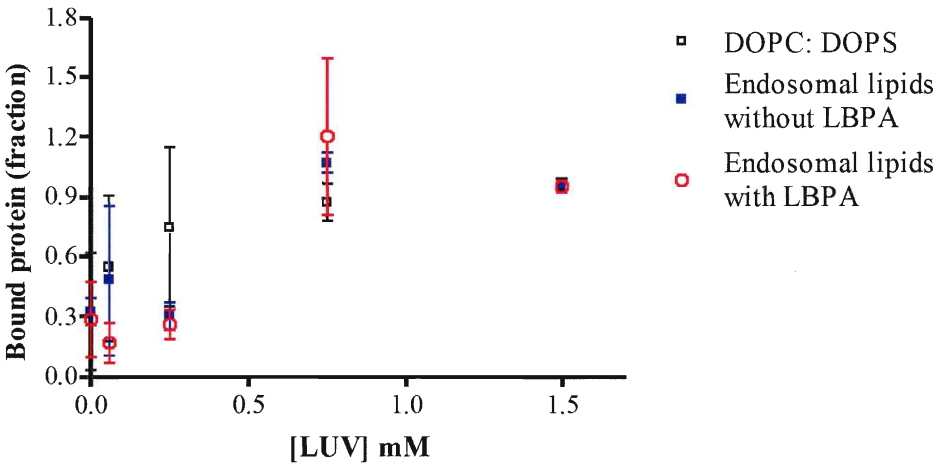

***Figure 32**: α-TTP binding to 200 nm LUVs at pH 5.7. The data are not fitted to a one-site binding curve due to large errors present. Data are from three independent measurements.*

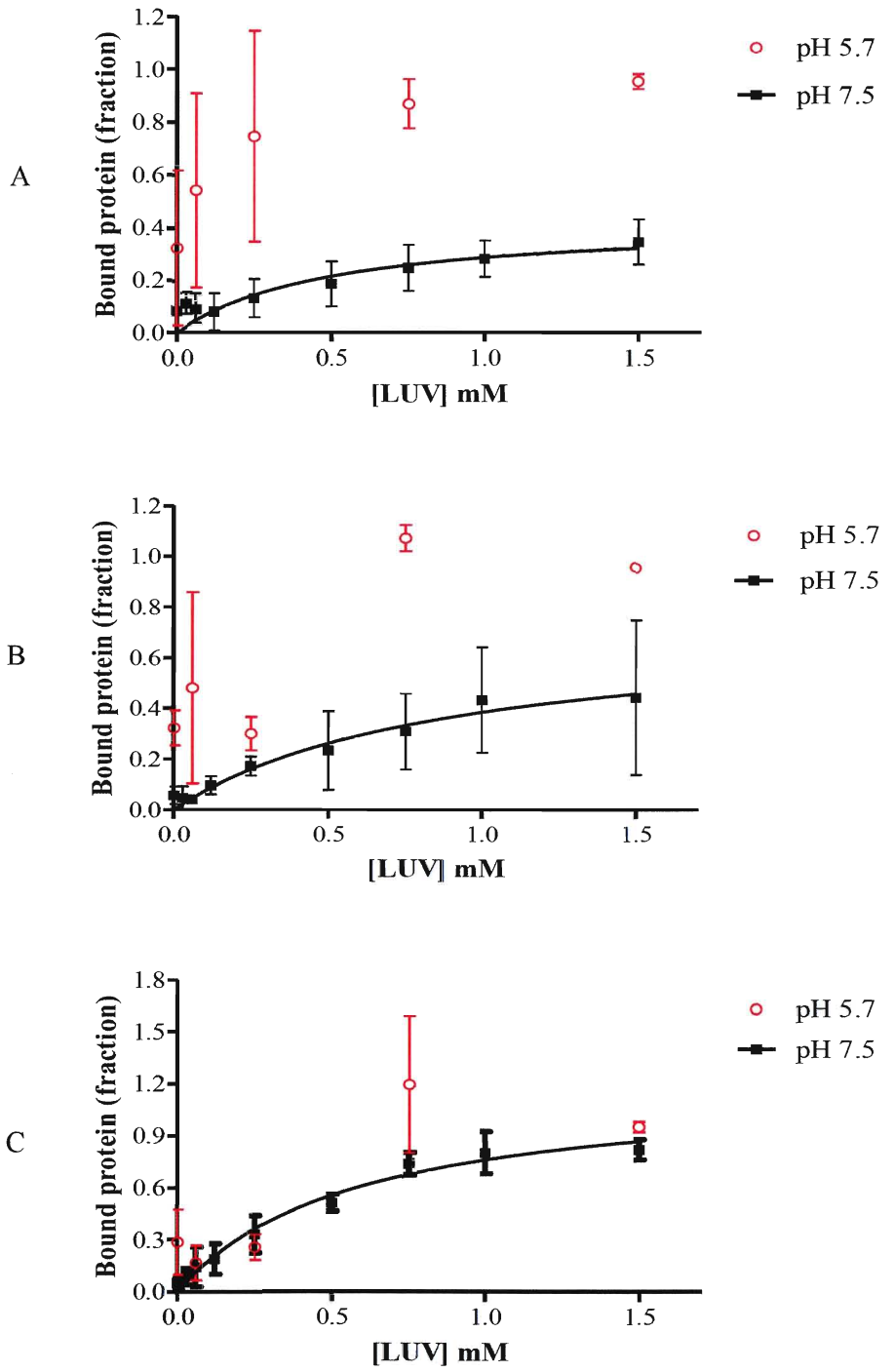

***Figure 33**: Comparison of binding trends between α-TTP and 200 nm LUVs of composed of DOPC: DOPS (A), endosomal lipids without LBPA (B) and endosomal lipids with LBPA (C) at neutral and acidic conditions. Data are from three independent measurements. The data for all three lipid mixtures at pH 5.7 are not fitted to a one-site binding curve due to the large errors present.*

We next performed a similar analysis with the 400 nm LUVs. Only the endosomal lipids with and without LBPA were used in this study (**Figure 34**). In this case, the amount of protein bound to endosomal lipids without LBPA was reduced. However, the endosomal lipids with LBPA still showed similar amount of bound-protein when compared to the 200 nm LUVs at pH 7.5.

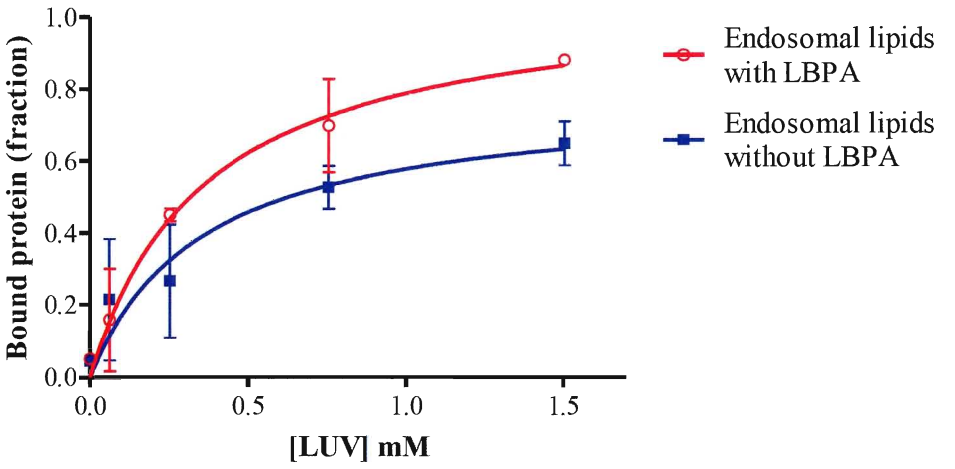

***Figure 34**: α-TTP binding to 400 nm LUVs at pH 5.7. Data are taken from three independent measurements.*

The fact that α-TTP binds to SUVs with nearly the same amount at both neutral and acidic conditions continues to support the idea that curvature is important in its binding. However, the loss of the binding enhancement (possibly due to curvature stresses) by LBPA in 200 nm LUVs at pH 5.7 can be rationalized as follows. α-TTP's tendency to be more hydrophobic at acidic conditions compared to a neutral environment, may account for the increased binding seen with the 200 nm LUVs at pH 5.7. A reduction in the amount of α-TTP bound to the 400 nm LUVs for endosomal lipids without LBPA was observed when compared to the 200 nm LUVs at pH 5.7 (**Figure 35**). Further investigation is required to confirm whether the

reduction in amount of proteins bound to 400 nm endosomal lipids without LBPA at pH 5.7 is real or not.

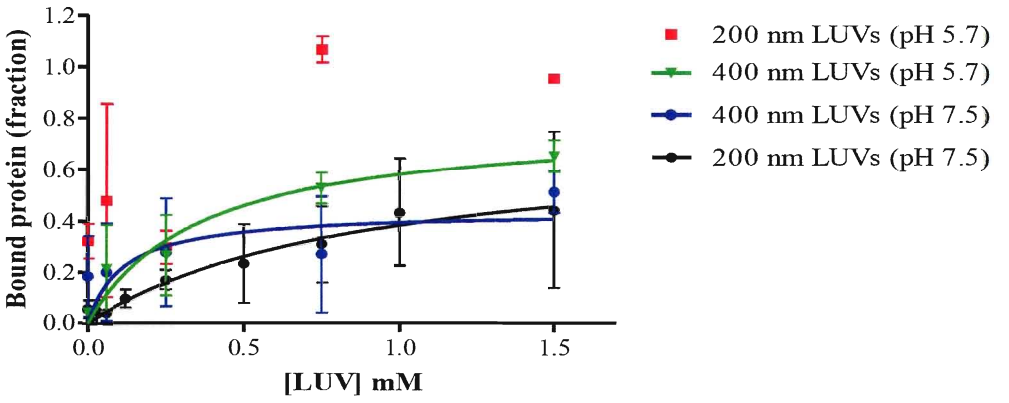

***Figure 35**: Comparison of the binding trends of α-TTP to 200 and 400 nm endosomal LUVs without LBPA at neutral and acidic pH conditions. 200 nm LUVs at pH 5.7 showed the highest amount of bound-protein. A reduced amount of protein bound to the 400 nm LUVs at pH 5.7 is observed. Data are taken from three independent measurements.*

Another explanation for the increased affinity of α-TTP to 200 nm LUVs at pH 5.7 stems from the fact that vesicles in acidic conditions can undergo physical changes [102]. These changes, which include invaginations and budding are influenced by vesicle size and lamellarity and have been observed in giant unilamellar vesicles (GUVs) [102]. It should be noted that the GUVs used were first prepared at neutral pH and then injected into an acidic medium [102] as opposed to the vesicles used in this project which are prepared directly in acidic buffer. However, this does not exclude the possibility that LUV's may still undergo these physical changes. If invaginations and budding are occurring in the LUVs, this would require that highly curved membrane surfaces are present, at least transiently. α-TTP's preference for

curvature and the presence of this curved membrane surfaces may account for the increased binding to LUVs at pH 5.7.

A better methodology to investigate the pH effect on α-TTP's binding to membranes is to use LUVs with a pH gradient in the vesicle binding assay. This means preparing vesicles with an internal pH of 5.7 but keeping the external environment neutral, mimicking the late endosome. It would also be worthwhile to examine the binding of α-TTP to membranes using DPI analysis at acidic conditions. This could, in principle, show if protein-membrane binding affinity is similar to results obtained from the vesicle binding assay, despite the flatness of surface adsorbed bilayers in the DPI. One of the objectives of this project was to conduct this DPI analysis, however, due to limited stability of α-TTP at low pH and the lipid precipitation problems the examination could not be pursued at this time.

3.5 Structural Effect On α-TTP's Interactions With Lipid Membranes

So far, all LBPA investigations performed involved the use of the 3, 1′ isoform. Matsuo *et al.* showed that the 2, 2′ isoform of LBPA, which is also believed to be the in vivo form, had a higher activity in multivesicular formation than the 3, 3′ form [45]. For this reason, the final investigation was to study the effect of the 2, 2′-LBPA on the binding of α-TTP to membranes using the vesicle binding assay. Since the 2, 2′-LBPA isoform is a costly lipid, it was only possible to proceed with the vesicle binding assay at this time. Moreover, since the effect of LBPA is most obvious in LUVs the 2, 2′-LBPA isoform was tested in 400 nm LUVs in both neutral and acidic environments.

The results obtained under neutral conditions showed a significant increase in the binding of α-TTP to 400 nm LUVs when 2, 2′-LBPA was present. A comparison

can be seen between endosomal lipids without and with LBPA of the two isoform in **Figure 36.**

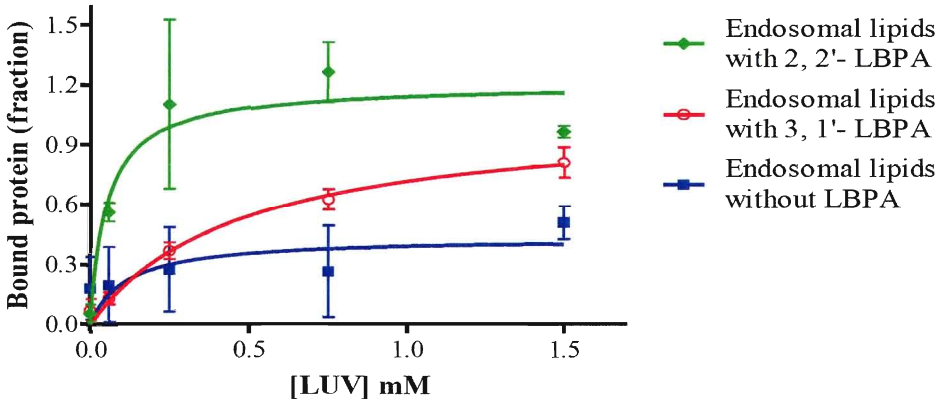

***Figure 36**: Comparison between α-TTP binding to 400 nm vesicles containing 2, 2′-LBPA and 3, 1′-LBPA at neutral pH. Increased in amount of α-TTP bound to 2, 2′-LBPA vesicles are seen compared to 3, 1′- LBPA vesicles. Results for endosomal lipids without LBPA were added for comparison purposes. Data are from three separate measurements.*

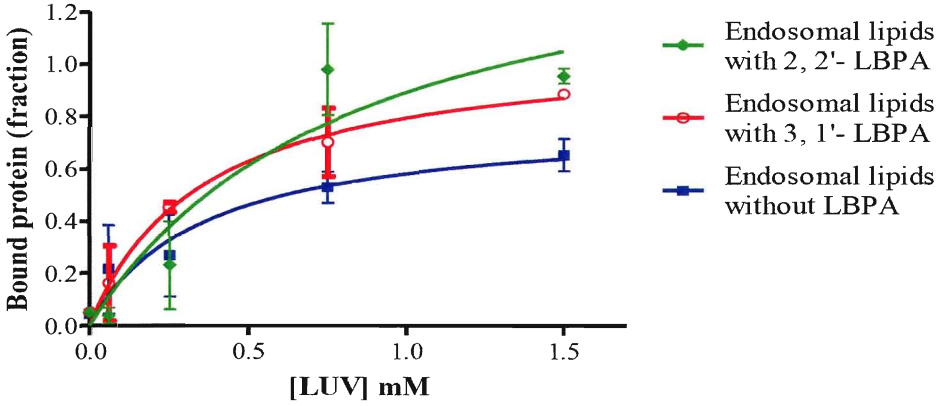

***Figure 37**: Comparison between α-TTP binding to 400 nm vesicles containing 2, 2′-LBPA and 3, 1′-LBPA at acidic conditions. Amount of α-TTP bound to 2, 2′- LBPA vesicles were similar to 3, 1′-LBPA vesicles. The binding curve for endosomal lipids without the presence of LBPA is shown for comparison purposes. Data are from three separate measurements.*

When similar investigations were conducted under acidic conditions, the increased amount of bound-protein as seen for the neutral pH was not visible here. Instead, the amount of α-TTP bound to 2, 2′-LBPA LUVs was closely similar to that of 3, 1′-LBPA LUVs (**Figure 37**). It was expected that a higher amount of α-TTP will bind to 2, 2′-LBPA vesicles at lower pH. However, the results in **Figure 37** show otherwise. One explanation stems from Frederick *et al.*'s work which observed that LBPA rapidly hydrolyzes under acidic conditions – within four days after rehydration of the vesicles [90]. Whether one form of LBPA has a higher rate of hydrolysis compared to another is not known. In addition it has been reported that the acyl chains on the 2, 2′ position are thermodynamically unstable and can migrate to the 3, 1′ position [45]. This takes place under either basic or acidic conditions [103]. This fact may also contribute towards the unchanged binding affinity of α-TTP to 2, 2′-LBPA LUVs at pH 5.7 compared to 3, 1′-LBPA. The final explanation could also stem from an increased hydrophobic α-TTP as described in the previous section. However, the outcome from the investigation at neutral pH is consistent with previous reports regarding the 2, 2′-LBPA – that it is able to generate the curvature effect to a greater extent. While at this pH level it may not be able to produce multilamellar morphology, it may still be able to contribute to curvature stress. The extent of curvature stress may be greater than compared to 3, 1′-LBPA due to the changes in the overall LBPA structure.

4. CONCLUSION

In summary, results from DPI analyses showed that α-TTP binding to membranes is greater in the presence of LBPA at physiological pH conditions. However, with this methodology, lipid membranes are believed to be flat. Amethod vesicle binding assay was then employed to investigate α-TTP binding to membranes that are curved. By means of this assay, α-TTP bound to LBPA-containing LUVs (200 and 400 nm) with greater affinity, just as was seen with the DPI analysis at neutral pH. These results are consistent since the surface of an LUV would appear flat to α-TTP as it approaches the membrane. On the other hand, when SUVs replaced the LUVs, more protein was bound to the vesicles regardless of whether LBPA was present or not. This suggests the importance of membrane curvature in influencing α-TTP's association with lipid membranes. These observations are in agreement with recent findings on the increased ligand transfer rate by α-TTP with SUVs containing only PC [38]. The fact that α-TTP binds to flat lipid bilayers to a greater extent when LBPA is present implies that α-TTP is able to specifically recognize the local curvature generated by LBPA within this bilayers. DOPE which is also a curvature-forming lipid does not appear to have the same effect on α-TTP binding to membranes, perhaps due to an inherently lesser influence on curvature on a per mol lipid basis.

Consider the localization of α-TTP to late endosomes: the late endosome is a dynamic vesicle where constant budding and fusion is taking place due to intracellular trafficking. Only in this vesicle, the LBPA content is found to be as high as 15 mol% of the total lipid content. LBPA is believed to play an important role in the development of the multivesicular bodies within the late endosomes. It is then possible that as LBPA in the limiting membrane of late endosomes forms

multivesicular bodies within the lumen of late endosomes, there are specific areas on the limiting membrane that develops high surface curvature and/or curvature stress. As these factors favour α-TTP binding to membranes, α-TTP then binds to these highly curved and stressed regions of the late endosome where it can insert and/or retrieve α-tocopherol. Taking into account the location of α-tocopherol within a bilayer, the highly negative curved surface signifies more free space between the lipid head-groups of the outer monolayer which then allows easier access of α-TTP to its ligand.

Since the internal lumen of late endosomes are acidic (pH 5.5) and this condition is vital for the formation of multivesicular bodies by LBPA, the effect of pH was also investigated on the binding of α-TTP to membranes. The results obtained from the vesicle binding assays showed that pH did not alter the binding of α-TTP to SUVs. Whereas with LUVs, the increased binding to only LBPA-containing LUVs was diminished more for the 200 nm LUVs compared to the 400 nm LUVs. One reason was described which stems from the increased hydrophobicity of α-TTP at pH 5.7.

Matsuo *et al.* showed that the 2, 2′-LBPA had a higher activity in promoting multivesicular morphology in contrast to the 3, 3′-LBPA [45]. Therefore the final investigation was to examine the effect of this form of LBPA on α-TTP binding to membranes using the vesicle binding assay. At neutral pH, the amount of α-TTP bound to 400 nm LUVs containing 2, 2′-LBPA were significantly higher compared to 3, 1′-LBPA. However, at acidic conditions, no significant changes in the protein binding were observed between both forms of LBPA. This could possibly be due to either the increased hydrophobicity of α-TTP as mentioned above or the instability of the 2, 2′-LBPA LUVs as result of hydrolysis of LBPA or acyl chain migration. The

enhanced binding of α-TTP to 2, 2′-LBPA-vesicles at neutral pH should not be overlooked. Since this form of LBPA is believed to exist in vivo and produces more curvature, the results seen here signify the importance of this LBPA form in α-TTP binding to membranes.

A better method for testing the pH effect of α-TTP binding to membranes using the vesicle binding assay involves the use of LUVs with a pH gradient, where the internal environment is acidic while the external environment remains neutral. This pH gradient appears to be vital for multivesicular formation [45]. Also this pH gradient will mimic the late endosome, since only the late endosome lumen is acidic while the exterior or cytoplasm is at physiological pH. In addition, using pH gradient LUVs will eliminate the problem with α-TTP's increased hydrophobicity at pH 5.7. Acidic liposomes can be prepared by using nigericin, an ionophore, which moves protons into the LUV when incubated in a low pH buffer [45, 101]. The nigericin is then removed and the external buffer is replaced with a neutral one. This procedure is performed on a PD-10 desalting and buffer exchange column [45]. Furthermore, it would also be advantageous to investigate α-TTP binding to lipid membranes at pH 5.7 employing the DPI method with both the 3, 1′ and 2, 2′-LBPA as a means of comparison with the vesicle binding assay. So far all analyses performed with DPI only took into consideration the deposition of mass layers. Information can also be extracted from the rates of formation and dissociation of the mass layer, which can be conducted in future DPI analyses.

Since the results obtained from this project cannot rule out that no specific interaction occurs between α-TTP and LBPA, further examination should be performed to elucidate this uncertainty. One technique that can be employed here is a protein-lipid overlay assay [104]. In this assay, the phospholipid of interest is spotted

onto a nitrocellulose membrane at varying concentrations. The nitrocellulose membrane is then incubated with the protein of interest. If the protein specifically interacts with the lipid, then any bound protein on the nitrocellulose membrane can be analyzed via immunoblotting [104].

It is important to mention that while other factors may contribute to the increased binding of α-TTP to LBPA such as charge, the main emphasis in this thesis was on the curvature effect generated by LBPA. LBPA is an anionic lipid and whether this negative charge influences the binding of α-TTP to LBPA vesicles can be explained as follows. Recent study showed that the ligand transfer rates by α-TTP to anionic SUVs, such as PS, PI and LBPA, showed no significant difference in the transfer rates compared to PC vesicles [38]. Although transfer rates differs from binding measurements, in order for α-TTP to transfer its ligand between donor and acceptor vesicles, binding must first occur to the donor vesicles to retrieve its ligand and then transfer it to the acceptor vesicles. Since the presence of anionic vesicles did not influence the transfer rate and therefore the binding of α-TTP to these vesicles, it can be deduced that the negative charge does not influence α-TTP binding to lipid membranes. For this reason the effect of anionic lipids on α-TTP association to lipid membranes was not investigated in this project.

It has been mentioned previously that LBPA has been proposed to adopt a cone shape, but no actual physical measurement has been performed to confirm this fact. One control method to determine the effect of cone-shaped lipids on α-TTP binding to lipid membranes is to use an alternative cone-shaped lipid in place of LBPA for example DOPE. This investigation has been previously carried out [81], whereby lipid mixtures consisting of DOPC and varying amounts of DOPE were introduced into the Analight Bio200. However, the thickness measurements of these

bilayers were found to increase as the proportion of DOPE increased, about 18 nm for 60:40 DOPC:DOPE lipids. This implies that the presence of DOPE influences the proper formation of lipid bilayers on the Analight Bio200 as explained in Section 3.2.1. Therefore, the binding of α-TTP to these lipids were not able to be investigated. Consequently, this control measure was not included in this project.

It is also noteworthy to emphasize that there is evidence to show LBPA does not undergo lateral phase segregation in mixed bilayers of 1-palmitoyl-2-oleoyl-phosphatidylcholine (POPC) and LBPA [105]. This then rules out the notion that binding of α-TTP to lipid membranes may be due to the interaction of α-TTP to LBPA-enriched microdomains.

In conclusion, the overall results from this project provide preliminary evidence that membrane curvature is an important factor in influencing α-TTP's binding to lipid membranes – specifically the local curvature generated by LBPA. Recent work by Zhang *et al.* also supports the role of membrane curvature in α-TTP binding to membranes [38]. The consistency in results is promising, however more investigations are required at this stage, some of which were described above, to fully elucidate the importance of LBPA to the mechanism of ligand transfer by α-TTP.

5. BIBLIOGRAPHY

1. Kamal-Eldin, A. & Appelqvist, L. (1996). The chemistry and antioxidant properties of tocopherols and tocotrienols. *Lipids*, 31, 671-701.
2. Brigelius-Flohe, R. & Traber, M. G. (1999). Vitamin E: function and metabolism. *FASEB Journal*, 13, 1145-1155.
3. Azzi, A. & Stocker, A. (2000). Vitamin E: non-antioxidant roles. *Progress in Lipid Research*, 39, 231-255.
4. Bjorneboe, A., Bjorneboe, G. & Drevon, C. (1990). Absorption, transport and distribution of vitamin E. *Journal of Nutrition*, 120, 233-242.
5. Evans, H.M & Bishop, K. S. (1922). On the existence of a hitherto unrecognized dietary factor essential for reproduction. *Science*, 56, 650-651.
6. Wang, X. & Quinn, P. J. (1999). Vitamin E and its function in membranes. *Progress in Lipid Research*, 38, 309-336.
7. Burton, G. W. & Ingold, K. U. (1986). Vitamin E: application of the principles of physical organic chemistry to the exploration of its structure and function. *Accounts of Chemical Research*, 19, 194-201.
8. Halliwell, B. (1996). Antioxidants in human health and disease. *Annual Review of Nutrition*, 16, 33-50.
9. Burton, G. W. & Ingold, K. U. (1989). Vitamin E as an in vitro and in vivo antioxidant. *Annals of the New York Academy of Sciences*, 570, 7-22.
10. Burton, G. W. & Traber, M. G. (1990). Vitamin E: Antioxidant activity, biokinetics and bioavailability. *Annual Reviews of Nutrition*, 10, 357-382.
11. Halliwell, B. & Chirico, S. (1993). Lipid peroxidation: its mechanism, measurement, and significance. *The American Journal of Clinical Nutrition*. 57(S), 715S-725S.

12. Wolf, R., Wolf, D. & Ruocco, V. (1998). Vitamin E: the radical protector. *Journal of the European Academy of Dermatology and Venereology*, 10, 103-117.

13. Traber, M. G. & Sies, H. (1996). Vitamin E in humans: demand and delivery. *Annual Review of Nutrition*, 16, 321-347.

14. Wang, X. & Quinn, P. J. (2000). The location and function of vitamin E in membranes (review). *Molecular Membrane Biology*, 17, 143-156.

15. Atkinson, J., Epand, R. F. & Epand, R. M. (2008). Tocopherols and tocotrienols in membranes: a critical review. *Free Radical Biology and Medicine*, 44, 739-764.

16. Bender, D. A. (2003). *Nutritional biochemistry of the vitamins*, 2 ed., Cambridge University Press, Cambridge.

17. Kayden, H. J. & Traber, M. G. (1993). Absorption, lipoprotein transport, and regulation of plasma concentrations of vitamin E in humans. *Journal of Lipid Research*, 34, 343-358.

18. Herrera, E. & Barbas, C. (2001). Vitamin E: action, metabolism and perspectives. *Journal of Physiology & Biochemistry*, 57, 43-56.

19. Traber, M. G., Burton, G. W., Ingold, K. U. & Kayden, H. J. (1990). RRR- and SRR-α-tocopherols are secreted without discrimination in human chylomicrons, but RRR-α-tocopherol is preferentially secreted in very low density lipoproteins. *Journal of Lipid Research*, 31, 675-685.

20. Traber, M. G. (2007). Vitamin E Regulatory Mechanisms. *The Annual Review of Nutrition*, 27, 347-362.

21. Catignani, G. L. & Bieri, J. G. (1977). Rat liver α-tocopherol binding protein. *Biochimica et Biophysica Acta,* 497, 349-357.

22. Mowri, H., Nakagawa Y., Inoue, K. & Nojima, S. (1981). Enhancement of the transfer of α-tocopherol between liposomes and mitochondria by rat-liver protein(s). *European Journal of Biochemistry*, 117, 537-542.

23. Murphy, D. J. & Mavis, R. D. (1981). Membrane transfer of α-tocopherol. *The Journal of Biological Chemistry*, 256, 10464-10468.

24. Sato, Y., Hagiwara, K., Arai, H & Inoue, K. (1991). Purification and characterization of the α-tocopherol transfer protein from rat liver. *FEBS Letters*, 288, 41-45.

25. Yoshida, H., Yusin, M., Ren, I., Kuhlenkamp, J., Hirano, T., Stolz, A. & Kaplowitz, N. (1992). Identification, purification, and immunochemical characterization of a tocopherol-binding protein in rat liver cytosol. *Journal of Lipid Research*, 33, 343-350.

26. Hosomi, A., Arita, M., Sato, Y., Kiyose, C., Ueda, T., Igarashi, O., Arai, H., Inoue, K. (1997). Affinity for α-tocopherol transfer protein as a determinant of the biological activities of vitamin E analogs. *FEBS Letters* 409, 105-108.

27. Panagabko, C., Morley, S., Hernandez, M., Cassolato, P., Gordon, H., Parsons, R., Manor, D. & Atkinson, J. (2003). Ligand specificity in the CRAL-TRIO protein family. *Biochemistry* 42, 6467-6474.

28. Catignani, G. L. (1975). An α-tocopherol binding protein in rat liver cytoplasm. *Biochemical & Biophysical Research Communications*, 67, 66-72.

29. Kuhlenkamp, J., Ronk, M., Yusin, M., Stolz, A. & Kaplowitz, N. (1993). Identification and purification of a human liver cytosolic tocopherol binding protein. *Protein Expression & Purification*, 4, 382-389.

30. Arita, M., Sato, Y., Miyata, A., Tanabe, T., Takahashi, E., Kayden, H. J., Arai, H. & Inoue, K. (1995). Human α-tocopherol transfer protein: cDNA cloning, expression and chromosomal localization. *Biochemical Journal*, 306, 437-443.

31. Manor, D. & Morley, S. (2007). The α-tocopherol transfer protein. *Vitamins & Hormones*, 76, 45-65.

32. Qian, J., Atkinson, J. & Manor, D. (2006). Biochemical consequences of heritable mutations in the α-tocopherol transfer protein. *Biochemistry*, 45, 8236-8242.

33. Yokota, T., Igarashi, K., Uchihara, T., Jishage, K., Tomita, H., Inaba, A., Li, Y., Arita, M., Suzuki, H., Mizusawa, H. & Arai, H. (2001). Delayed-onset ataxia in mice lacking α-tocopherol transfer protein: model for neuronal degeneration caused by chronic oxidative stress. *Proceedings of the National Academy of Sciences USA*, 98, 15185-15190.

34. Arita, M., Nomura, K., Arai, H. & Inoue, K. (1997). α-tocopherol transfer protein stimulates the secretion of α-tocopherol from a cultured liver cell line through a Brefeldin A-insensitive pathway. *Proceedings of the National Academy of Sciences USA,* 94, 12437-441.

35. Meier, R., Tomizaki, T., Schulze-Briese, C., Baumann, U. & Stocker, A. (2003). The molecular basis of vitamin E retention: structure of human α-tocopherol transfer protein. *Journal of Molecular Biology*, 331, 725-734.

36. Min, K. C., Kovall, R. A. & Hendrickson, W. A. (2003). Crystal structure of human α-tocopherol transfer protein bound to its ligand: implications for ataxia with vitamin E deficiency. *Proceedings of the National Academy of Sciences USA,* 100, 14713-14718.

37. Morley, S., Cecchini, M., Zhang, W., Virgulti, A., Noy, N., Atkinson, J. & Manor, D. (2008). Mechanism of ligand transfer by the hepatic tocopherol transfer protein. *Journal of Biological Chemistry*, 283, 17797-17804.

38. Zhang, W. X., Frahm, G., Morley, S., Manor, D. & Atkinson, J. (2009). Effect of bilayer phospholipid composition and curvature on ligand transfer by the α-tocopherol transfer protein. *Lipids*, 44, 631-641.

39. Traber, M. G., Burton, G. W. & Hamilton, R. L. (2004). Vitamin E trafficking. *Annals of New York Academy of Sciences*, 1031, 1-12.

40. Qian, J., Morley, S., Wilson, K., Nava, P., Atkinson, J., & Manor, D. (2005). Intracellular trafficking of vitamin E in hepatocytes: the role of tocopherol transfer protein. *Journal of Lipid Research*, 46, 2072-2082.

41. Horiguchi, M., Arita, M., Kaempf-Rotzoll D. E., Tsujimoto, M., Inoue, K. & Arai, H. (2003). pH-dependent translocation of α-tocopherol transfer protein (α-TTP) between hepatic cytosol and late endosomes. *Genes to Cells*, 8, 789-800.

42. Rupar, C. A., S. Albo, and J. D. Whitehall. (1992). Rat liver lysosome membranes are enriched in alpha-tocopherol. *Biochemistry & Cell Biology,* 70**,** 486–488.

43. Hayakawa, T. Makino, A., Murate, M., Sugimoto, I., Hashimoto, Y., Takahashi, H., Ito, K., Fujisawa, T., Matsuo, H. & Kobayashi, T. (2007). pH-dependent formation of membranous cytoplasmic body-like structure of ganglioside$_{GM1}$/ Bis(Monoacylglycerol)Phosphate mixed membranes. *Biophysical Journal*, 92, L13-L16.

44. Kobayashi, T., Beuchat, M., Chevallier, J., Makino, A., Mayran, N., Escola, J., Lebrand, C., Cosson, P., Kobayashi, T. & Gruenberg, J. (2002). Separation and characterization of late endosomal membrane domains. *The Journal of Biological Chemistry*, 277, 32157-32164.

45. Matsuo, H., Chevallier, J., Mayran, N., Le Blanc, I., Ferguson, C., Faure, J., Blanc, N. S., Matile, S., Dubochet, J., Sadoul, R., Parton, R. G., Vilbois, F. & Gruenberg, J. (2004). Role of LBPA and Alix in multivesicular liposome formation and endosome organization. *Science*, 303, 531-534.

46. Poorthuis, B. & Hostetler, K. (1975). Biosynthesis of bis(monoacylglyceryl)phosphate and acylphosphatidylglycerol in rat liver mitochondrial. *The Journal of Biological Chemistry*, 250 (9), 3297-3302.

47. Hullin-Matsuda, F., Kawasaki, K., Delton-Vanderbroucke, I., Xu, Y., Nishijima, M., Lagarde, M., Schlame, M. & Kobayashi, T. (2007). De novo biosynthesis of the late endosome lipid, bis(monoacylglycero)phosphate. *Journal of Lipid Research*, 48, 1997-2008.

48. Van Meel, E. & Klumperman, J. (2008). Imaging and imagination: understanding the endo-lysosomal system. *Histochemistry & Cell Biology*, 129, 253-266.

49. Lakkaraju, A. & Rodriguez-Boulan, E. (2008). Itinerant exosomes: emerging roles in cell and tissue polarity. *Trends in Cell Biology*, 18, 199-209.

50. Clague, M. J. & Urbe, S. (2008). Multivesicular bodies. *Current Biology*, 18, R402-R404.

51. Gruenberg, J. & Stenmark, H. (2004). The biogenesis of multivesicular endosomes. *Nature Reviews Molecular Cell Biology*, 5, 317-323.

52. Ganley, I. G., Carroll, K., Bittova, L. & Pfeffer, S. (2004). Rab9 GTPase regulates late endosome size and requires effector interaction for its stability. *Molecular Biology of the Cell*, 15, 5420-5430.

53. Van der Goot, F. G. & Gruenberg, J. (2006). Intra-endosomal membrane traffic. *Trends in Cell Biology*, 16, 514-521.

54. Uchil, P. & Mothes, W. (2005). Viral entry: a detour through multivesicular bodies. *Nature Cell Biology*, 7, 641-642.

55. Keller, S., Sanderson, M. P., Stoeck, A. & Altevogt, P. (2006). Exosomes: from biogenesis and secretion to biological function. *Immunology Letters*, 107, 102-108.

56. Van Niel, G., Porto-Carreiro, I., Simoes, S. & Raposo, G. (2006). Exosomes: a common pathway for a specialized function. *The Journal of Biochemistry*, 140, 13-21.

57. Luyet, P., Falguieres, T., Pons, V. & Gruenberg, J. (2007). Endosomal membrane dynamics. *Journal of Oral Biosciences*, 49, 231-243.

58. Perret, E., Lakkaraju, A., Deborde, S., Schreiner, R. & Rodriguez-Boulan, E. (2005). Evolving endosomes: how many varieties and why? *Current Opinion in Cell Biology*, 17, 423-434.

59. Piper, R.C. & Katzmann, D. J. (2007). Biogenesis and function of multivesicular bodies. *Annual Review of Cell and Developmental Biology*, 23, 519-547.

60. White, I. J., Bailey, L. M., Aghakhani, M. R., Moss, S. E. & Futter, C. E. (2006). EGF stimulates annexin 1-dependent inward vesiculation in a multivesicular endosome subpopulation. *The EMBO Journal*, 25, 1-12.

61. Subra, C., Laulagnier, K., Perret, B. & Record, M. (2007). Exosome lipidomics unravels lipid sorting at the level of multivesicular bodies. *Biochimie*, 89, 205-212.

62. Trajkovic, K., Hsu, C., Chianta, S., Rajendran, L., Wenzel, D., Wieland, F., Schwille, P., Brugger, B. & Simons, M. (2008). Ceramide triggers budding of exosomes vesicles into multivesicular endosomes. *Science*, 319, 1244-1246.

63. Kobayashi, T., Stang, E., Fang, K. S., de Moerloose, P., Parton R. G. & Gruenberg, J. (1998). A lipid associated with the antiphospholipid syndrome regulates endosome structure and function. *Nature*, 392, 193-197.

64. Kobayashi, T., Beuchat, M., Lindsay, M., Frias, S., Palmiter R. D., Sakuraba, H., Parton, R. G. & Gruenberg, J. (1999). Late endosomal membranes rich in lysobisphosphatidic acid regulate cholesterol transport. *Nature Cell Biology*, 1, 113-118.

65. McMahon, H. T. & Gallop, J. L. (2005). Membrane curvature and mechanisms of dynamic cell membrane remodelling. *Nature*, 438, 590-596.

66. Pencer, J., Jackson, A., Kucerka, N., Nieh, M-P. & Katsaras, J. (2008). The influence of curvature on membrane domains. *European Biophysics Journal*, 37, 665-671.

67. Haque, M. E., McIntosh, T. J. & Lentz, B. R. (2001). Influence of lipid composition on physical properties and PEG-mediated fusion of curved and uncurved model membrane vesicles: "nature's own" fusogenic vesicles. *Biochemistry*, 40, 4340-4348.

68. Van Meer, G. & Sprong H. (2004). Membrane lipids and vesicular traffic. *Current Opinion in Cell Biology*, 16, 373-378.

69. De Matteis, M. A. & Godi, A. (2004). Protein-lipid interactions in membrane trafficking at the Golgi complex. *Biochimica et Biophysica Acta*, 1666, 264-274.

70. Chernomordik, L. V. & Kozlov, M. M. (2003). Protein-lipid interplay in fusion and fission of biological membranes. *Annual Review of Biochemistry*, 72, 175-207.

71. Le Blanc, I., Luyet, P-P., Pons, V., Ferguson, C., Emans, N., Petiot, A., Mayran, N., Demaurex, N., Faure, J., Sadoul, R., Parton, R. G & Gruenberg, J. (2005). Endosome-to-cytosol transport of viral nucleocapsids. *Nature Cell Biology*, 7, 653-664.

72. Bigay, J., Casella, J., Drin, G., Mesmin, B. & Antonny, B. (2005). ArfGAP1 responds to membrane curvature through the folding of a lipid packing sensor motif. *The EMBO Journal*, 24, 2244-2253.

73. Hubner, S., Couvillon, A. D., Kas, J. A., Bankaitis, V. A., Vegners, R., Carpenter, C. L. & Janmey, P. A. (1998). Enhancement of phosphoisotide 3-kinase (PI 3-kinase) activity by membrane curvature and inositol-phospholipid-binding peptides. *European Journal of Biochemistry*, 258, 846-853.

74. Rich, R. L. & Myszka, D. G. (2001). BIACORE J: a new platform for routine biomolecular interaction analysis. *Journal of Molecular Recognition*, 14, 223-228.

75. Besenicar, M., Macek, P., Lakey, J. H. & Anderluh, G. (2006). Surface Plasmon resonance in protein-membrane interactions. *Chemistry and Physics of Lipids*, 141, 169-178.

76. Sonesson, A. W., Callisen, T. H., Brismar, H. & Elofsson, U. M. (2007). A comparison between dual polarization interferometry (DPI) and surface plasmon resonance (SPR) for protein adsorption studies. *Colloids and Surfaces B: Biointerfaces*, 54, 236-240.

77. Swann, M. J., Peel, L. L., Carrington, S. & Freeman, N. J. (2004). Dual-polarization interferometry: an analytical technique to measure changes in protein structure in real time, to determine the stoichiometry of binding events, and to differentiate between specific and nonspecific interactions. *Analytical Biochemistry* 329, 190-198.

78. Cross, G. H., Reeves, A., Brand, S., Swann, M. J., Peel, L. L., Freeman, N. J. & Lu, J. R. (2003). The metrics of surface adsorbed small molecules on the Young' fringe dual-slab waveguide interferometer. *Journal of Physics D: Applied Physics*, 37, 74-80.

79. Terry, C. J., Popplewell, J. F., Swann, M. J., Freeman, N. J. & Fernig, D. G. (2006). Characterisation of membrane mimetics on dual polarisation interferometer. *Biosensors and Bioelectronics*, 22, 627-632.

80. Johnson, J. E., Rao, N. M., Hui, S-W & Cornell, R. B. (1998). Confirmation and lipid-binding properties of four peptides derived from the membrane-binding domain of CTP: phosphocholine cytidyllyltransferase. *Biochemistry*, 37, 9509-9519.

81. Virgulti, A. (2007). Investigation of human α-tocopherol transfer protein (α-TTP) through altered lipid composition. BSc (Hons) thesis. Brock University.

82. Zimmerberg, J. (2006). Membrane biophysics. *Current Biology*, 16, R272-276.

83. Morley, S., Panagabko, C., Shineman, D., Bernhanrd, M., Stocker, A., Atkinson, J. & Manor, D. (2004). Molecular determinants of heritable vitamin E deficiency. *Biochemistry*, 43, 4143-4149.

84. Schonherr, H., Johnson, J. M., Lenz, P., Frank, C. W. & Boxer, S. G. (2004). Vesicle adsorption and lipid bilayer formation on glass studied by atomic force microscopy. *Langmuir*, 20, 11600-11606.

85. Popplewell, J., Freeman, N., Carrinton, S., Ronan, G., McDonnell, C. & Ford, R. C. (2005). Quantification of the effects of melittin on liposome structure. *Biochemical Society Transactions*, 33, 931-933.

86. Hamai, C., Yang, T., Kataoka, S., Cremer, P. S. & Musser, S. M. (2006). Effect of average phospholipid curvature on supported bilayer formation on glass by vesicle fusion. *Biophysical Journal*, 90, 1241-1248.

87. Booth, P. J. (2005). Sane in the membrane: designing systems to modulate membrane proteins. *Current Opinion in Structural Biology*, 15, 435-440.

88. Van der Brink-van der Laan, E., Killian, J. A. & de Kruijff, B. (2004). Nonbilayer lipids affect peripheral and integral membrane proteins via changes in the lateral pressure profile. *Biochimica et Biophysica Acta: Biomembranes*, 1666, 275-288.

89. Bezrukov, S. M. (2000). Functional consequences of lipid packing stress. *Current Opinion in Colloid & Interface Science*, 5, 237-243.

90. Frederick, T. E., Chebukati, J. N., Mair, C. E., Goff, P. C. & Fanucci, G. E. (2009). Bis(monoacylglycero)phosphate forms stable small lamellar vesicle structures: insights into vesicular body formation in endosomes. *Biophysical Journal*, 96, 1847-1855.

91. Feng, J., Wehbi, H. & Roberts, M. F. (2002). Role of tryptophan residues in interfacial binding of phosphatidylinositol-specific phospholipase C. *The Journal of Biological Chemistry*, 277, 19867-19875.

92. Wehbi, H., Feng, J., Kolbeck, J., Ananthanarayanan, B., Cho, W. & Roberts, M. F. (2003). *Biochemistry*, 42, 9374-9382.

93. Weiss, S. Millner, P. & Nelson, A. (2005). Monitoring protein binding to phospholipid bilayers using electrochemical impedance spectroscopy. *Electrochimica Acta*, 50, 4248-4256.

94. Szoka, F. Jr. & Papahadjopoulos, D. (1980). Comparative properties and methods of preparation of lipid vesicles (liposomes). *Annual Reviews of Biophysics and Bioengineering*, 9, 467-508.

95. Marsh, D. (1996). Intrinsic curvature in normal and inverted lipid structures in membranes. *Biophysical Journal*, 70, 2248-2255.

96. Attard, G. S., Templer, R. H., Smith, W. S., Hunt, A. N. & Jackowski, S. (2000). Modulation of CTP:phosphocholine cytidylyltransferase by membrane curvature elastic stress. *The Proceedings of the National Academy of Sciences*, 97, 9032-9036.

97. Davies, S. M. A., Epand, R. M., Kraayenhof, R. & Cornell, R. B. (2001). Regulation of CTP:phosphocholine cytidylyltransferase activity by the physical properties of lipid membranes: an important role for stored curvature strain energy. *Biochemistry*, 40, 10522-10531.

98. Van der Brock-van der Laan, E., Dalbey R. E., Demel, R. A., Killian, J. A., & de Kruijff, B. (2001). Effect of non-bilayer lipids on membrane binding and insertion of the catalytic domain of leader peptidase. *Biochemistry*, 40, 9677-9684.

99. Koeppe II, R. E. & Andersen, O. S. (2007). Bilayer thickness and membrane protein function: an energetic perspective. *The Annual Review of Biophysics and Biomolecular Structure*, 36, 107-130.

100. Rukmini, R., Rawar, S. S., Biswas, S. C. & Chattopadhyay, A. (2001). Cholesterol organization in membranes at low concentrations: effects of curvature stress and membrane thickness. *Biophysical Journal*, 81, 2122-2134.

101. Magzoub, M., Pramanik, A. & Graslund, A. (2005). Modelling the endosomal escape of cell-penetrating peptides: transmembrane pH gradient driven translocation across phospholipid bilayers. *Biochemistry*, 44, 14890-14897.

102. Nacka, F., Cansell, M., Gouygou, J. P., Gerbeaud, C, Meleard, P. & Entressangles, B. (2001). Physical and chemical stability of marine lipid-based liposomes under acidic conditions. *Colloids and Surfaces B*, 20, 257-266.

103. Jiang, G., Xu. Yong & Prestwich G. D. (2006). Practical enantiospecific syntheses of lysobisphosphatidic acid and its analogues. *Journal of Organic Chemistry*, 71, 934-939.

104. Takahashi, T., Yamashita, H., Nagano, Y., Nakamura, T., Kohriyama, T. & Matsumoto, M. (2006). Interactions of Synphilin-1 with phospholipids and lipid membranes. *FEBS Letters*, 580, 4479-4484.

105. Holopinen, J. M., Soderlund, T., Alakoskela, J., Saily, M., Eriksson, O. & Kinnunen P. (2005). Intermolecular interactions of lysobisphosphatidic acid with phosphatidylcholine in mixed bilayer. *Chemistry and Physics of Lipids*, 133, 51-67.

APPENDIX I: BINDING CURVES FOR α-TTP PLOTTED FROM FREE PROTEIN FRACTIONS

Below is the representation of data analyzed directly from the free protein fractions. The free protein fractions were normalized against the amount of protein recovered when no lipid was present, which is taken as the total amount of free protein. Although this method of data manipulation produces qualitatively similar binding trends as those obtained from the lipid-bound fractions, the loss of proteins at low acidic conditions in the free protein fractions affected the binding trend. For this reason this data analysis was not chosen for the 'Results & Discussion' section. Instead it is shown here as alternate method for analyzing the vesicle binding assay results.

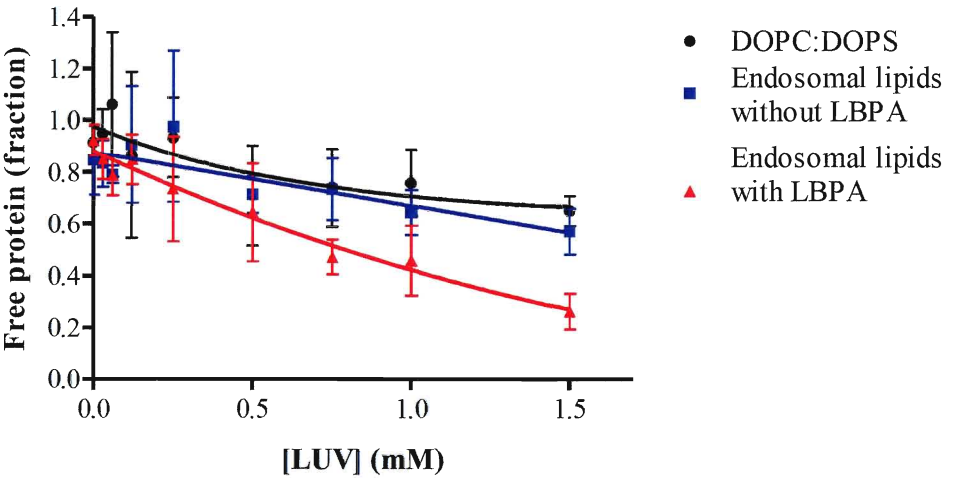

***Appendix I Figure 1**: Binding curves of α-TTP to 200 nm LUVs of DOPC:DOPS, endosomal lipids with and without LBPA at pH 7.5. Data are analysed from the free protein fractions and represent three separate measurements.*

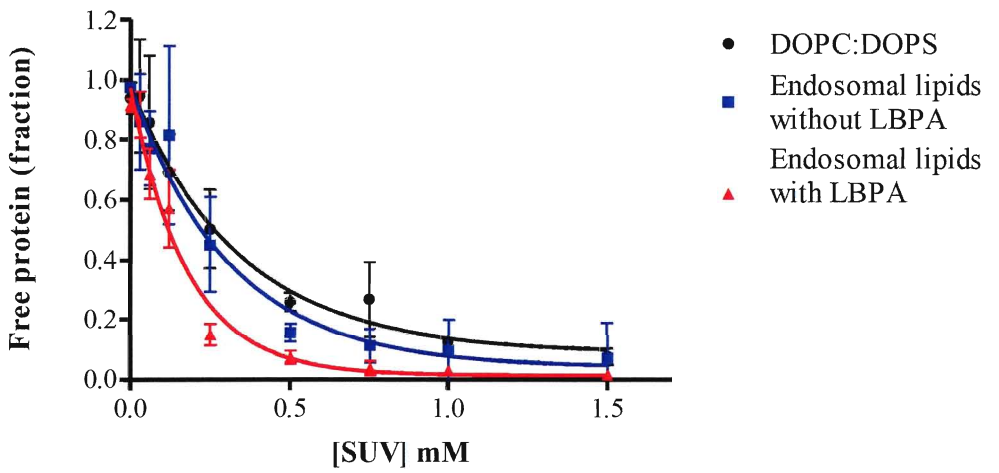

***Appendix I Figure 2**: Binding curves of α-TTP to SUVs of DOPC:DOPS, endosomal lipids with and without LBPA at pH 7.5. Data are analysed from the free protein fractions and represent three separate measurements.*

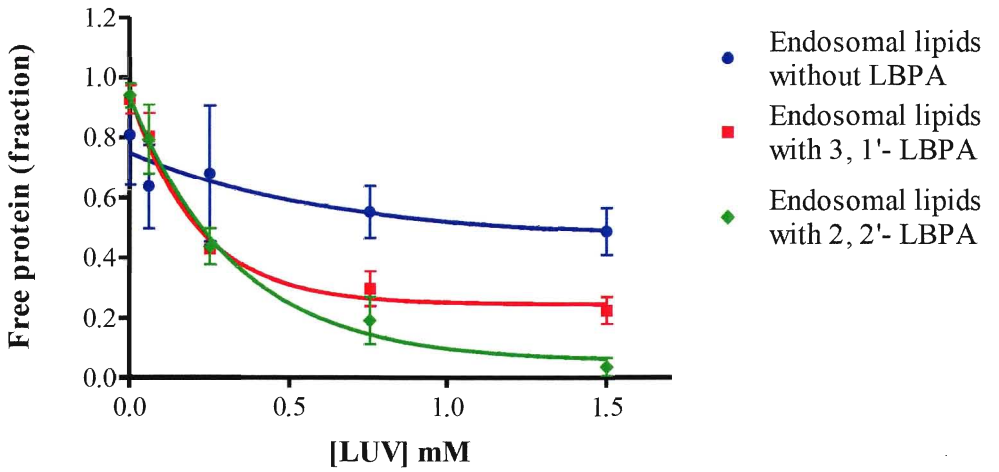

***Appendix I Figure 3**: Binding curves of α-TTP to 400 nm LUVs of endosomal lipids without LBPA, endosomal lipids with 3, 1′ and 2, 2′-LBPA at pH 7.5. Data are analysed from the free protein fractions and represent three separate measurements.*

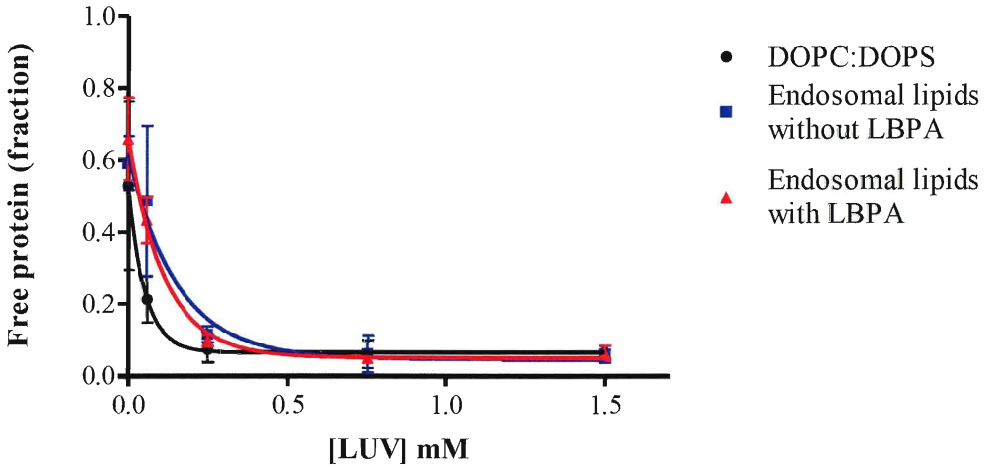

***Appendix I Figure 4**: Binding curves of α-TTP to 200 nm LUVs of DOPC:DOPS, endosomal lipids with and without LBPA at pH 5.7. Data are analysed from the free protein fractions and represent three separate measurements.*

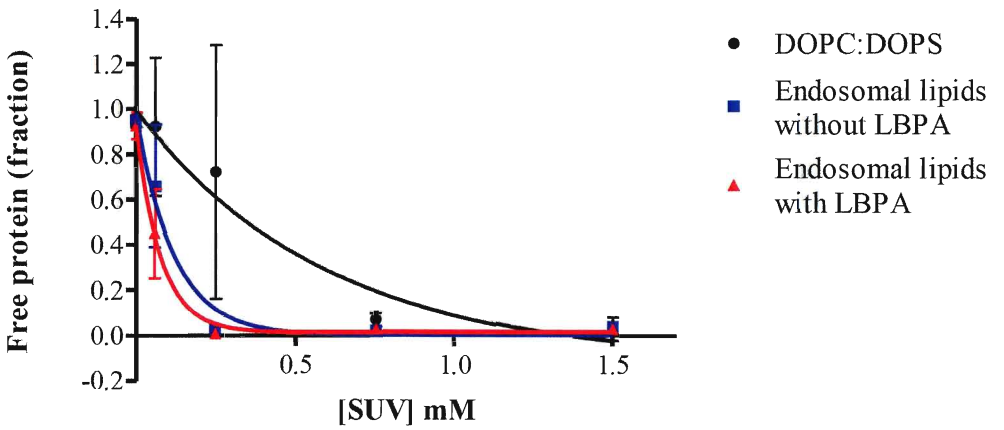

***Appendix I Figure 5**: Binding curves of α-TTP to SUVs of DOPC:DOPS, endosomal lipids with and without LBPA at pH 5.7. Data are analysed from the free protein fractions and represent three separate measurements*

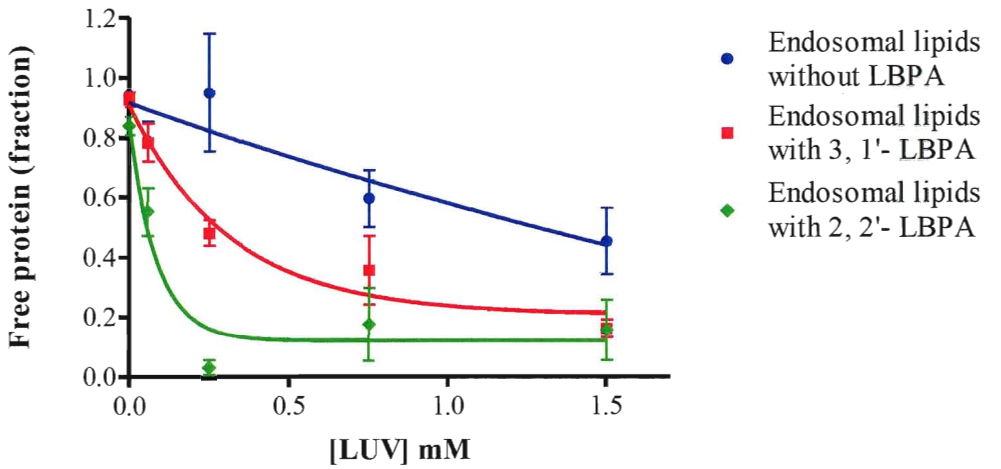

***Appendix I Figure 6**: Binding curves of α-TTP to 400 nm LUVs of endosomal lipids without LBPA, endosomal lipids with 3, 1′ and 2, 2′-LBPA at pH 5.7. Data are analysed from the free protein fractions and represent three separate measurements.*

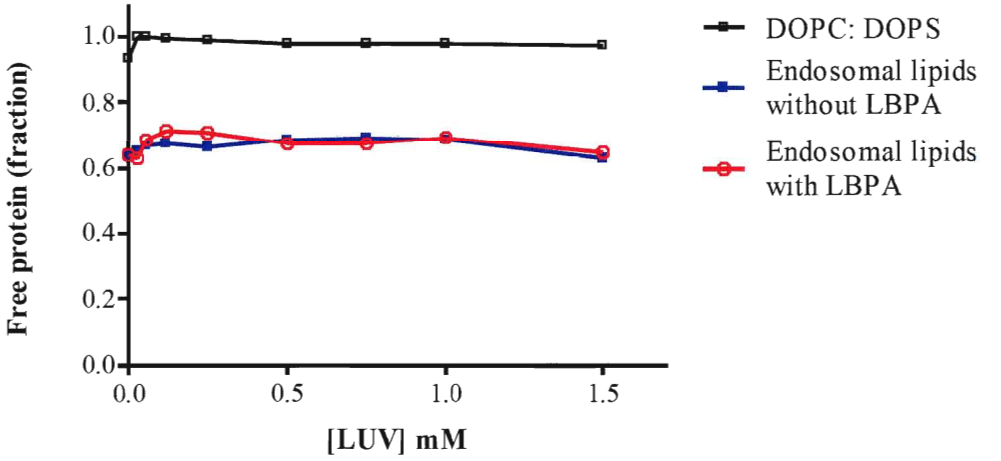

***Appendix I Figure 7**: Binding curves of BSA to 200 nm LUVs of DOPC:DOPS, endosomal lipids with and without LBPA at pH 7.5. Data are analysed from the free protein fractions and each point represents one measurement.*

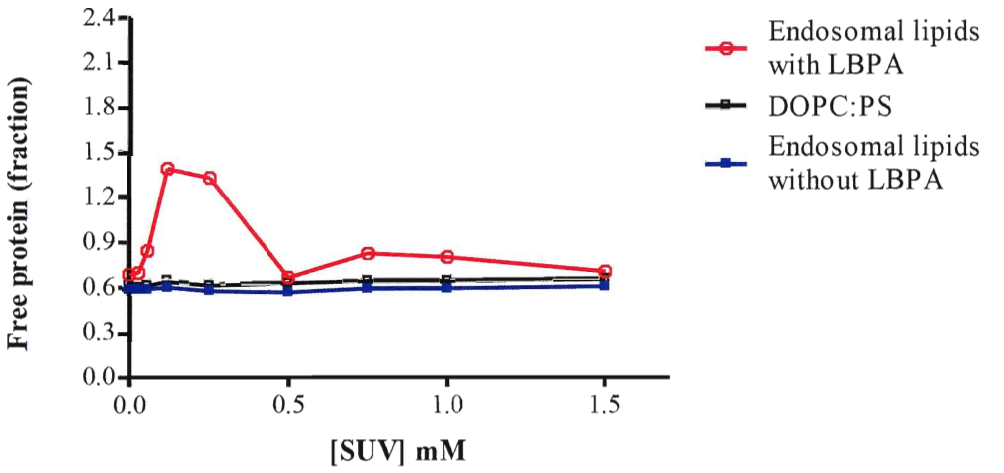

***Appendix I Figure 8**: Binding curves of BSA to SUVs of DOPC:DOPS, endosomal lipids with and without LBPA at pH 7.5. Data are analysed from the free protein fractions and each point represents one measurement.*

APPENDIX II: BINDING CURVES FOR α-TTP BOUND FRACTIONS ANALYZED FROM FREE PROTEIN FRACTIONS

The data from the free protein fractions can also be analyzed in another method [90-91]. The lipid-bound fractions were determined by (1 – Pf/Pt) [91]. Pf represents the free protein recovered when lipid was present while Pt is the free protein recovered when no lipid was present. Therefore Pt represents the total amount of free protein. The lipid-bound fractions are represented as Pb/Pt where Pb is the amount of lipid-bound protein. Since this analysis involves the free protein fractions, the similar explanation describes why this method was not used for the 'Results & Discussion' section.

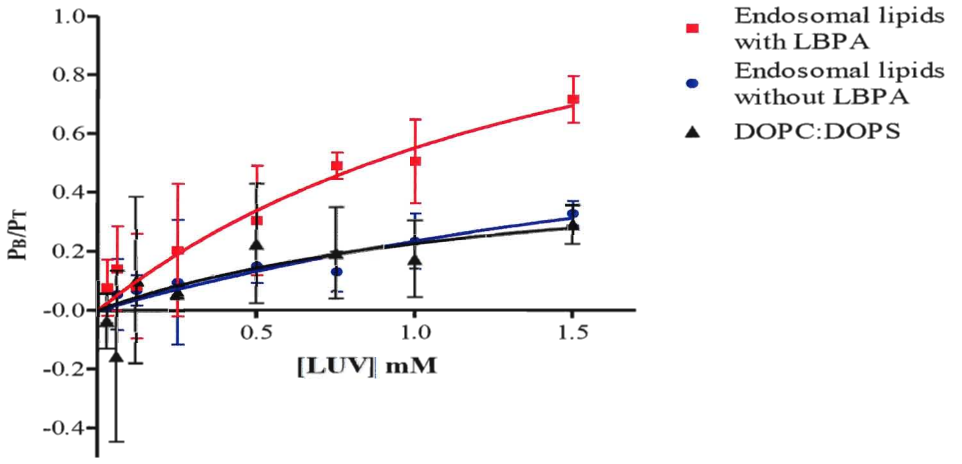

***Appendix II Figure 1**: Binding curves of α-TTP to 200 nm LUVs of DOPC:DOPS, endosomal lipids with and without LBPA at pH 7.5. Data are analysed from the free protein fractions and represent three separate measurements.*

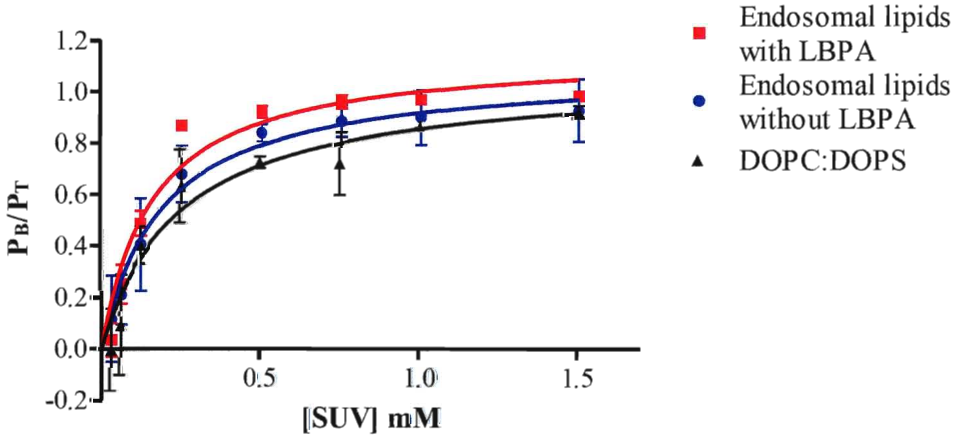

***Appendix II Figure 2**: Binding curves of α-TTP to SUVs of DOPC:DOPS, endosomal lipids with and without LBPA at pH 7.5. Data are analysed from the free protein fractions and represent three separate measurements.*

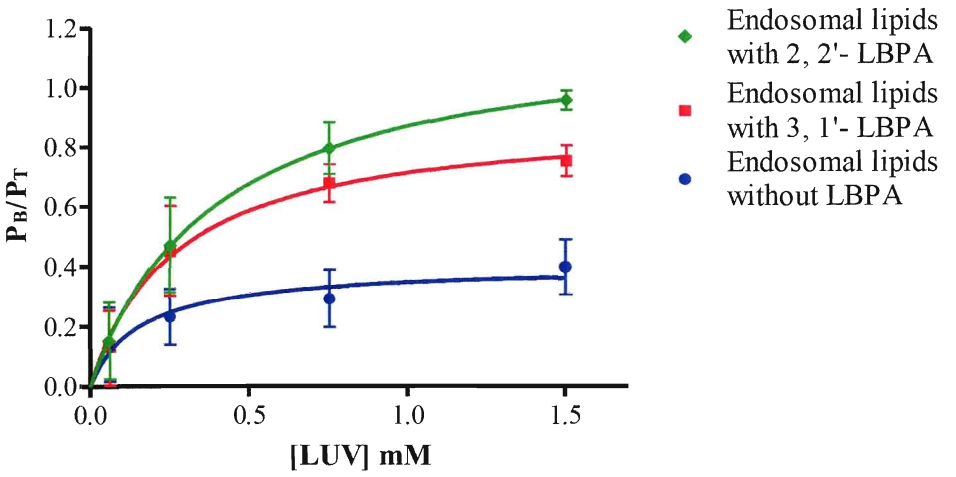

***Appendix II Figure 3**: Binding curves of α-TTP to 400 nm LUVs of endosomal lipids without LBPA, endosomal lipids with 3, 1' and 2, 2'-LBPA at pH 7.5. Data are analysed from the free protein fractions and represent three separate measurements.*

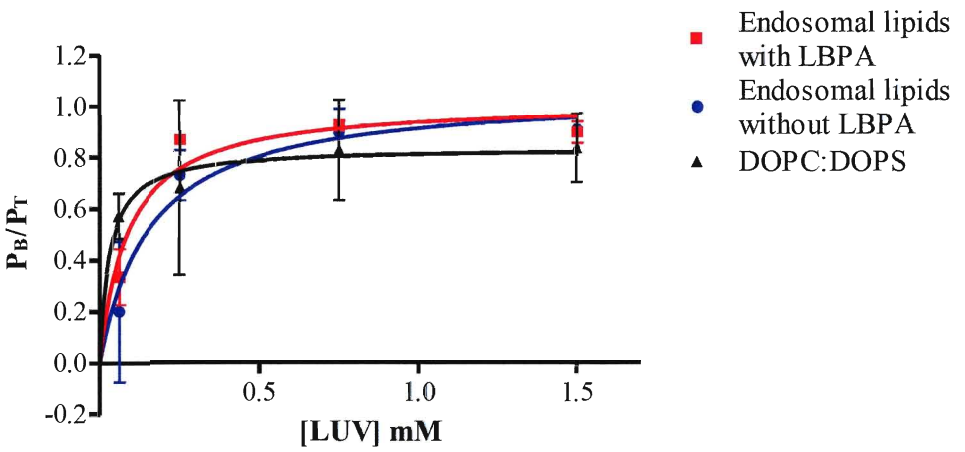

***Appendix II Figure 4**: Binding curves of α-TTP to 200 nm LUVs of DOPC:DOPS, endosomal lipids with and without LBPA at pH 5.7. Data are analysed from the free protein fractions and represent three separate measurements.*

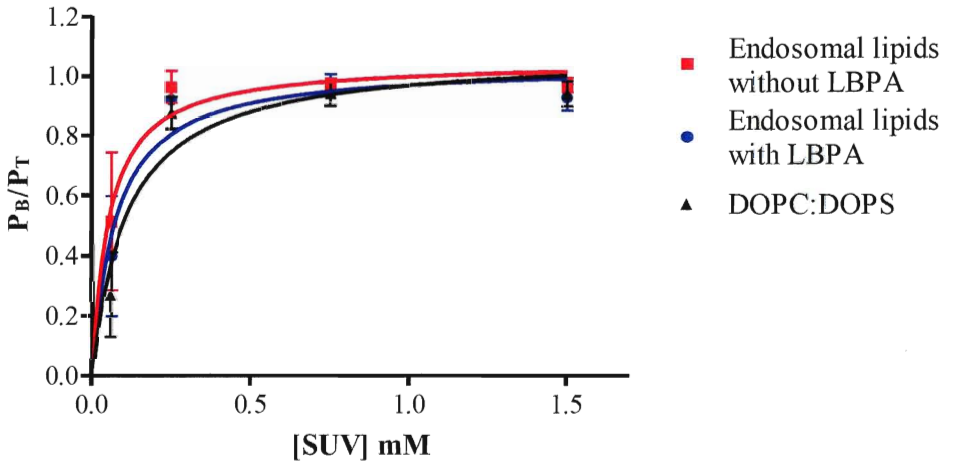

***Appendix II Figure 5**: Binding curves of α-TTP to SUVs of DOPC:DOPS, endosomal lipids with and without LBPA at pH 5.7. Data are analysed from the free protein fractions and represent three separate measurements.*

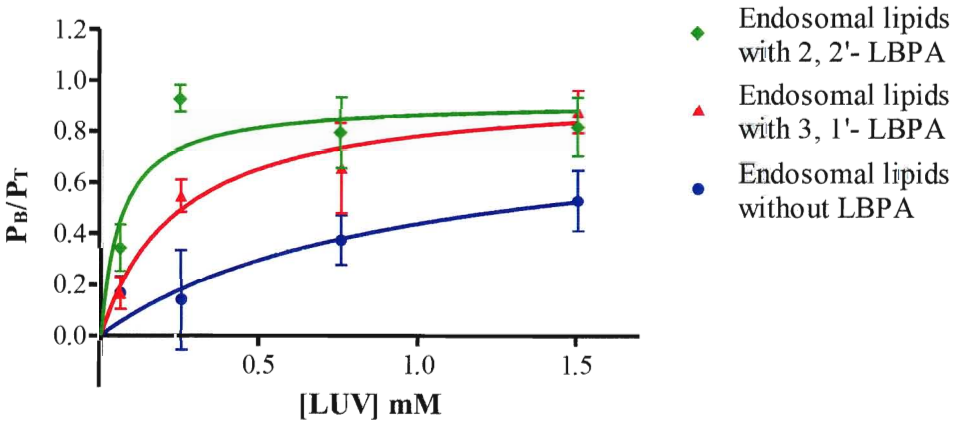

***Appendix II Figure 6**: Binding curves of α-TTP to 400 nm LUVs of, endosomal lipids without LBPA, endosomal lipids with 3, 1′ and 2, 2′-LBPA at pH 5.7. Data are analysed from the free protein fractions and represent three separate measurements.*

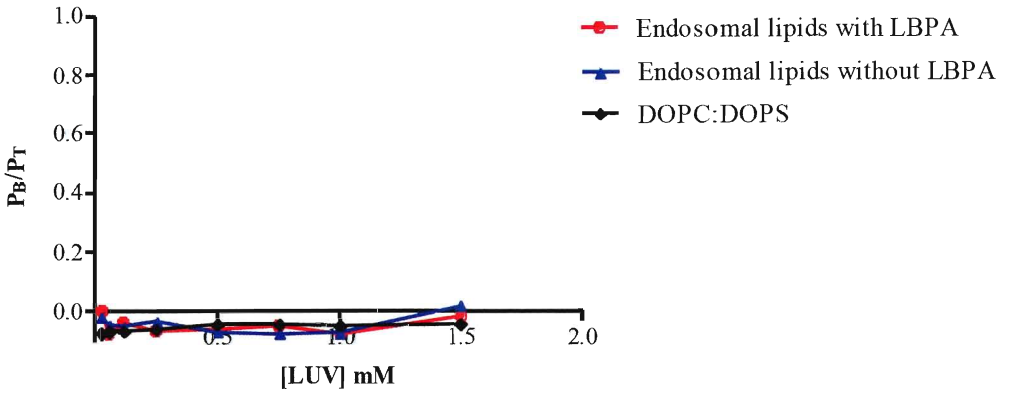

***Appendix I Figure** 7: Binding curves of BSA to 200 nm LUVs of DOPC:DOPS, endosomal lipids with and without LBPA at pH 7.5. Data are analysed from the free protein fractions and each point represents one measurement.*

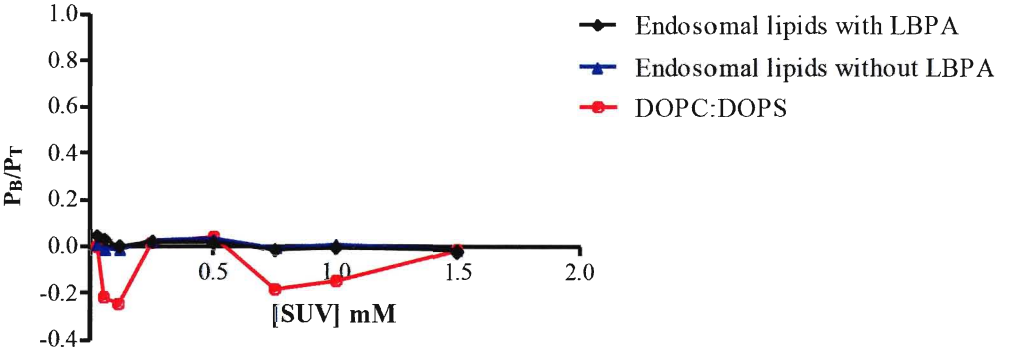

***Appendix I Figure 8**: Binding curves of BSA to SUVs of DOPC:DOPS, endosomal lipids with and without LBPA at pH 7.5. Data are analysed from the free protein fractions and each point represents one measurement.*